Institute for Laser Physics of SC "Vavilov State Optical Institute"
&
Company Lasers and Optical System, Ltd.

Crystalline Media for SRS Conversion
of High Power
1.32 Micron Radiation

Final Report

SPC 97- 4080

F61708 - 97- W025S

Director of the Institute   Prof. Arthur A.Mak

Principle Investigator   Sergey N.Karpukhin

St.-Petersburg

1999

19990413 067

AQF99-07-1292

REPORT DOCUMENTATION PAGE

Form Approved OMB No. 0704-0188

1. AGENCY USE ONLY (Leave blank)	2. REPORT DATE 1999	3. REPORT TYPE AND DATES COVERED Final Report

4. TITLE AND SUBTITLE

Delivery of Crystalline Media for SRS Conversion of High Power 1.32 Micron Radiation

5. FUNDING NUMBERS

F6170897W0255

6. AUTHOR(S)

Dr. Sergey Karpukhin

7. PERFORMING ORGANIZATION NAME(S) AND ADDRESS(ES)

Company
Birzhevaya line 12
St. Petersburg 199034
Russia

8. PERFORMING ORGANIZATION REPORT NUMBER

N/A

9. SPONSORING/MONITORING AGENCY NAME(S) AND ADDRESS(ES)

EOARD
PSC 802 BOX 14
FPO 09499-0200

10. SPONSORING/MONITORING AGENCY REPORT NUMBER

SPC 97-4080

11. SUPPLEMENTARY NOTES

12a. DISTRIBUTION/AVAILABILITY STATEMENT

Approved for public release; distribution is unlimited.

12b. DISTRIBUTION CODE

A

13. ABSTRACT (Maximum 200 words)

This report results from a contract tasking Company as follows: The contractor will (1) deliver SRS crystal samples currently available, and analyze the principal limitations of SRS conversion of 1.32 micron radiation; (2) deliver SRS crystal samples available at this stage of the contract, and operate the laser with rep rate of up to 20 Hz and energy of 20mJ single mode and 150mJ multi-mode, and grow larger SRS-active crystals; and (3) produce final SRS crystal samples, and study SRS conversion parameters (vary beam focus within and outside the cavity), measure spectral and coherence properties of the radiation, investigate SRS amplification of single mode radiation with multi-mode pumping, and prepare final report.

14. SUBJECT TERMS

EOARD, Laser Raman Conversion

15. NUMBER OF PAGES

78

16. PRICE CODE

N/A

17. SECURITY CLASSIFICATION OF REPORT	18. SECURITY CLASSIFICATION OF THIS PAGE	19. SECURITY CLASSIFICATION OF ABSTRACT	20. LIMITATION OF ABSTRACT
UNCLASSIFIED	UNCLASSIFIED	UNCLASSIFIED	UL

NSN 7540-01-280-5500

Standard Form 298 (Rev. 2-89)
Prescribed by ANSI Std. 239-18
298-102

Contents

1. Introduction

This Report is delivered on the completion of the third final stage of the work in the frame of the Contract F61708-97-W0255. According to the Contract provisions on the final stage we had to study the SRS conversion parameters (to vary beam focus within and outside the cavity), to measure the spectral and the coherence properties of the radiation, to investigate the SRS amplification of single mode radiation, with the multi-mode pumping and had also to grow up the large-size SRS-active crystal. The study was carried out by the Company LOS Ltd., St.-Petersburg, Russia with the participation of the scientists of the Research Institute for Laser Physics, St.- Petersburg , Russia, and of the Research Center "Vavilov State Optical Institute", St.-Petersburg , Russia.

In the First Interim Report we have analyzed the basic physical limitations of the approach on the base of the literature data on the studies of the SRS in crystals. The said report contains the review of the available literature as well as the some original numerical simulation results, related to the thermal optics behavior of the SRS process in the pulse-repetitive mode. The experimental setup is described in the Second Interim Report. This Report contains only the original results, and the literature data is used only when it is necessary for the analysis.

2. Measuring of SRS gain for the pump wavelength of 1.32 μm

In the First Interim Report we have noted that the SRS gain (the amplification coefficient) is the main characteristic of the crystal, determining its SRS activity. To this moment the literature has lacked the data on this gain values, so we have started the work by its measurements. One can directly evaluate the gain measuring the amplification of the input signal. Such an approach seems to be the most accurate, but its realization requires the detailed account for the spatial and temporal overlap of the signal and pumping beams. For instance[1], the measurement accuracy was improved by the use of the CW input signal, amplified in the field of the pulsed pump. One can also provide the automatic spatial and temporal coincidence of the pulses when measuring SRS excitation from the spontaneous Raman scattering signal. This method is based on measurement of the SRS threshold.

Let us first evaluate the possibility to use in the gain measurements the multi-frequency single-mode radiation of the pumping laser, described in the Second Interim Report. One can see from the following equation that within some limits the width of the pump spectrum does not influence onto the value of the local gain Γ [cm^{-1}] of the collinear SRS [2]:

$$\Gamma = gI_0 - 2\pi\Delta\nu_p(1/\upsilon_s - 1/\upsilon_p), \quad \text{for} \quad gI_0 > 2\pi\Delta\nu_p(1/\upsilon_s - 1/\upsilon_p)$$

here g is the SRS gain, I_0 is the intensity of the pump, entering the crystal, $\Delta\nu_p$ is the width of the pump spectrum and υ_s, υ_p are the group velocities of the Stokes and pumping waves. As it follows from this relationship, when the inequality is fulfilled, the value of the gain for the multi-frequency radiation does not differ from that for the single-frequency radiation. The physical sense of this inequality is that the gain,

3

accumulated along the length, which is equal to the difference of the coherent lengths of the interacting waves, has to exceed one. In other words, the gain is to be sufficiently high. Let us evaluate this inequality fulfillment for the single-pass SRS excitation in our case. It is well known, that, according to the results of the theoretical and experimental studies of the stimulated nonlinear processes, the intensity of the Stokes wave can reach the level, comparable to the intensity of the pump ($I_s/I_p \sim 1\%$), when the total gain is equal approximately 10^{13} or e^{30} [3]. This large value is universal for all the stimulated processes; it describes the experimental threshold of the stimulated scattering $\Gamma L = 30$ (here L is the length of the crystal). Indeed for the fixed geometry of the experiment the reduce of the pump intensity in just 20% below the threshold results in the signal intensity reduce in 400 times, i.e. in the practically complete dumping of the stimulated scattering. However, the additional detailed account for the angle, where takes place the spontaneous Raman scattering signal amplification, has resulted in more accurate evaluation of the total threshold gain [2]. The more accurate value equals 20-25 for the parallel pumping beam and 30-35 for the focused single mode beam. So at the threshold of the SRS excitation in the focused single-mode beam the left side of the given inequality has to be equal 30/L.; L in our case was equal 6 cm, so the local gain value has to be equal $\Gamma=5$. Note, that in the right side $(1/\upsilon_s - 1/\upsilon_p) = 1/c(1/n_s - 1/n_p)$, that the width of the laser emission spectrum was $\Delta\nu_p = 0.4$ cm^{-1} and that $(1/n_s - 1/n_p) < 0.01$. So the right side of the inequality is <0.03, i.e. inequality is fulfilled. Consequently, we can use the method of the gain measuring by measuring the single-pass SRS excitation threshold. This method is based on the following. The single-mode radiation, whose energy exceeds the SRS threshold, is focused into the crystal. In the focal waist the radiation propagates as the plain wave, and hence the gain is described by the following product:

$$M_F = g\,(P/S_F)\,l_F \qquad (1)$$

here P is the pump power, S_F is the square of the pumping beam's section $(S_F = \frac{\pi}{4}(F\theta_0)^2)$, F is the focal length of the lens, θ is the Gaussian beam divergence $(\frac{4}{k_0 D_0})$ and l_F is the length of the beam waist. The length of the beam waist in the crystal is described by the following equation [2]:

$$l_F = F^2 \frac{\theta\,n}{D_0} \qquad (2)$$

here D_0 is the Gaussian beam diameter before lens $(D_0 = \frac{D_{0.8\,E}}{\sqrt{\pi}})$ and n is the refraction index. Combination of (1) and (2) with the account for the expressions for S_F and θ results in the expression:

$$g = \frac{\pi}{2} \frac{M_F}{k_0\,P_{th}\,n} \qquad (3)$$

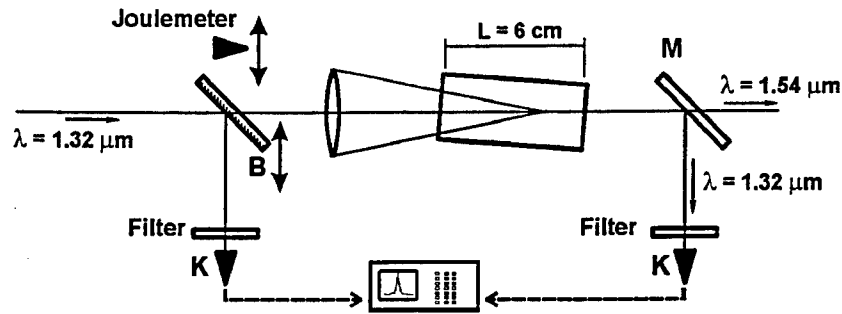here $M_F = 30 \div 35$, $k_0 = \frac{2\pi}{\lambda}$.

Fig. 2.1. The scheme of experimental setup for measuring an amplification gain.

In the Fig.2.1 is shown the scheme of the experimental setup for measuring of the amplification gain. The dimensions of $Ba(NO)_3$ crystal equaled 10×10×60mm and dimensions of KGW crystal were $\varnothing$5×55mm. The focal length of the lens, mounted at the distance 120 cm from the coupling mirror of the cavity, equaled 20 cm. The diameter of the Gaussian beam, which was measured with the use of the apertures, equaled 1.24 mm (the diameter of the aperture inside the laser cavity was in 0,1 mm smaller than the diameter of the aperture, resulting in the second laser mode excitation). The Gaussian distribution across the beam was checked by measuring its divergence: the relationship $\theta_{0.8E} = \lambda/D_{0.8E}$ was fulfilled. The length of the beam waist (6.8 cm) has slightly exceeded the length of the crystal; hence the threshold increment was accumulated along the smaller length. The measuring of the amplification gain has accounted for this difference: the correction coefficient, equal to the lengths' ratio, was used.

The threshold power was measured by means of registration of the pump pulse shape at the crystal input and output. We have evaluated the power, which was corresponding (with the account for the nonlinear losses) to the moment of the character break of the temporal profile of the pumping pulse at the crystal output. This break corresponds to the start of the process of the energy conversion. In the Fig.2.2 are shown the temporal profiles of the pump pulse at the crystal input and of the pulse, which has passed through the crystal without conversion. The Table summarizes the results of the gain measurements as well as the values, which were measured earlier for the wavelengths of 1.064 µm and of 0.532 µm. One can see that the gain reduce with the wavelength grow is described by the law, which faster than the just inversely proportional. The possible reason is the influence of the resonant terms in the expression for the Raman scattering, accounting for the structure of the crystalline electron levels [4].
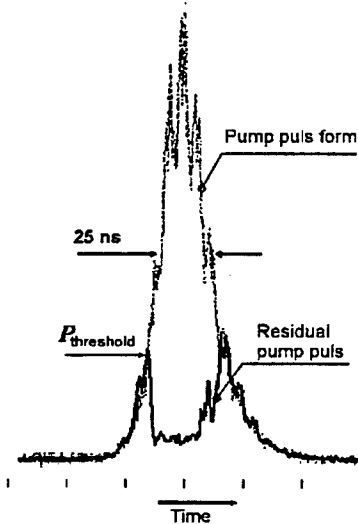

Fig2.2. Temporal profiles of the pump pulse at the crystal input and of the pulse, which has passed through the crystal without conversion.

5

Parameters of SRS crystals

Materials	Polarization	$g \cdot 10^3$ cm/MW			ν, cm^{-1}
		$\lambda = 0.5$ μm	$\lambda = 1.06$ μm	$\lambda = 1.32$ μm	
Ba(NO$_3$)$_2$		47	11	7.1	1046 1047*
KGd(WO$_4$)$_2$	n_m - axis	–	6	–	901.5
	n_p - axis	–	6	–	767.3

* T.T. Basiev, W. Jia, H. Liu, P.G. Zverev, Raman Spectroscopic and Nonlinear Optical Properties of Barium Nitrate Crystal., OSA TOPS on Advanced Solid-State Lasers.,1996, v.1, p.554-559.

In addition to the said measurements in the barium nitrate crystal we have made an attempt to measure the gain in the KGW crystal in the similar experimental conditions. However, in this crystal the threshold of SRS has exceeded the breakdown threshold. Thus the gain in the KGW crystal was evaluated on the base of measuring of the threshold of the generation in the cavity (see Section 4).

So we have measured the value of the SRS gain in the crystal of barium nitrate at the wavelength 1.32 μm. It is equal 0.0071 cm/MW.

3. Generation in the focused beams

This section presents the results of the experimental study of the Stokes radiation generation in the focused single and multi mode beams. Special attention was paid to the conversion efficiency and to the spectral and spatio-angular parameters of the radiation. In the Fig.3.1 is shown the spectrum of the radiation, generated via the single mode beam focusing. (The spectrum was produced due to

Fig.3.1. Spectrum of the radiation, generated via the single mode beam focusing: *a* -pump; *b* - first Stokes; *c* – second Stokes.

the dispersion of the Stokes radiation in the glass prism and was photographed from the screen with the photosensitive layer.) Note the splitting of the second Stokes component line. One can see that its longer wavelength subcomponent reveals lower intensity. The reason of this effect is the threshold-less four-wave mixing conversion of the weak pumping component at the wavelength 1.338 μm (see the First Interim Report) to the Stokes components. The said wavelength is rather close to that of the main component. Hence the wave mismatch of the corresponding parametric process is small ($\Delta k_{S,2} = (k_{P,1} - k_{S,1}) - (k_{p,2} - k_{S,2})$, $\Delta k_{SS,2} = (k_{S,1} - k_{SS,1}) - (k_{S,2} - k_{SS,2})$, here the indexes p, s and ss correspond to the pump, to the first and to the second Stokes components, and the indexes 1 and 2 correspond to the pump components at the wavelengths 1.319 and 1.338 μm) and interaction is rather efficient. In all the experiments which we shall discuss further were observed not more than two Stokes components. The energy of the second Stokes component was measured with the use of the selective glass filter, cutting off the first Stokes component.

We have experimentally measured the dependence of the efficiency of the conversion to the both Stokes components vs. the focal length of the lens in order to determine the optimal focal length. The optical scheme of the experiment is shown in
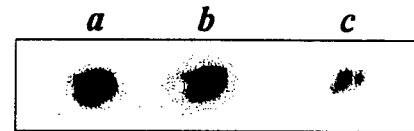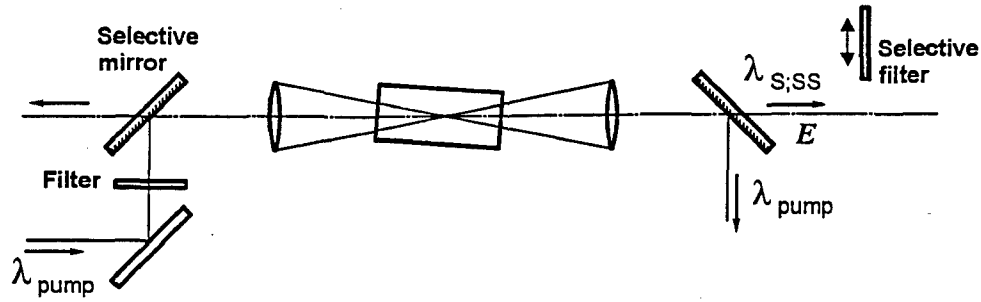
6

Fig.3.2. The optical scheme of the experiment for generation in the focused beams.

the Fig.3.2. The crystals were tilted in order to prevent the generation in the direction, perpendicular to their butt-ends. In the Fig.3.3 are shown the results of these measurements for the single and the multi-mode beams at the constant energy. One can see that in the case of the single mode beam (Fig.3.3 a) the curve is saturated for the short focal length. The reason is that for the focal length of 20 cm the length of the focal waist practically coincides with the length of the crystal. Further shortening of the focal length results in just negligible growth of the increment, while the focal density of the intensity grows. Such a growth is not desirable in the case of pulse-repetitive mode of laser action. (For example, in the experiments with the copper vapor laser [5] radiation, focused by lens with the focal length of 50 cm, after some period of the experiments there was observed the occasional breakdown of the crystal, while in course of the consequent experiments with the focal length of 60 cm no damage occurred). That is why we have chosen for our experiments the focal length of the lens equal to 20 cm.

In the case of the multi-mode pumping the length of the focal waist exceeded the length of the crystal for all the lens we have used. Hence the conversion efficiency was reducing with the focal length growth (see Fig.3.3 b). However, in our further experiments we have not used the focal lengths, shorter than 20 cm, due to the higher energy in the pulse of the multi-mode pump and to the limitations, imposed by the possibility of the optical damage. The threshold of the optical damage can be evaluated as 60 J/cm^2. The most recently grown crystals were not damaged by such an intensity. However, in the crystals, which were grown up earlier and which were characterized by the stronger scattering of the He-Ne laser radiation, the damage sometimes was produced by such an intensity (depending upon the point of radiation focusing).
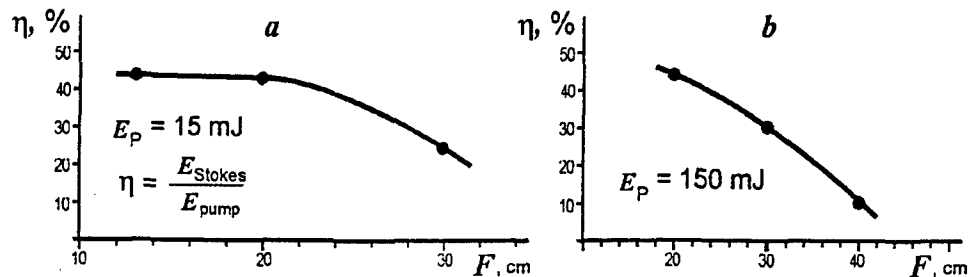

Fig.3.3 Dependence of the conversion efficiency
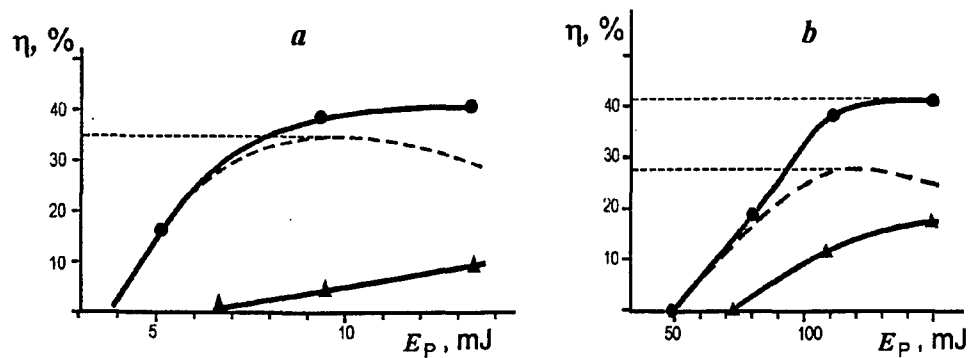to the both Stokes components vs. the focal length of the lens.

Fig.3.4 Conversion efficiency to the separate Stokes components vs. pump energy for single mode beam (a) and multy mode beam (b).
● - total output Raman radiation, − − − − - first Stokes component, ▲ - second Stokes component;

In the Fig.3.4 are shown the results of measuring of the conversion efficiency to the separate Stokes components vs. pump energy. As one would expect, the efficiency of the conversion to the most interesting first Stokes component was limited by the excitation of the second Stokes component. Both Stokes components were excited only in the forward direction; the reason is the slightly smaller gain of the backward SRS amplification in the field of the multi-frequency pump in our case. The maximal technical efficiencies reached 35% for the single-mode pump and 27% for the multi-mode pump. The corresponding values of the physical efficiency (accounting for the Fresnel reflection at the butt-ends and for the incomplete transmission through the selective mirror) were thus 41% for the single-mode and 32% for the multi-mode pump. One can see that in the case of the single-mode pumping the influence of the second Stokes generation onto the efficiency of the first Stokes component generation is smaller. The reason of this effect is as follows. The process of the second Stokes component generation involves the parametric process. In the both regimes the pump has the plain wavefront along the overall length of the crystal. Hence both of the pumping regimes reveal one and the same increments along the length of the nonlinear parametric conversion to the second Stokes component ($gI_s/\Delta k_{SS}$, here $\Delta k_{SS} = k_P - 2k_s + k_{SS}$). At the same time in the single-mode variant of pumping the diffraction divergence of the second Stokes component ($\theta = \lambda_{SS}/D_{0,8E}$, $\lambda_{SS} = 1.82$ μm) exceeds that for the multi-mode pump because of the much (approximately in 5 times) narrower beam in the first case. This effect obviously results in extra-losses while excitation of the second Stokes component.

The relatively low conversion efficiency results of the temporal profile of the pulse, where the large amount of energy contains in the forward and the backward tails of the pulse. That is why the Stokes pulse is shorter and has the nearly rectangular shape (Fig.3.5). This, however, is not the only reason. We have discovered the additional channel of losses, caused by the nonlinear absorption of radiation. It is more emphasized for the single-mode radiation. We have first measured the energy balance between the input and output beams when the peak intensity in the pulse was sufficiently lower than the SRS threshold. Such an experimental conditions were provided when the radiation passed through the crystal without focusing (pulse energy of 15 mJ). The output energy was in this case equal to the input energy with the account for the reflection from the edges, i.e. the linear losses were negligible. In the case of focusing of the beam with the energy beyond the
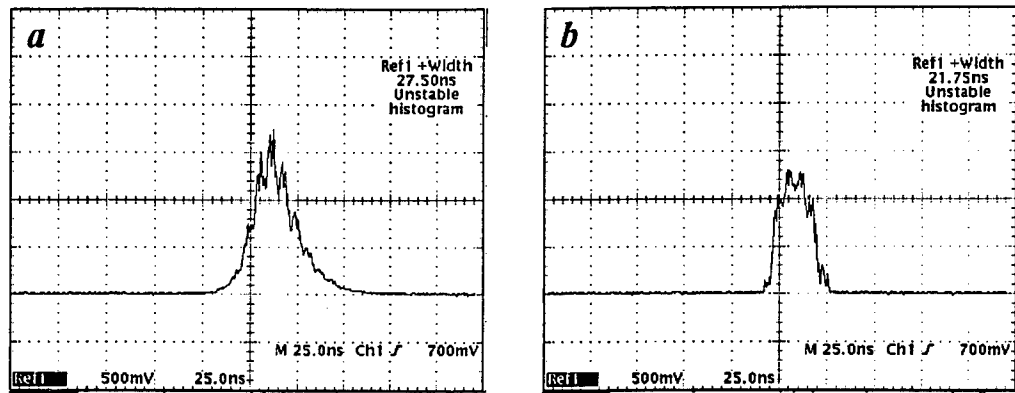
Fig. 3.5. Temporal profile of the one mode pump pulse(a) and Stokes pulse(b).

threshold, when no SRS took place, for the single-mode pump the energy balance (with the account for the reflexes) was frustrated. Extra-losses equaled 6% of the input energy. For the saturated SRS these losses grew up to 11-13%. In the case of the multi-mode pumping the nonlinear losses in the saturated regime were smaller than in the single-mode case; in the mode of the single-pass saturated SRS their value did not exceed 4-6%. The most possible reason of these nonlinear losses is the resonant multi-photon absorption, caused by the continuous spectrum of the electron states in the crystalline zone structure. The difference in the losses for two variants of the pump results, probably, of the different spectral density of radiation. The multi-mode radiation opposite the single-mode radiation contains the transverse oscillations and thus its energy is distributed across the larger amount of the frequency components. (This feature also reveals itself in the much smoother temporal profile of the multi-mode radiation pulse).

Another variant of the experiment geometry (Fig.3.6) has revealed higher efficiency of the energy conversion to the first Stokes component of the multi-mode radiation. In this case the radiation was focused by lens (with the longer focal length) in the direction, which was perpendicular to the butt-ends of the crystal. In this case the butt-end edges act as the cavity mirrors, and the SRS excitation threshold is approximately two times lower than in the case of the tilted edges. In such the geometry there is also observed the excitation of the backward SRS. However, such an experiment can not be treated as the generation in the cavity: one can see from the divergence measurements (see further) that in this case the structure of the angular distribution of the output radiation energy reproduct that of the pump. The optical scheme of the measurements in this geometry is shown in the Fig.3.6, while the results of these measurements are shown in the Fig.3.7. One can see that the second Stokes component is excited only for the triple threshold ratio. The reason is the threshold reduce and thus in the weaker parametric process of the second Stokes component generation, whose rate is proportional to the product of the pump intensity and intensity of the first Stokes component. Note also that the radiation focusing into the auxiliary crystal (Fig.3.6 b) did not result in the improvement of the first Stokes component generation efficiency.
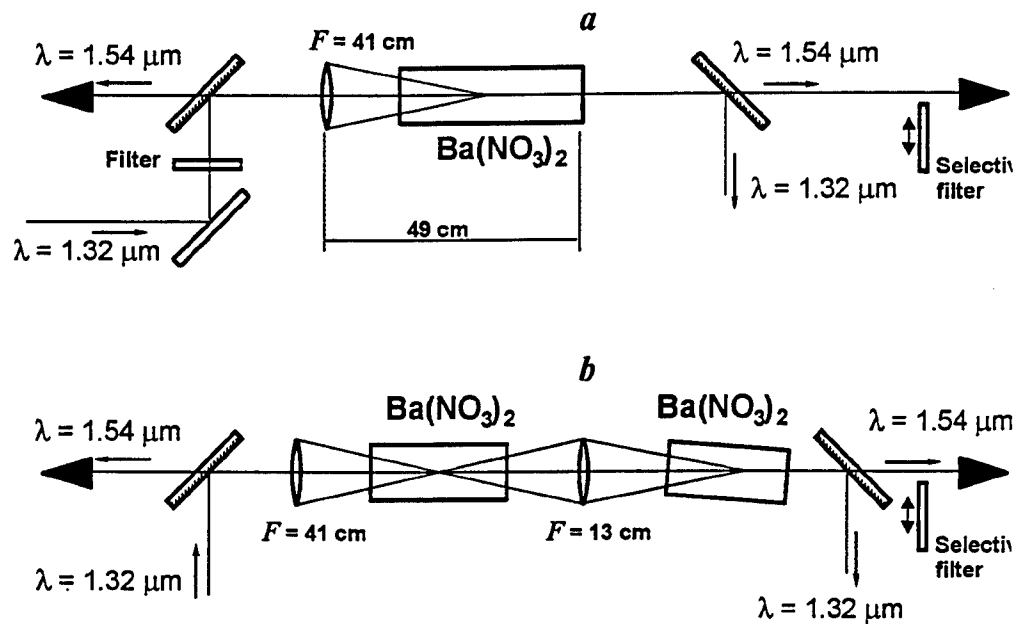
Fig.3.6. The optical scheme for generation in the focussed beams with butt ends of a crystal perpendicular to pumping beam direction (à) and with repeated focusing in the second crystal (b) .
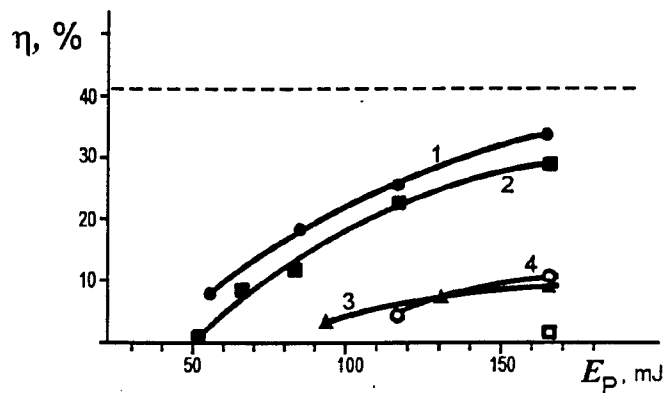

Fig.3.7 Conversion efficiency to Stokes components vs. pump energy.
1 - two crystal scheme (total output Raman radiation); 2 - one crystal scheme (first Stokes component); 3 - backward SRS (for one and two crystal scheme); 4 - second Stokes component (two crystal scheme); □ - second Stokes component (one crystal scheme).
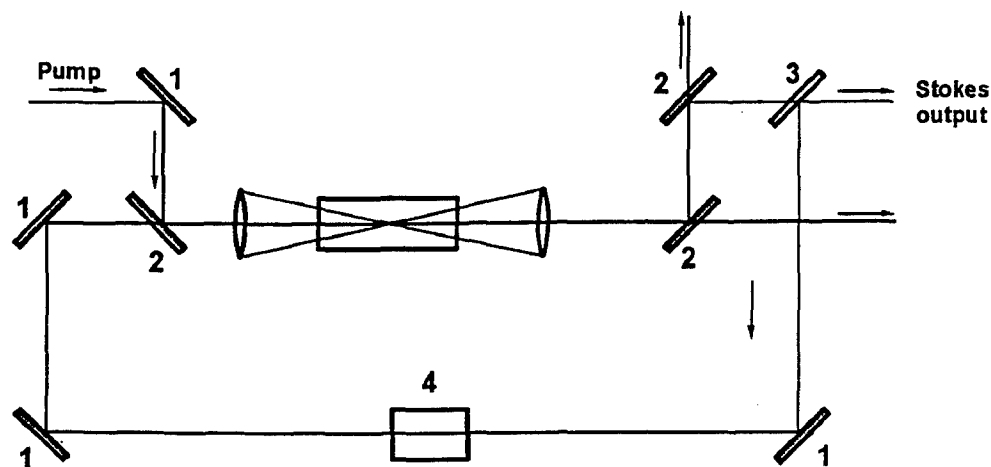
10

Fig.3.8 The optical scheme for effective generation
of the first Stokes component in focused beams.
1 - mirror; 2 - selective mirror; 3 - polarizer for Stokes radiation; 4 - 90° polarization rotator

Summation of the forward and the backward SRS radiation in the scheme, shown in the Fig.3.8, will result in the utmost conversion efficiency of 41%.

We have tested in the experiment that the parameters of the converted beams did not vary up to the pulse repetition rates of 20 Hz.

Radiation divergence was measured with the use of the pinholes, mounted in the beam waist after the special measuring lens (Fig.3.9). We have also measured (for the comparison purposes) the divergence of the pumping beam. In this case the beam energy was attenuated beyond the SRS threshold by the thin neutral filter, and the selective mirror was taken off the scheme. The results of the divergence
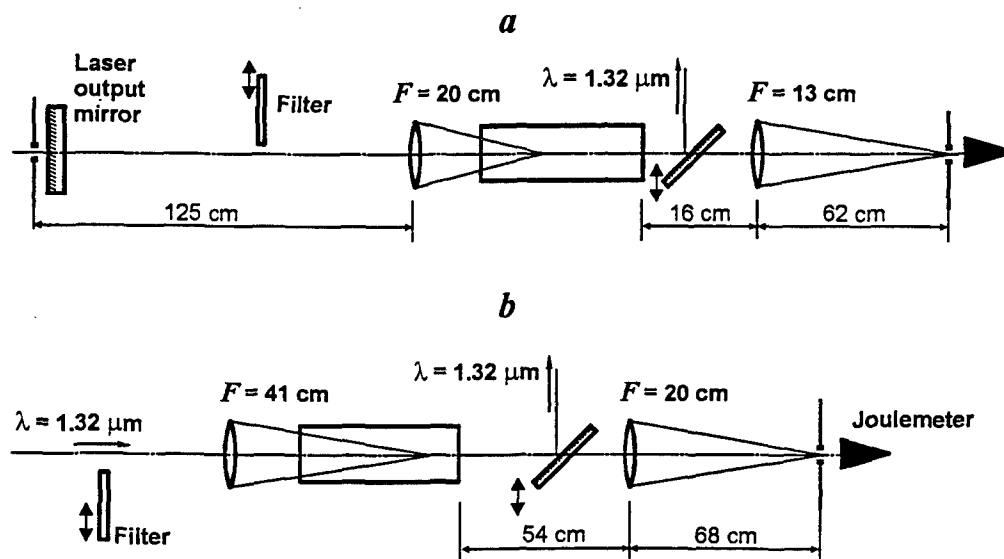
a

b

Fig. 3.9. The optical scheme for divergence measurement with
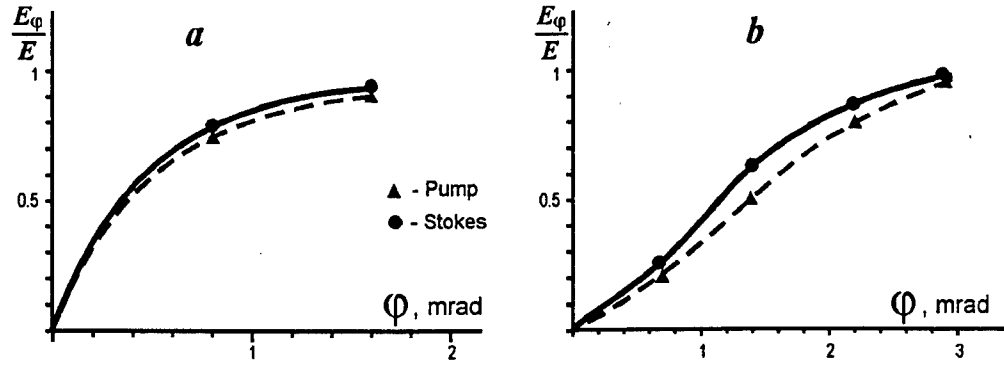one mode pump beam (a) and multy mode (b).

11

Fig.3.10. The results of the divergence measurements

measurements are shown in the Fig.3.10. One can see that - both for the single-mode and the multi-mode pumping - the Stokes beam divergence was slightly less than that of the pumping beam. In the case of the single mode beam such a situation is possible only due to the beam diameter increase at the measuring lens. This, in turn, means that the diameter of the beam of the Stokes radiation in the crystal is smaller than that of the pump beam (such a result was theoretically predicted [6]), and the near-field diffraction results in the wider beam in the plane of the measurement lens. Let us, for a conclusion, repeat the main results of this Section:

1. In the focused beam the generation with the wave front reproduction takes place up to the level of saturation. That is why the divergence of the Stokes radiation is close to that of the pump divergence.
2. Efficiency of the conversion to the first forward Stokes component is limited by the excitation of the second Stokes component. Conversion efficiency in the single-mode focused beam (35%) is higher than that in the multi-mode beam (27%). Efficiency of the first Stokes component for multi-mode generation can be improved up to 41% by means of summation of the forward and the backward scattering in the scheme of the low-quality cavity, which does not influence onto the reproduction of the pump wave front in that of the Stokes component.
3. We have realized ~ 1 W of the average power at the eye-safe wavelength of 1.53 μm.

4. Generation in the cavity

We have improved the efficiency of the single-mode pump conversion with the use of the generation in the cavity. The parameters of the cavity, which are shown in the Fig.4.1a, were chosen with the account for the mutual adjustment of the volume of the zero mode of this cavity and of the focused pumping beam. The Gauss diameter of the zero mode was determined according to the formula [7]:

$$d_0 = 2\sqrt{\frac{\lambda_s}{\pi}} \sqrt{L'(R - L')} \qquad (3.1)$$

$$L' = L - l\left(1 - \frac{1}{n}\right)$$

12

It was equal 0.42 mm. The Gauss diameter of the pumping beam in the crystal when focused by the lenses with the focal lengths 41 cm and 30 cm ($d_{0p} = (\lambda/D_0)F$) was equal to 0.25 and 0.18 mm correspondingly. The diameter at the level 80% of the total energy was 0.44 and 0.32 mm correspondingly.

The Gaussian diameter of the cavity mode exceeding that of the pumping beam has, seemingly, resulted in the growth of the generation threshold and, maybe, in the better selectivity of the cavity. The coupling mirror reflected the pump completely. According to the results of the paper [8] this also increase in the discrimination of the second Stokes component generation. When the butt-end edges of the crystal were orthogonal to the cavity axis we have observed the dual mode generation. Small tilt of the crystal has resulted in generation of the single mode (Fig.4.2). Fig.4.3 a illustrates the results of measuring of the dependence of the conversion efficiency vs. pump intensity. The maximal efficiency was as high as 55% (accounting for the possibility of the AR coating of the input edge of the crystal). Account for the incomplete transmission of the output mirror indicates the physical level of 58.%. Note that no generation of the second Stokes component was observed.

No modification of the generation parameters took place for the pulse-repetitive modes of action (repetition rate - up to 20 Hz).

With the use of the multi-mode pump we have started from the similar scheme of radiation focusing into the volume of the zero mode of the cavity. The most interesting was to reveal the possibility to improve the radiation divergence. The parameters of the cavity we have studied are indicated in the Fig.4.1b.
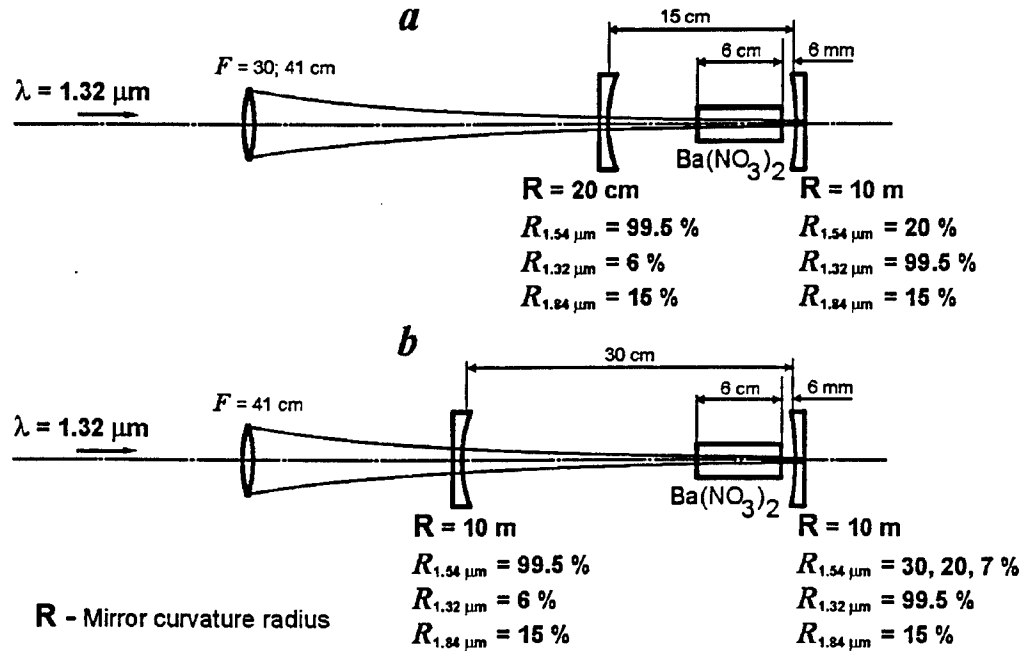

Fig. 4.1 The parameters of the cavity for generation with single-mode pumping (a) and multimode pumping (b).

13

We have used the symmetrical cavity with the concave mirrors. In this case one has to replace in the formula (3.1) L by L/2 so as to evaluate the mode volume. Neglecting in the long cavity by the cavity length modification due to the refraction in the crystal we get for the Gaussian diameter of the zero mode the value of 1.54 mm. For the focal length of the focusing lens 41cm the diameter of the beam in the crystal (energy.level 0.8) was equal 1.64 mm.
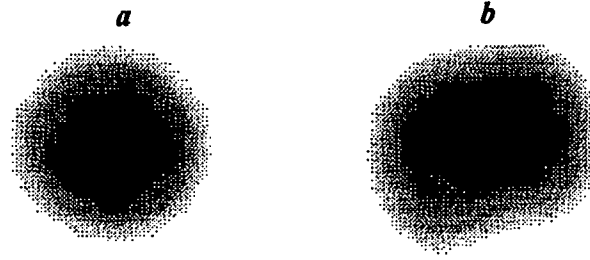

Fig. 4.2. Far field patterns for generation in the cavity with single- mode pumping.
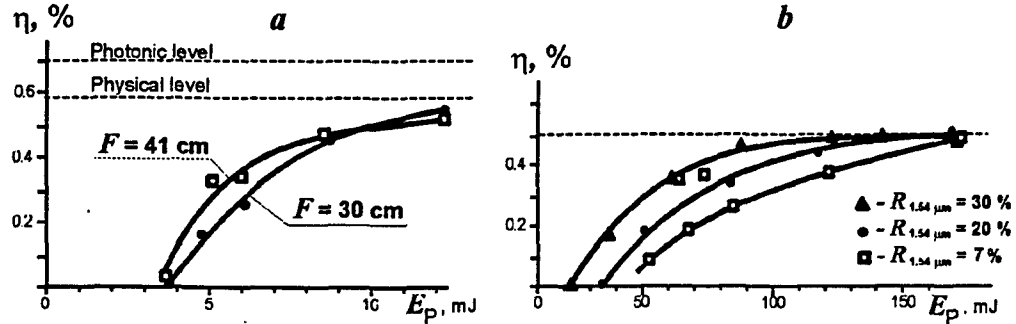a – tilted crystal; b – parallel crystal.

Fig. 4.3. Dependence of the conversion efficiency vs. pump pulse energy for generation in the cavity with single- mode pumping (a) and multy- mode pumping (b).

In the Fig.4.3 b are shown the results of measuring the conversion efficiency vs. the pumping energy for the different coefficients of the mirror reflectivity. Note, that for the mirror with the reflectivity 7% the threshold is just slightly lower than in the case of the single-pass SRS when the crystal edges are orthogonal to the optical axis (Fig.3.7). The reason is that in the mode of the wave front reproduction the increment of the Stokes wave amplification twice exceeds the corresponding value for the waves in the cavity, which are not spatially correlated with the pump [6]. The maximal efficiency (without the account for the reflection by the input edge of the crystal) was equal 50%. Hence both variants of the pump reveal approximately one and the same conversion efficiency, but not the radiation divergence. The Gaussian angle of the zero mode divergence in the described cavity can be calculated according to the formula [7]:

14

$$\Delta\theta = 2\frac{\sqrt{\dfrac{\lambda}{\pi}}}{\sqrt[4]{\dfrac{L}{2}\left(R-\dfrac{L}{2}\right)}}$$

It is equal 1.2 mrad. In the Fig.4.4 are shown the results of measuring of the energy distributions in the near (17 cm from the coupling mirror) and far-field zones. One can see from these figures that the Stokes radiation contains the core and the wide wings. High quality of the core radiation can be seen also from the Fig.4.5. The

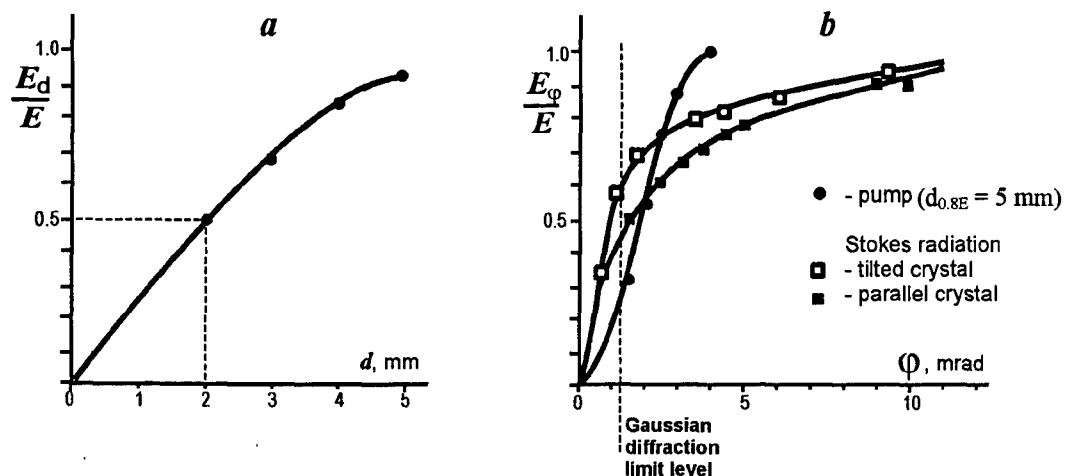Fig.4.4. Near field distribution (*a*) and angular energy distribution *(b)* for generation in the cavity with multy-mode pumping.
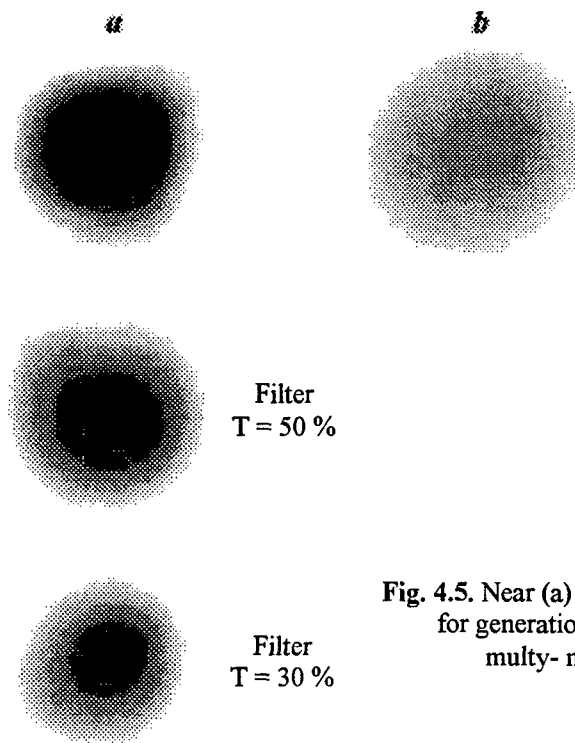

Filter
T = 50 %

Filter
T = 30 %

Fig. 4.5. Near (a) and far (b) field patterns for generation in the cavity with multy- mode pumping.

brightness improvement was measured with the higher accuracy in the following experiment. At some distance from the coupling mirror we have mounted the aperture (Fig.4.6), cutting off the main part of the radiation wings. The efficiency of the conversion in the presence of such an aperture was 25% (the butt-end edges of the crystal were not tilted). In such a geometry we have also measured the near and the far-field energy distributions; the results are shown in the Fig.4.7. The coefficient of the brightness improvement k, recalculated for the equal beam diameters according to the following formula, equaled 5.9:

$$k = \eta \left(\frac{D_p}{D_s} \right)^2 \left(\frac{\theta_p}{\theta_s} \right)^2$$

Here D_p is the pumping beam diameter before the focusing lens, θ_p is the pumping beam divergence for the given diameter, and D_s and θ_s are the same parameters of the Stokes radiation in the plane of the measuring lens.

Hence the SRS generation in the cavity makes it possible to improve significantly the brightness of the remote object irradiation.

The described cavity differs from the schemes we have described before: it reveals the significant reduce of the efficiency with the growth of the pulse repetition
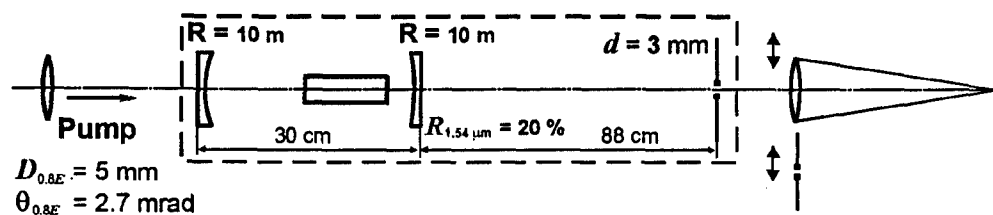

Fig. 4.6 Optical scheme for measuring the brightness improvement for generation in the cavity with multy-mode pumping.

Fig. 4.7. Near field and angular energy distributions for generation in the cavity with multy-mode pumping and external spatial filter.
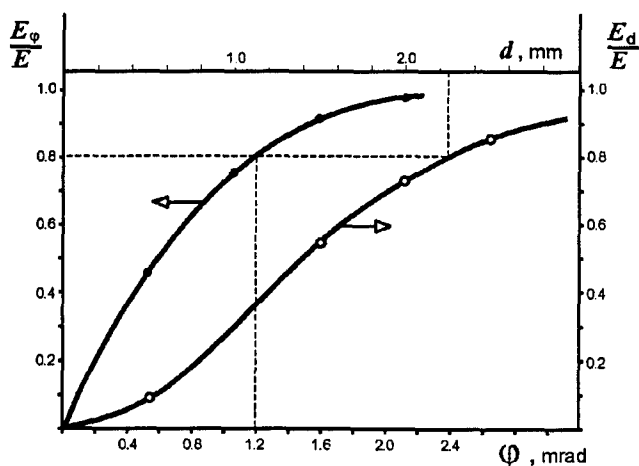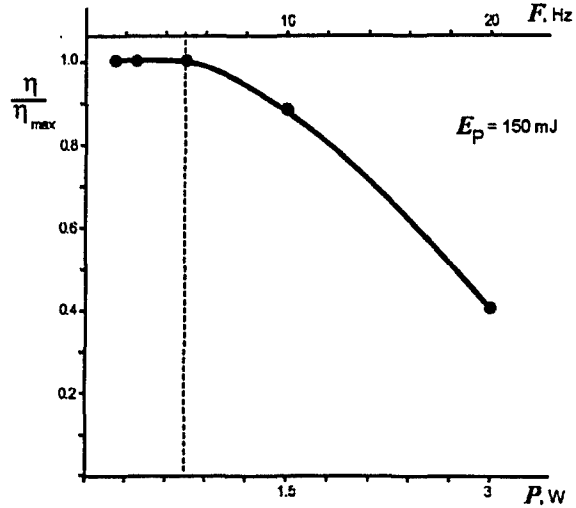
Fig. 4.8. Dependence of the conversion efficiency for generation in the cavity with multy-mode pumping vs. pump pulse frequency.

rate (Fig.4.8). We have found out that the reason is the negative thermal lens, which modifies the cavity quality. In the Fist Interim Report we have described the model of the thermo-optical distortions in barium nitrate crystal. It was shown that the account of the relationships between the photoelastic coefficients (($p_{1.3}$ -$p_{1.2}$)/$p_{1.2}$ << 1) makes it possible to use the theory, elaborated for the crystals of higher symmetry. The average value of the optical force of the thermal lens for two orthogonal eighen - polarizations is described by the formula [9]:

$$F = \frac{2\chi S}{PP_h}$$ (3.1)

where P_h is the heating power, S is the beam section area, χ is the thermal conductivity coefficient, $P = \beta - \frac{\alpha n_0^3}{4}\frac{1+v}{1-v}(p_{11}+p_{12}) = -7.9\times10^{-5}$ degree^{-1}, $\beta = \frac{dn}{dT}$,

n is the refraction index, α is the coefficient of linear expansion, v is the Poisson coefficient and p_{11}, p_{12} are the photoelastic coefficients.

One can see from these relationships that the thermal lens reveals the negative optical force. This force was measured in the optical scheme, which is shown in the Fig.4.9. Diameter of the beam in the crystal was enlarged up to 2.2 mm (0.9E, nearly flat top distribution) by means of the spherical mirror, replacing one of the flat mirrors
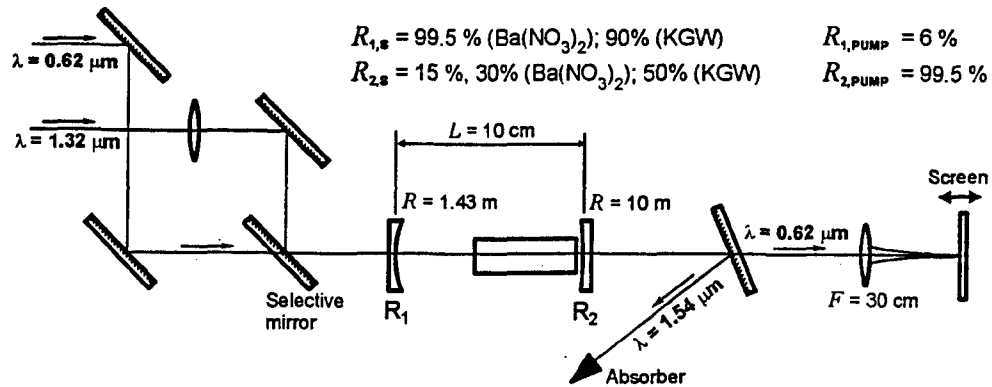

$R_{1,s}$ = 99.5 % (Ba(NO$_3$)$_2$); 90% (KGW) $R_{1,PUMP}$ = 6 %
$R_{2,s}$ = 15 %, 30% (Ba(NO$_3$)$_2$); 50% (KGW) $R_{2,PUMP}$ = 99.5 %

Fig. 4.9. Optical scheme for measuring thermal lens.

17

in the pumping laser cavity. We have measured in the experiment the distance from the plain of the auxiliary lens to the center of the focal waist of the He-Ne laser radiation beam. Such measurements were done in the presence of the SRS excitation in the cavity and in its absence. The calculation was done with the use of the lens formula. ((Preliminary – in the absence of SRS – we have measured the radius of the He-Ne laser beam wave front curvature in the plane of the crystal). For the pulse energy 115 mJ, pulse repetition rate 20 Hz, efficiency of generation to the first Stokes component 50% and to the second one 7% the measured value of the thermal lens focal distance was equal minus 150 cm.

It was interesting to compare this value of the thermal lens focal length with the value, calculated for the deposed thermal power:

$$P_h = P_p \left(\eta_1 \frac{\Omega}{v_S} + \eta_2 \frac{2\Omega}{v_{SS}} \right) \qquad (3.2)$$

Here η_S and η_{SS} are the efficiencies of the pump conversion to the first and to the second Stokes components and v_S and v_{SS} are the frequencies of these components.

If one uses in the formula (3.1) the value of the thermal losses of 0.24 W and the values of some other constants (see Table 2 of the First Interim Report), he will evaluate the focal length of the lens as rather short – equal to minus 35 cm. This is a contradiction with the experimental result. One can use the experimental value of the focal length for evaluation of the thermooptical constant P. It is thus equal to 2.3×10^{-5} degree^{-1}, while calculated value is 7.9×10^{-5} degree^{-1}. This constant is calculated as the difference between two constants, and is thus rather sensitive to the accuracy of measuring them. (Let us, for example, assume, that the real value of β exceeds twice the value, available from the literature, and let us also assume, that the value of α is, vice versa, twice smaller. In this case the calculated value of the P would change in an order of magnitude and would be thus 2.5 times smaller than the experimentally measured.)

We have also tried to measure the thermal lens in the crystal of KGW in the similar cavity. Unfortunately, the use of the pulse-repetitive pump has destroyed the AR coating on the butt-ends of the crystal. However, before this damage occurred we have carried out the series of the preliminary adjustment experiments. In this experiments we have, in particular, registered on the photosensitive paper the near field distribution. On this basis we can make a statement that for the various pulse repetition rates the near field distribution does not change. In the barium nitrate experiment under the similar conditions we have observed the noticeable modification of the near field distribution due to the thermal lens action. Hence, one can state that in the crystal of KGW the thermooptical constant P is smaller than that in the crystal of the barium nitrate. Worth mentioning that in the crystal of YAG its value is 7.7×10^{-7} degree^{-1}, i.e. is smaller more than in order of magnitude [8].

In the First Interim Report we have analyzed the possibility to eliminate for the thermally induced birefringency. It was done experimentally using the optical scheme, shown in the Fig.4.10. The geometrical axis in the crystal was parallel to the crystallographyc axis [$\bar{1}10$]. Lateral faces were crystallographyc planes {111} and {112}. (The angle between axis [100] and lateral face {111} is equal 35°.) In the Fig.4.11 are shown the dependencies of the efficiency of the pump conversion to the Stokes radiation in the cavity vs. the pump power for the various crystal orientations. For the optimal orientation, when polarization of pump radiation is parallel to
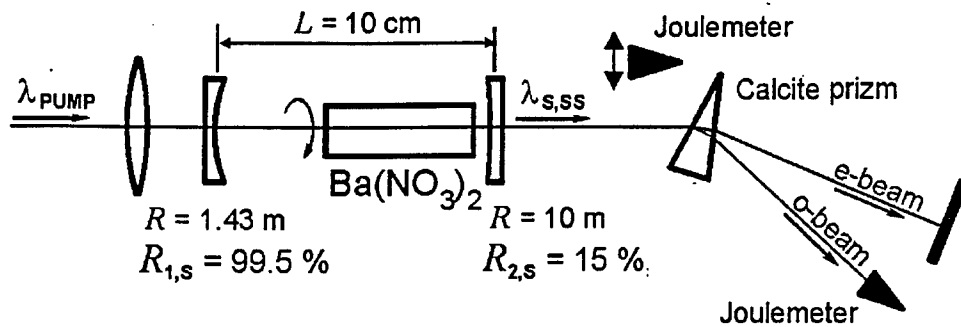
Fig. 4.10. Optical scheme for measuring influence of radiation depolarization
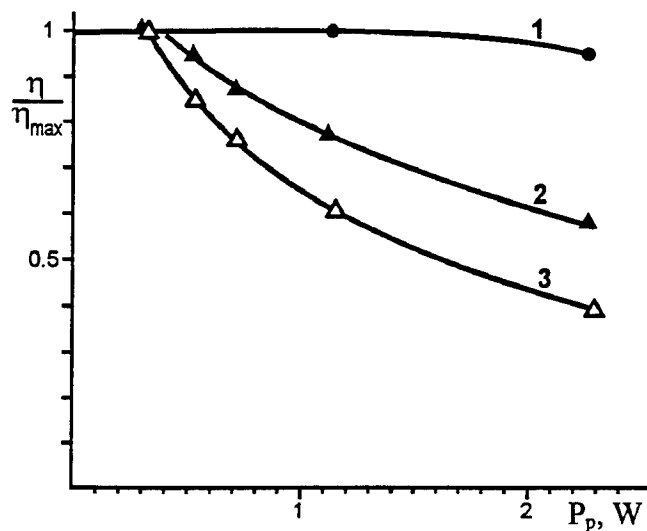on generation efficiency in the cavity.

Fig. 4.11. Dependence of relative generation efficiency in the cavity
vs. mean pump power.

1- pump radiation polarization vector is parallel to axis [100] .
2- polarization vector is directed under angle 45° to an axis [100].
3- separately for Stokes radiation with polarization vector parallel to pump vector.

crystallographic axis [100], the rate of depolarization was negligible, and for the
orientation with angle 45° between them the depolarization has reached its maximal
value, resulting in reduce of the conversion efficiency. The minor depletion of the
efficiency, observed for the optimal orientation, results of the thermal lensing (the
focal length of the thermal length at the maximal repetition rate is compatible with the
focal length of the cavity's spherical mirror). So one can say that there was observed
the correlation of the theoretical predictions and of the experimental results
concerning the possibility to eliminate for the depolarization.

Let us conclude this section by the evaluation of the gain in the KGW crystal. It can
be done on the base of the of the generation threshold values, measured for the KGW

100

η, %

50

Fig. 4.12 Dependence of the
conversion efficiency for
generation in the cavity
vs. pump pulse energy.

1-R_{2S}=15%, Ba(NO₃)₂;
2-R_{2S}=30% Ba(NO₃)₂;
3- R_{2S}=50%, R_{1S}=90%, KGW.

50   100 E_n, mJ
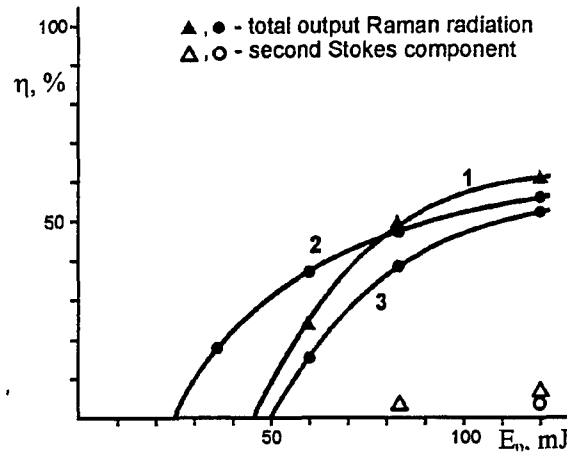
crystals; mounted in the same cavity which was used for the thermal lens measurements. In the Fig.4.12 are shown the dependencies of the generation efficiency vs. the pump energy; the value of the threshold was determined from their extrapolation till crossing the abscissa axis. The crystal KGW was mounted in the orientation, where the oscillation with the shift of 770 cm^{-1} is active. The end surfaces of the KGW crystal were covered by untireflection coating for pump and Stokes radiation. Length of the crystal was 55mm.The gain value was determined with the use of the formula for the generation threshold (g I- (ln (1/R_1R_2))/2 l)υτ =30; here τ is the pulse duration, υ = c/nξ, ξ = (L+ l (n-1))/nl – the coefficient, accounting for the incomplete fill of the cavity by the crystal, L is the cavity length and l is the crystal length. This formula accounts for the presence of the over-threshold intensity surplus, which is necessary to overcome the energy threshold [10]. With the use of this formula and the relation of measured threshold energies for KGW and Ba(NO)₂ at first was determined the relation of gain values in these crystals. They are equal 2.2 and 1.7 accordingly for reflectivities of output mirrors 30 and 15 % for generation in Ba(NO)₂. For a value of the gain in KGW it is accepted medial between two values obtained with the use gain in Ba(NO)₂ (from section 2) and this two relations. It is equal 3.7×10⁻³cm / MW. Note that at the wavelength of 1.06 μm the gain in KGW was twice lower than that in the barium nitrate. According to the results of our measurements the growth of the wavelength did not result in the significant variation of this ratio.

Let us in conclusion enumerate the main results of this Section:
1. We have shown that the use of the generation in the cavity can provide the 55% - conversion efficiency of the single-mode pumping beam to the single-mode beam of the first Stokes component.
2. In the case of the multi-mode pumping the Stokes beam brightness was improved in approximately six times in comparison with the pumping beam.
3. We have measured the thermal constant, which determines the thermal lens in the barium nitrate crystal.
4. We have confirmed in the experiment for the wavelength 1.32 μm the possibility to eliminate the influence of the depolarization onto the efficiency for the optimal orientation of the barium nitrate crystal.

20

5. Amplification of the diffraction-limited beams in SRS media, pumped by laser beam with a wide angular spectrum

5.1. Introduction

Yet in 70-es [11] it was shown that one can amplify the diffraction-limited beams, preserving their spatial structure, in the SRS-amplifier, pumped by the beam, whose divergence is in one or two orders of magnitude higher than that of the amplified beam. The possibility of such an amplification is explained by two different theoretic models, namely by the model of plain waves and by the model of the speckle-field.

In the model of plain waves [11,12] the possibility to preserve the angular divergence of the diffraction-limited beam while its amplification is explained by the dumping of the parametric generation of the non-axial Stokes components. Such a dumping takes place when the relationship

$$CR_1 = 2(\Gamma k_S / k_L^2 \theta_L^2)^2 \ll 1, \tag{5.1}$$

is valid. Here Γ is the local increment of SRS, k_S and k_L are the wave numbers of the Stokes wave and of the pumping wave in the SRS-active medium, and θ_L is the angular divergence of the pumping beam.

In the model of the speckle-field [2] this possibility to preserve the diffraction limited divergence of the amplified beam is explained by the averaging of the pumping field inhomogeneity. Efficient averaging is possible only for the sufficiently small-scaled speckle inhomogeneity of the pumping field. The criterion of the efficient averaging looks like:

$$CR_2 = \frac{16\Gamma^2}{k_L^2 \theta_L^3 \theta_D} \arctg\left(\frac{1}{4} L k_L \theta_L \theta_D\right) \ll 1. \tag{5.2}$$

Here L is the length of the SRS-active medium and θ_D is the diffraction limited divergence angle.

One can see from the relationships (5.1) and (5.2) that the criteria reveal their qualitative nature. These two formulae contain different parameters and reveal the different law of dependence upon the pump divergence angle θ_L. Thus their use for the evaluation of the pumping beam divergence, for which it is possible to realize the distortions-lacking amplification of the Stokes beam, results in quite different values. One can see this from the Fig.5.1, presenting the dependencies of CR_1 and CR_2 vs.
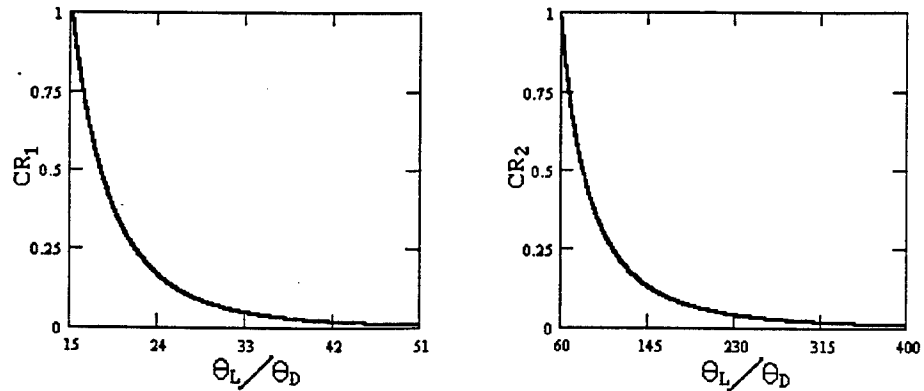

Fig.5.1. Dependence of the criteria figures of merit vs. angular divergence

θ_L/θ_D. The calculations were carried out for $Lk_L\theta_D^2/4 = 9 \times 10^{-3}$ and $2\left(\Gamma/k_L\theta_D^2\right)^2 = 5.5 \times 10^4$.

So one can see that the requirements to the angular divergence of the pump are quite unclear. That is why it is interesting to carry out the numerical simulation of the diffraction limited beam amplification in the field of the pump with the wide angular spectrum and thus to determine the values of the criteria (5.1) and (5.2) which correspond to the amplification of the Stokes wave without the significant distortion of its wavefront. Especially interesting are such amplification regimes when the criteria (5.1) and (5.2) are frustrated, but the angular divergence of the pump is still high. Such a situation is usual for the pumping by the solid-state laser emission.

5.2. The model of SRS amplifier: basic equations and relationships

The numerical simulation of amplification of the Stokes wave with the primarily diffraction limited quality in the field of the wide angular spectrum laser beam was carried out in the stationary two dimensional approximation. It was done on the base of the following set of equations, which is widely used in the theory of SRS:

$$\left[\frac{\partial}{\partial z} - \frac{i}{2k_s}\frac{\partial^2}{\partial x^2}\right]E_s = \frac{1}{2}g|E_L|^2 E_s,$$

$$\left[\frac{\partial}{\partial z} - \frac{i}{2k_L}\frac{\partial^2}{\partial x^2}\right]E_L = -\frac{1}{2}g\frac{k_L}{k_s}|E_s|^2 E_L, \qquad (5.3)$$

$$E_s|_{z=0} = E_{SO}, \qquad E_L|_{z=0} = E_{LO},$$

Here E_L, E_S are the electric tensions of the pumping and Stokes waves, g is the gain of SRS, x and z are the transverse and the longitudinal coordinates.

It is well known [11] that the set of equations (5.3) provides the quite adequate description of the Stokes wave amplification for the wide range of the SRS-active media parameters when the duration of the relaxation process is negligibly short. For the condensed media this duration is in the picosecond range [13]. That is why the stationary approximation is applicable for pulse with the nanosecond duration.

One can generalize the calculations by the use of the dimension-less parameters:

$$\frac{z}{L} \Rightarrow z, \quad \frac{x}{x_o} \Rightarrow x. \quad \frac{E_s}{\sqrt{I_o}} \Rightarrow E_s, \quad \frac{E_L}{\sqrt{I_o}} \Rightarrow E_L,$$

Here L and $2x_o$ are the length and the width of the SRS-active medium. I_0 is the so-called normal intensity fluency. Thus the set of equations (5.3) is transformed into:

$$\left[\frac{\partial}{\partial z} - \frac{i}{4C_L}\frac{k_L}{k_s}\frac{\partial^2}{\partial x^2}\right]E_s = \frac{1}{2}G|E_L|^2 E_s,$$

$$\left[\frac{\partial}{\partial z} - \frac{i}{4C_L}\frac{\partial^2}{\partial x^2}\right]E_L = -\frac{1}{2}G\frac{k_L}{k_s}|E_s|^2 E_L, \qquad (5.4)$$

Here $G = gLI_0$, $C_L = k_L x_0^2/2L$ is the parameter, which characterizes the geometry of the amplifier (it is some analog of the Fresnel number). One can use various methods for establishment of the relationship between the dimension values of the Stokes and pumping beam intensities at the amplifier input, on the one hand, and the value of the normal intensity I_0, on the other hand. In the experiment it is most simple to measure the Stokes and pumping beam intensities, integrated across the beam section. Hence it is reasonable to use the following equations to establish the said relationship between the dimension and dimension-less values:

$$\int_{-1}^{1} |E_{LO}|^2 dx = 1, \quad \int_{-1}^{1} |E_{SO}|^2 dx = q, \qquad (5.5)$$

Here q is the coefficient, which determines the relationship between the Stokes beam power P_{SO} and the pumping beam power P_{LO} at the amplifier input $\left(q = P_{SO}/P_{LO}\right)$.

The goal of the calculations was to analyze the process of the SRS-amplification for the various configurations and positions of the pumping beam with respect to the Stokes beam. We have, in particular, analyzed the situation, when the the pumping wave is tilted with respect to the Stokes wave in some angle θ (with focusing of the pumping radiation and without; see Fig.5.2).
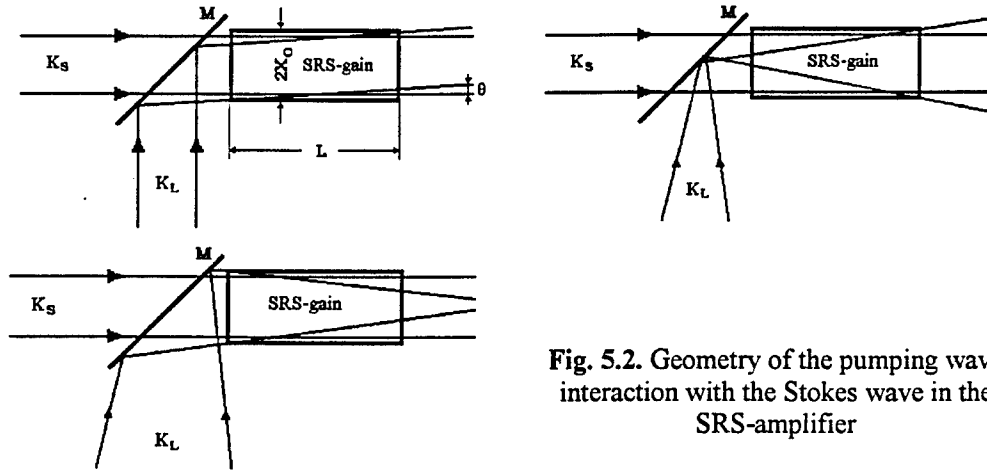
Fig. 5.2. Geometry of the pumping wave interaction with the Stokes wave in the SRS-amplifier

In the calculations the Stokes wave E_{SO} was described by the real hyper-Gauss function, and the pumping wave E_{LO} was described by the superposition of the finite number N_H of the Gauss-Hermit modes, whose random phases and amplitudes are distributed according to the definite law. Such a description of E_{SO} and E_{LO} is quite adequate to the experimental situation, because it describes the diffraction-limited beams and the beams with the wide angular spectrum, generated in the solid-state laser with the stable cavity [9]. Hence, E_{SO} and E_{LO} look like:

$$E_{SO} = \left[q \frac{x_O}{r_S} \frac{m2^{1/2m}}{\Gamma(1/2m)} \right]^{1/2} \exp\left[-\left(\frac{x_O}{r_S} x \right)^{2m} \right],$$

$$E_{LO} = \exp\left[i\left\{ C_R (x-h)^2 - k_L x_O \theta x \right\} \right] \sum_{n-0}^{N_H} a_n \exp(i\varphi_n) \Psi_n \left[\frac{x_O}{r_L}(x-h) \right],$$

(5.6)

Here $\Gamma(y)$ is the Gamma-function, m is the integer value, which describes the shape of the hyper-Gauss function, θ is the angle between the Stokes and the pumping beams, , $h = L\theta/2x_O$, $C_R = k_L x_O^2/2R$, R is the curvature radius of the wavefront, a_n are the real amplitudes, which are proportional to the function $\exp[-\gamma(n-n_m)^2]$, n_m is the number· of the mode with the largest amplitude, $\gamma > 0$ is the parameter, which determines the variation of the amplitudes a_n, φ_n are the random phases, which are uniformly distributed across the range $[0, 2\pi]$, r_S and r_L are the characteristic sizes (see further), and Ψ_n are the normal Gauss-Hermit modes, described by the formula:

$$\Psi_n\left(\frac{x_O}{r_L} x \right) = \left[\frac{2x_O^2}{\pi r_L^2} \right]^{1/4} (2^n n!)^{-1/2} H_n\left(\sqrt{2} \frac{x_O}{r_L} x \right) \exp\left[-\left(\frac{x_O}{r_L} x \right)^2 \right],$$

Here H_n are Hermit polynoms: $H_n(x) = 2xH_{n-1}(x) - 2(n-1)H_{n-2}(x)$, $H_o = 1$, $H_1 = 2x$.

One can see from the formula (5.6) that in the case, when the pumping beam is tilted with respect to the Stokes beam or when it is focused (θ, $1/R \neq 0$), the pumping field distribution contains the terms, which reveal strong oscillations. One can see that in the cases of practical interest the number of oscillations across the range $x \in [-1,1]$ can be as high as several hundreds. These oscillations to a large extent tantalize the numerical solution of the set of equations (5.4). That is why it is reasonable to describe the field $E_L(x,z)$ as a product of the slowly oscillating function $U_L(x.z)$ and of the fast oscillating function:

$$E_L(x,z) = U_L(x,z)\exp\left[iF_L(x,z) \right].$$

(5.7)

According to the estimations, one can replace the function $F_L(x,z)$ by some phase factor, which is one and the same for all the Gauss-Hermit modes. It is produced while the free-space propagation of the pumping beam E_{LO}. On the base of the Guigence-Fresnel principle and of the well-known relationships for the Hermit polynoms [14] one can outline the following relationship for the function $F_L(x,z)$:

$$F_L(x,z) = C_L\left[\alpha(x + 2hz - h)^2 - 4h(x + hz) \right],$$

(5.8)

Here $\alpha = \dfrac{z + C_R(zC_R + C_L)(r_L/x_O)^4}{z^2 + (zC_R + C_L)^2(r_L/x_O)^4}$.

With the help of the relationships (5.7) and (5.8) one can transform the set of equations (5.4) to:

$$\left[\frac{\partial}{\partial z} - \frac{i}{4C_L}\frac{k_L}{k_S}\frac{\partial^2}{\partial x^2}\right]E_S = \frac{1}{2}G|U_L|^2 E_S,$$

$$\left[\frac{\partial}{\partial z} - \{2h - \alpha(x + 2hz - h)\}\frac{\partial}{\partial x} - \frac{i}{4C_L}\frac{\partial^2}{\partial x^2}\right]U_L =$$

$$= -\left[\frac{1}{2}G\frac{k_L}{k_S}|E_S|^2 + \frac{\alpha}{2} - iC_L(\alpha^2 - \beta)(x + 2hz - h)^2\right]U_L,$$

(5.9)

Here $\quad \beta = \dfrac{1 + C_R^2(r_L/x_O)^4}{z^2 + (zC_R + C_L)^2(r_L/x_O)^4}$.

The characteristic size r_S, which determines the size of the zone, containing the main part of the Stokes wave field, and the characteristic size r_L, which determines the scale of the amplitude distribution inhomogeneity, were determined from the requirement of the small amplitude of the fields at $x = \pm 1$. The width of the zone of the SRS-active medium is to be limited by the finite range. Out of this range the intensities of the Stokes and of the pumping waves are to be negligible. From the corresponding estimations it is clear, that it will be provided if the relative values of the Stokes and of the pumping waves intensities were not more than 10^{-3} of the maximal value for $x = \pm 1$. The Table 5.1 summarizes the relationships for the determining of the characteristic sizes r_S and r_L, which were determined with the account for the above-said requirement and for the diffraction spreading out of the beams. The parameter $\rho > 1$ determines the size of the minimal region x_{min} ($x_{min} = 2x_o/\rho$); outside this region the amplitude of the wave field is not more than 10^{-3} of its maximal value. In the case of the beam focusing (see Fig.5.2) the parameter ρ describes the curvature radius of the wavefront R according to the following formulae:

$$C_R = -C_L + \sqrt{\rho^2 C_L^2 - x_O^4/r_L^4}, \qquad R > 0,$$

$$C_R = -C_L + \sqrt{C_L^2/\rho^2 - x_O^4/r_L^4}, \qquad R < 0$$

According to a rather simple analysis the range of values of the coefficient ρ, for which the minimal size of the zone of the pumping field concentration while its focusing x_{min} is laced in the plane $z = 0$ or $z = 1$, is limited. In particular, for $x_O^4/r_L^4 C_L^2 \ll 1$ the said values of the coefficient ρ are to fill into the interval:

$$1 + x_O^4/2r_L^4 C_L^2 < \rho < r_L^2 C_L/x_O^2 .$$

Table 5.1

x_o/r_s	$\rho\left[d_1 - \sqrt{d_1^2 - C_L^2}\right]^{1/2}$, $m = 1$, $d_1 = C_L^2/6\ln 10$		$\rho[3\ln 10]^{1/2m}$, $m > 1$, $C_L \gg 1$
C_R	0	>0	<0
x_o/r_L	$\left[d_2 - \sqrt{d_2^2 - C_L^2}\right]^{1/2}$	$\rho C_L/\sqrt{2d_2}$	$C_L/\sqrt{2d_2}$
N_H	0	>0	
d_2	$C_L^2(1 - h)^2/6\ln 10$	$\frac{1}{2}\left[C_L(1 - h)/(0,863\sqrt{N_H} + 2,087)\right]^2$	

In course of the solution of the system of equations (5.9) the range of the continuous variation of the argument x was replaced by the discrete set of the points with the coordinate:

$$x_n = -1 + (n-1)\delta, \quad n = 1,2,.....N, \quad \delta = 2/(N-1).$$

Correspondingly, the functions E_S and U_L were discretized on the variable x according to the relationships $E_{Sn} = E_S(x_n,z)$, $U_{Ln} = U_L(x_n,z)$, and their derivatives on x were replaced by the differential equations according to the well-known formulae [15]:

$$\frac{\partial W(x_n,z)}{\partial x} = \frac{1}{2\delta}\left(W_{n+1} - W_{n-1}\right),$$

$$\frac{\partial^2 W(x_n,z)}{\partial x^2} = \frac{1}{\delta^2}\left(W_{n+1} - 2W_n + W_{n-1}\right), \qquad (5.10)$$

$$n = 2,3,......N-1.$$

According to the results of investigations, for $x = \pm 1$, it is reasonable to use for the derivatives on x not the relationships (5.10), but the more complicated differential relationships:

$$\frac{\partial W(-1,z)}{\partial x} = -\frac{1}{6\delta}\left(10W_1 - 15W_2 + 6W_3 - W_4\right),$$

$$\frac{\partial W(1,z)}{\partial x} = \frac{1}{6\delta}\left(10W_N - 15W_{N-1} + 6W_{N-2} - W_{N-3}\right),$$

$$\frac{\partial^2 W(-1,z)}{\partial x^2} = \frac{1}{6\delta^2}\left(11W_1 - 27W_2 + 21W_3 - 5W_4\right),$$

$$\frac{\partial^2 W(1,z)}{\partial x^2} = \frac{1}{6\delta^2}\left(11W_N - 27W_{N-1} + 21W_{N-2} - 5W_{N-3}\right).$$

As a result, the system of the equations in the partial derivatives (5.9) transforms into the system of the usual differential equations. Accounting for the complexity of the functions E_S and U_L, this set consists of 4N equations. This system was solved with the use of the standard codes from the Fortran-77 library. The value of N was chosen to be N=226, which is determined by the available software. According to the results of test solutions, such a quantity is sufficient to describe without significant distortions the beams, containing up to 30..50 modes for $\rho \le (1,5-2)$ and for $h \le (0,1-0,2)$.

5.3. Results of calculations and discussion

The goal of the calculations was to determine the influence of the pumping wave field structure onto the spatial structure of the Stokes wave, and, in particular, onto its angular divergence and direction. With this purpose we have varied across the wide range the amplitude and the phase distribution of the pumping wave at the input of the amplifier, of the SRS gain, and of the relationship between the intensities of the Stokes and the pumping waves for various geometry of their interaction in the SRS-active medium. Our situations differs from that in the paper [16]. In the said paper there was numerically simulated the experiment with the XeCl eximer laser radiation and its SRS in hydrogen. We have simulated the experiment with the solid-state laser radiation and its SRS in the solid-state medium. Usually the angular divergence of

such a laser beam, used for the pumping purposes, equals to several dozens of the diffraction limits. That is why it was very interesting to investigate the dependence of the spatial distribution of the amplified Stokes beam upon the pumping beam quality without application of any special means of the forced control over the spatial coherence of this radiation (produced, for instance, by the aberrant).

Our studies have revealed the following main features:

- The most efficient approach to the Stokes beam angular distribution improvement is tilt of the pumping beam. If the angular divergence of the pumping beam θ_{LO} (θ_{LO} is the angle, containing 80% of pumping beam power at the amplifier input) equals several dozen diffraction limits, already for $\theta \approx (1-3)\theta_{LO}$ the angular divergence of the amplified Stokes beam is nearly diffraction limited, and its intensity distribution is rather smooth. The reduce of the pumping beam divergence is accompanied by the growth of the ratio θ/θ_{LO} for which one observes the significant reduce of the Stokes beam divergence. We are to note, however, that for the pumping beam divergence of several diffraction limits the aggravation of the Stokes beam divergence is not strong, while the improvement of the Stokes beam distribution, caused by the pumping beam tilt, is small.
- In the case of the collinear propagation of the Stokes and pumping beam through the amplifier and of the angular divergence of the pumping beam of several dozen diffraction limits, only some 50..60% of the amplified Stokes radiation fills into the angle of $(1-2)\theta_{SO}$ (here θ_{SO} is the angle, containing 80% of the Stokes beam power at the amplifier input). All other power is emitted to the wide wings. Further enlargement of the pump divergence up to 100..120 diffraction limits results in the reduce of the power, emitted to these wings.
- Seemingly, the criterion CR_1 is valid only for the case of the pumping beam tilt with respect to the Stokes beam. In this case one has to replace in the formula (5.1) the angle θ_L by the angle θ (however, this situation corresponds to the primary sense of the said criterion [12]).
- The criterion CR_2, seemingly, becomes valid for the very large (exceeding one hundred of diffraction limits) angular divergence of the pumping beam. For the smaller divergence of the pumping beam the value of this criterion does not correlate with the variation of the Stokes beam divergence.

Said features are illustrated by the following Figures. In the Fig.5.3 is shown for an example four variants of the primary distributions of the pumping beam intensity in the transverse direction and of the corresponding angular divergencies. In the first and in the second variants the pumping beam consisted of odd Gauss-Hermit modes ($N_H = 29$). In the second variant the beam was also focused (the value of the parameter $\rho = 1,2$). In the variants 3 and 4 the pumping beam consisted of both odd and even modes ($N_H = 50$ и 8). The angular distributions are presented as the functions of the current angle θ_R ratio to the angle θ_{DG}, which contains 80% of the diffraction-limited Gauss beam. Its amplitude at $x = \pm 1$ equals 10^{-3} of the maximal value. One can see in the same Figure the distributions of the Stokes beam intensity, described by the hyper-Gauss function at $m = 1$ and 5.
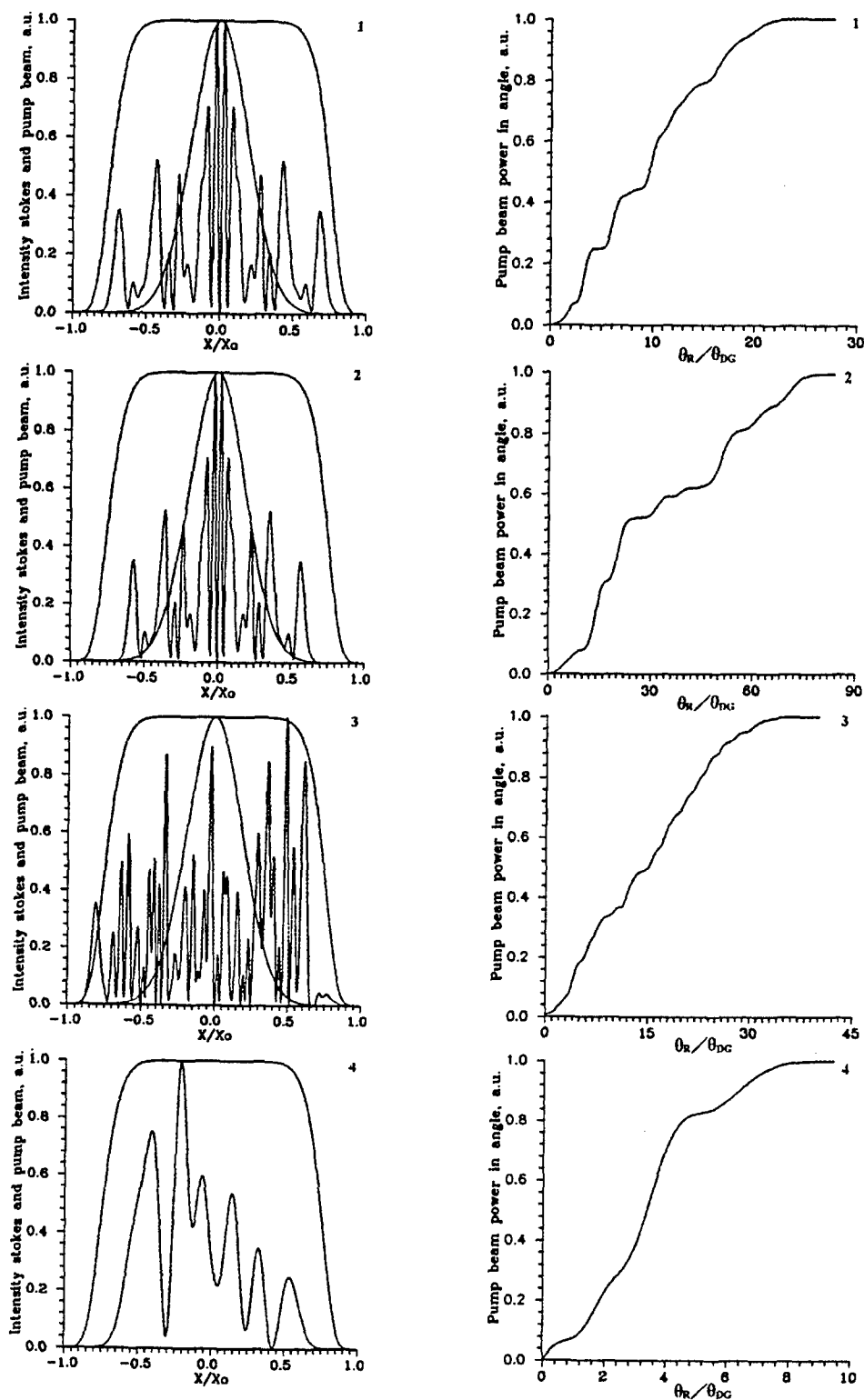
Fig. 5.3. Primary intensities of the Stokes beam and of the pumping beam in the transverse section of the amplifier and the angular distribution of the pumping beam power: θ_{LO}/θ_{DG} = 15.43 (1), 54.35 (2), 22.64 (3) and 4.55 (4).

28

In the Fig.5.4 are shown the results of studying of the dependence of the amplified Stokes beam divergence θ_S (θ_S is the angle, containing 80% of the power of the amplified Stokes beam) vs. the angle θ. The curves 1, 2 and 4 in the Fig.5.4 correspond to the variant 1, the curve 3 corresponds to the variant 2 (R>0, the diverging pumping beam), the curve 5 - to the variant 3 and the curve 6 - to the variant 4 of the primary distributions of the pumping beam field (see Fig.5.3). Other conventions are described in the caption for the Fig.5.4. The calculations were carried out for C_L = 1000, q = 0.01, k_L/k_S = 1.1 and variation of h from 0 to 0.1. The criterion CR_1 was calculated according to the formula (5.1), where the angle θ_L was replaced by the angle θ, and the local SRS increment Γ was determined from the gain G according to the relationship Γ = G/L. In the Figures 5.5-5.10 are shown the distributions of the intensity, phase and angular distributions of the amplified Stokes beam for h = 0 and 0.1, corresponding to the curves 1-6.
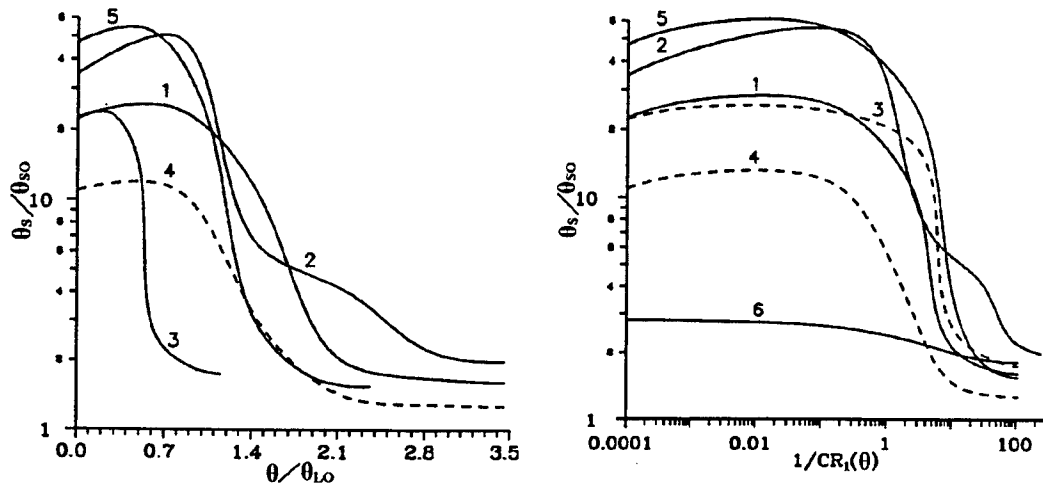

Fig. 5.4. Variation of the angular divergence of the amplified Stokes beam
with the pumping beam tilting:
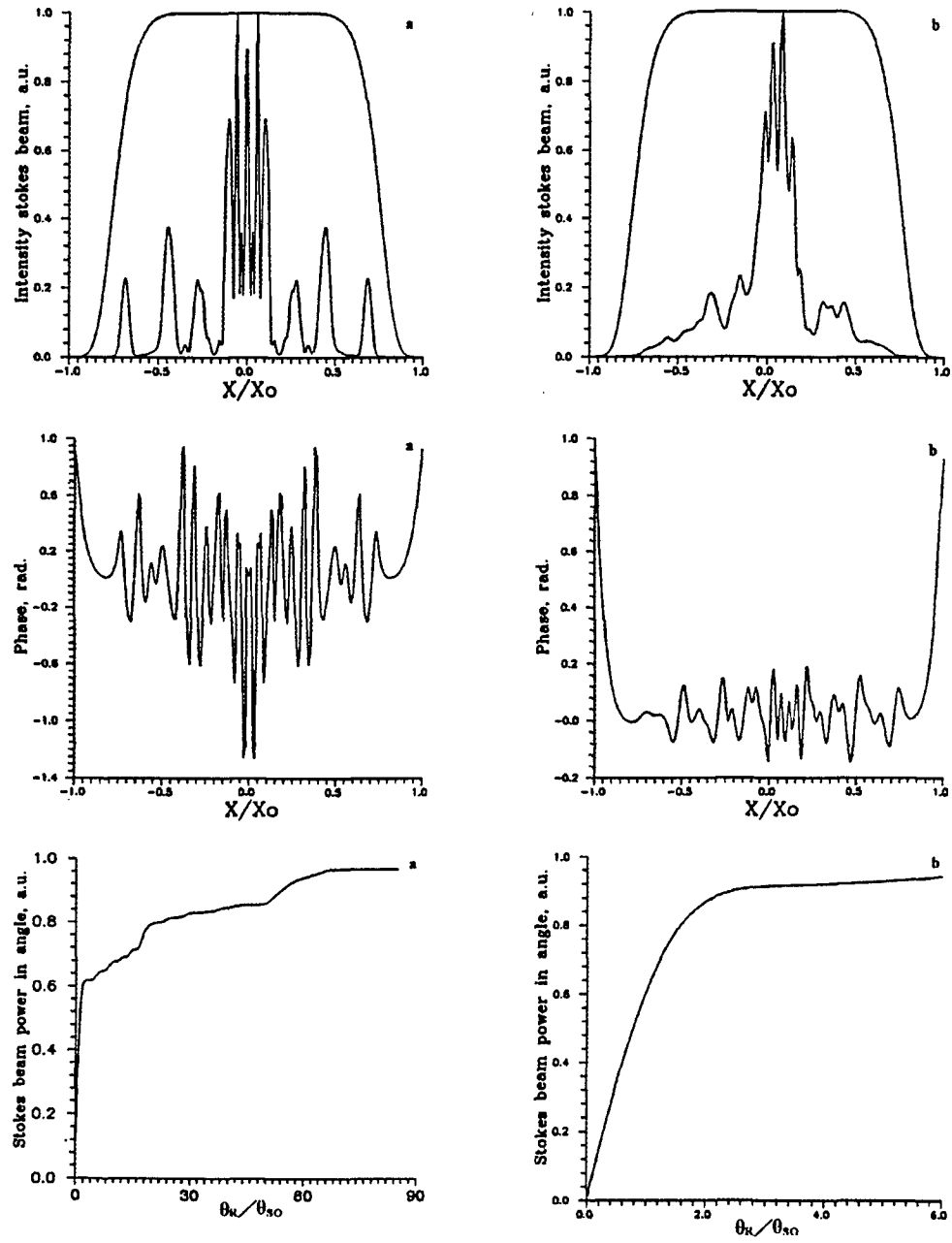G = 4 (2) and 6 (1, 3, 4, 5, 6), m = 1 (4) and 5 (1, 2, 3, 5, 6).

Fig.5.5. Distributions of the intensity, phase and angular distribution of the amplified
Stokes beam, corresponding to the curve 1 of Fig.5.4 for $\theta/\theta_{LO} = 0$ (a) and 3.46 (b).
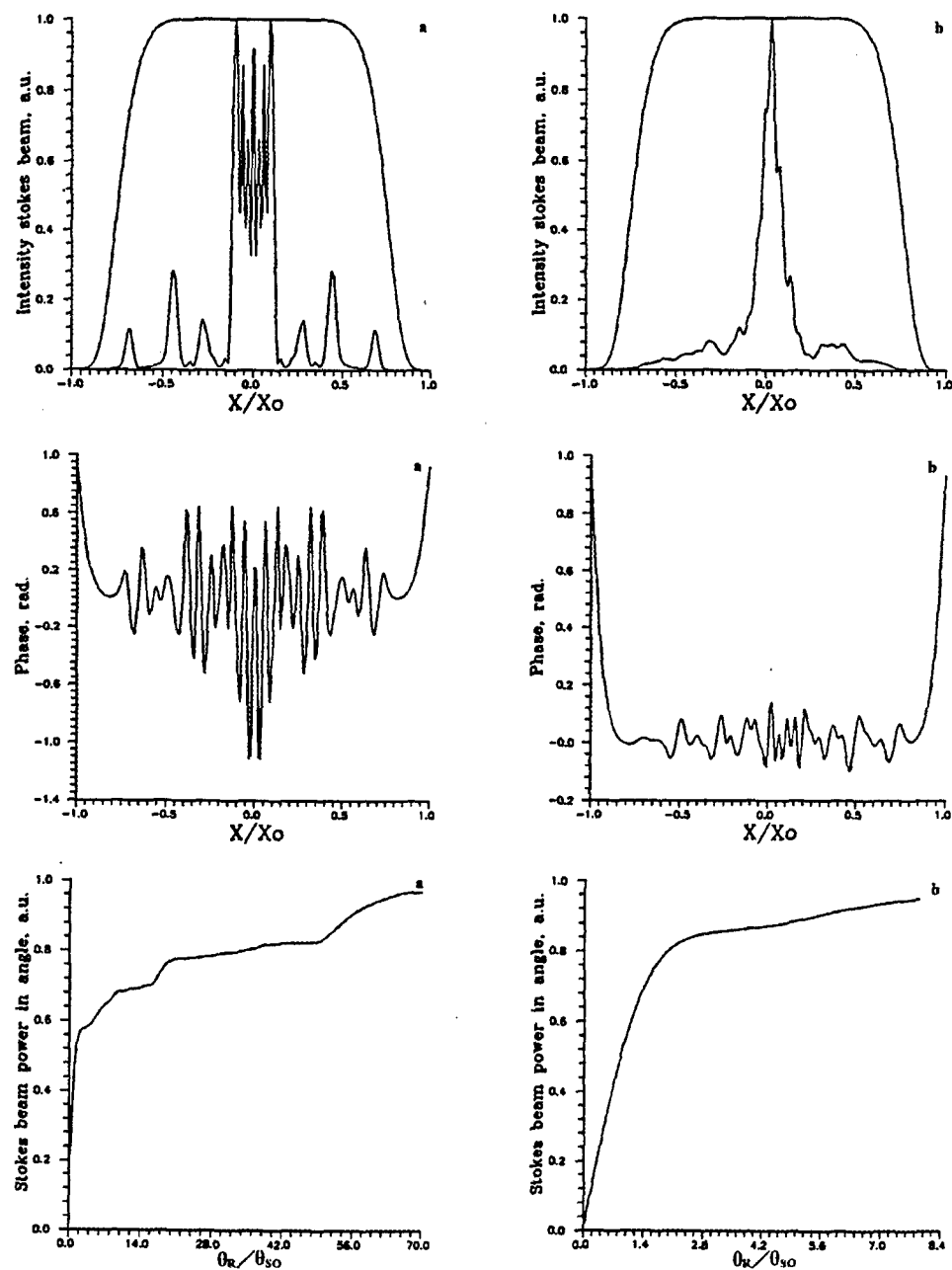
Fig.5.6. Distributions of the intensity, phase and angular distribution of the amplified Stokes beam, corresponding to the curve 2 of Fig.5.4 for $\theta/\theta_{LO} = 0$ (a) and 3.46 (b).

Fig. 5.7. Distributions of the intensity, phase and angular distribution of the amplified Stokes beam, corresponding to the curve 3 of Fig.5.4 for $\theta/\theta_{LO} = 0$ (a) and 1.15 (b).

Fig. 5.8. Distributions of the intensity, phase and angular distribution of the amplified Stokes beam, corresponding to the curve 4 of Fig.5.4 for $\theta/\theta_{LO} = 0$ (a) and 3.46 (b).
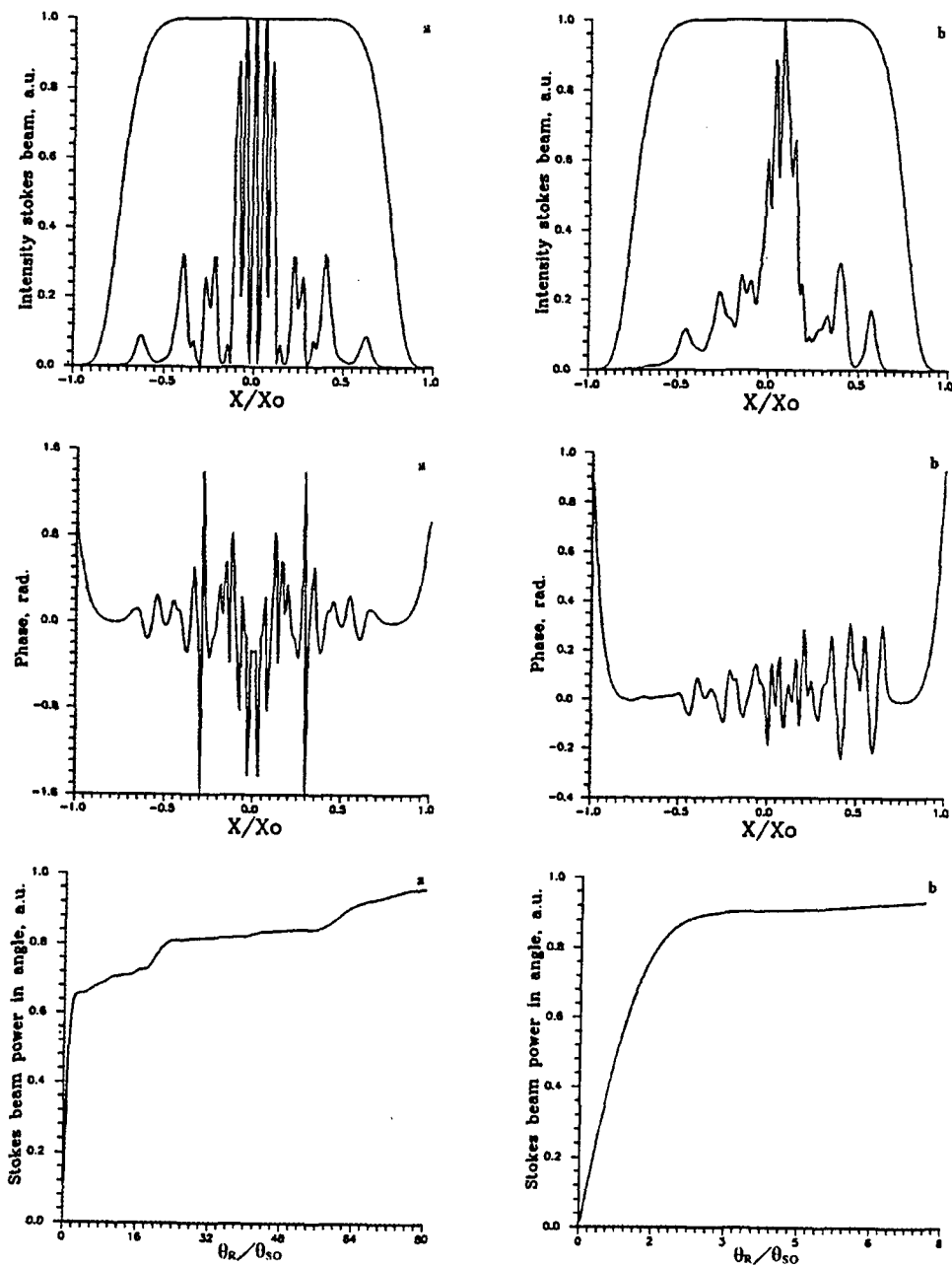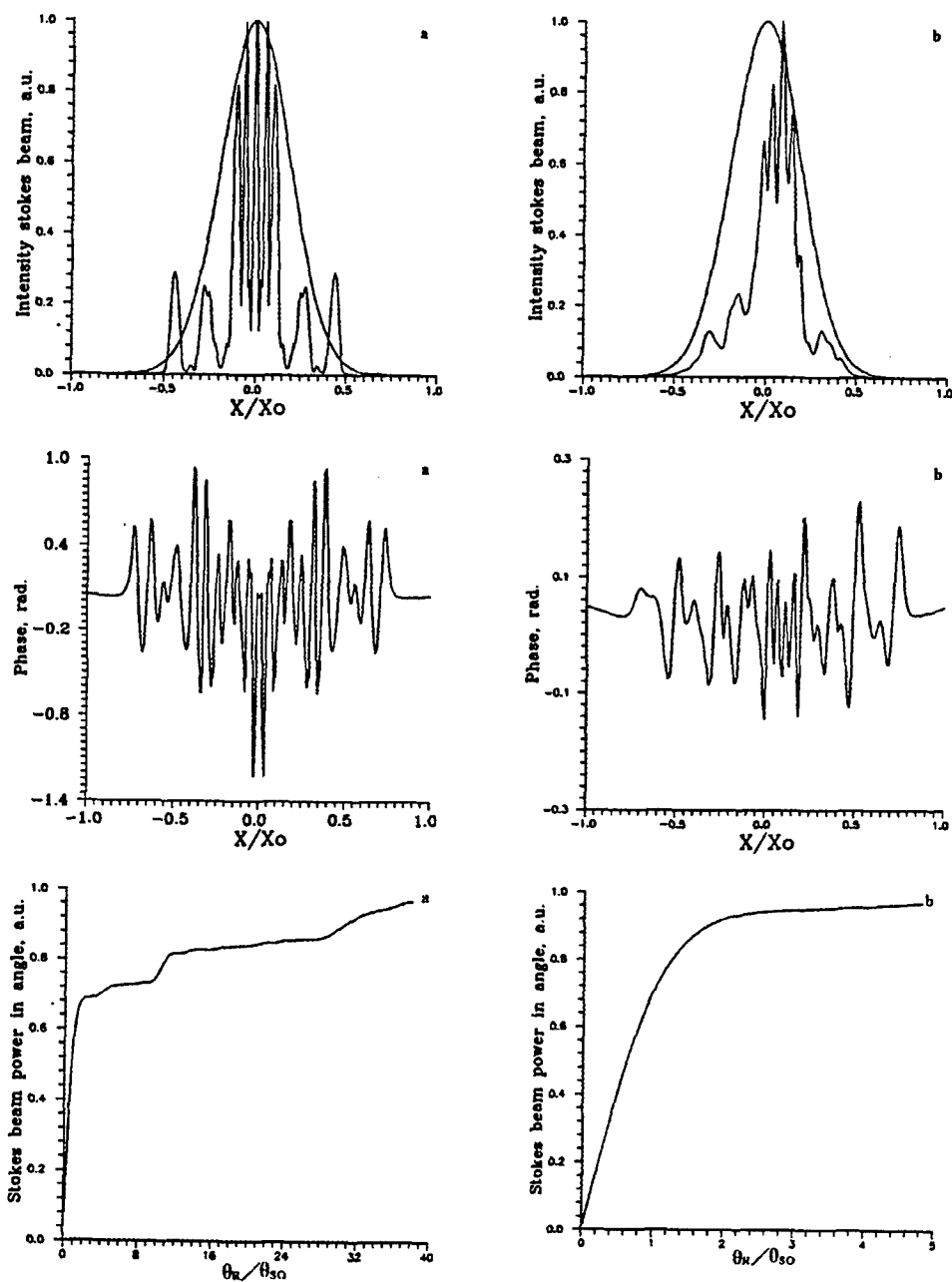
Fig. 5.9. Distributions of the intensity, phase and angular distribution of the amplified Stokes beam, corresponding to the curve 5 of Fig.5.4 for $\theta/\theta_{LO} = 0$ (a) and 2.36 (b).

Fig. 5.10. Distributions of the intensity, phase and angular distribution of the amplified Stokes beam, corresponding to the curve 6 of Fig.5.4 for $\theta/\theta_{LO} = 0$ (a) and 11.74 (b).
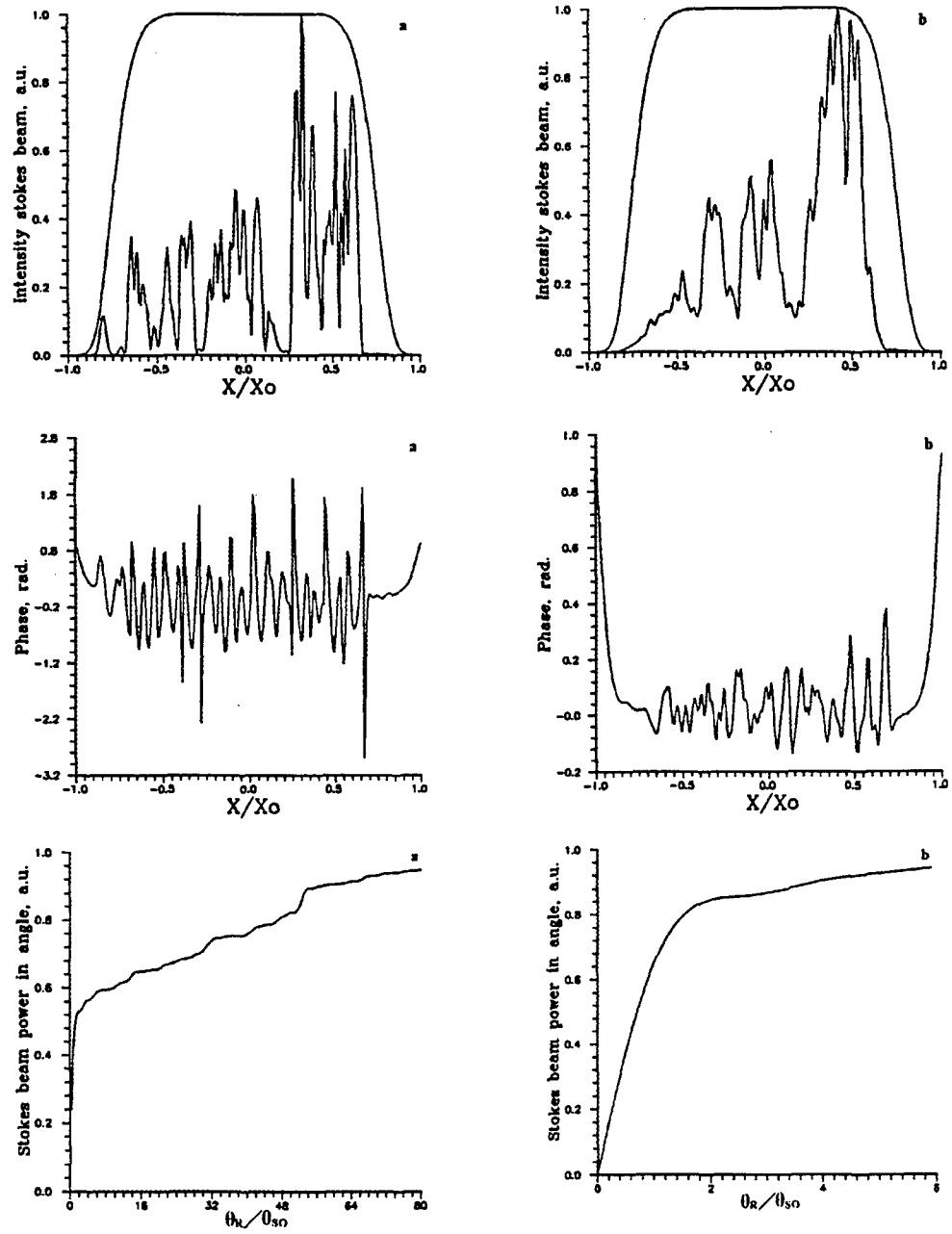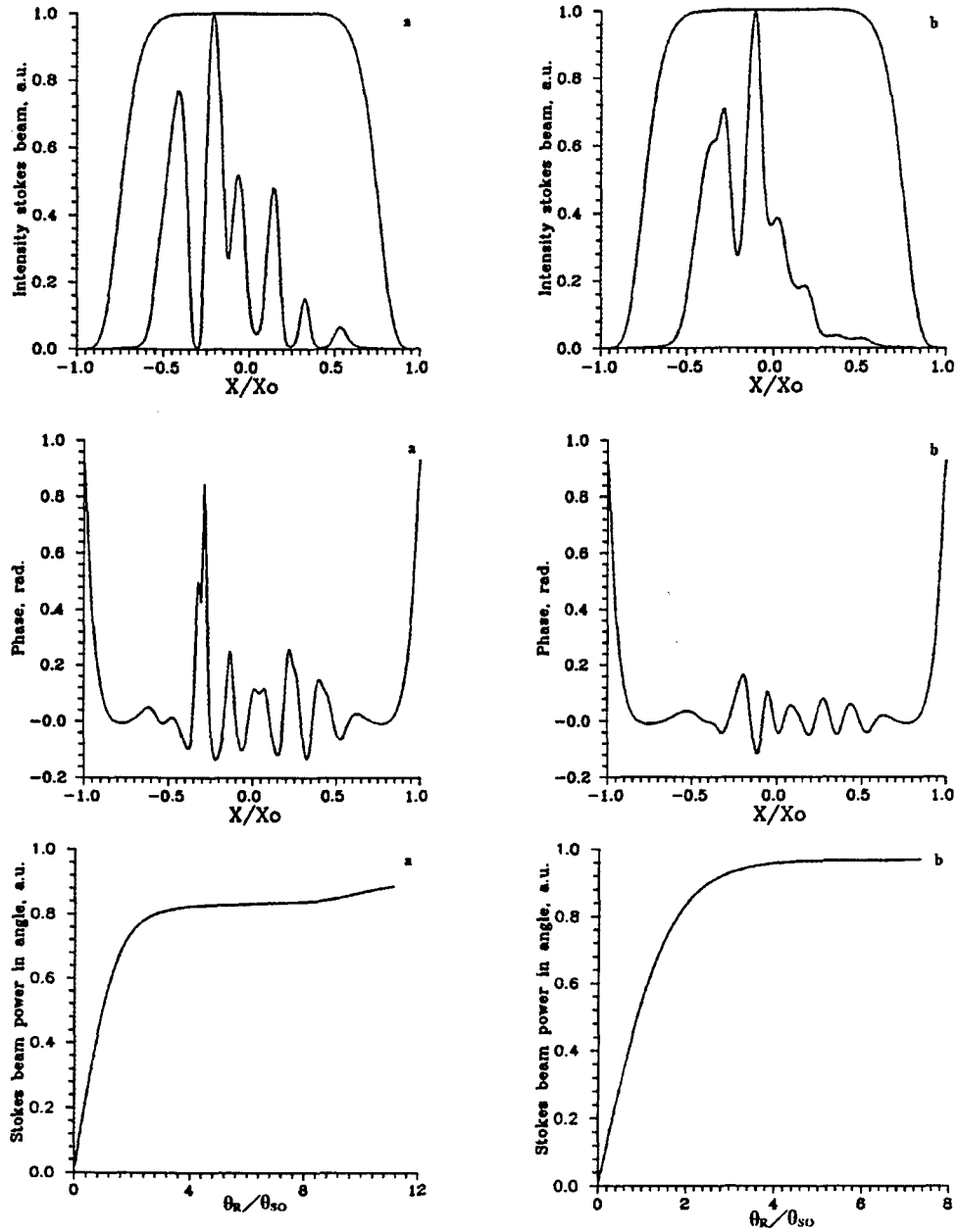
The presented data obviously evidence that the amplified Stokes beam spatial structure varies in a similar way for a wide range of the amplifier and pumping beam parameters. One can see from the given curves that when $\theta = 0$ even for the pumping beam divergence of several dozens of diffraction limits 50-60% of the Stokes radiation power at the amplifier output P_S contains in 1.5-3 diffraction limited angles (see Fig.5.11). Pumping beam tilt results first of all in dumping of the wings in the angular distribution of the Stokes radiation. Such an evolution of the Stokes beam divergence quite corresponds to the theory of the parametric mechanism of generation

35

of the Stokes radiation with the wide angular spectrum [12]. For the higher divergence of the pumping beam, equal to $(10\text{-}20)\theta_{DG}$, the divergence of the amplified Stokes beam is close to the diffraction limit already for $\theta \approx (1\text{-}3)\theta_{LO}$. However, in this case the criteria CR_1 (with the angle θ_{LO}) and CR_2 are not fulfilled. Worth mentioning, that for the variation of the angle θ in the said limits the efficiency of the pumping use (it was determined according to the formula $G_{ex} = q(P_S/P_{SO} - 1)$) has varied within the range of 15..30% of its average value (see Fig.5.12).

Fig. 5.11. The fragment of the angular distribution of the amplified Stokes beam for $\theta=0$,corresponding to the curve 5 of the Fig.5.4.
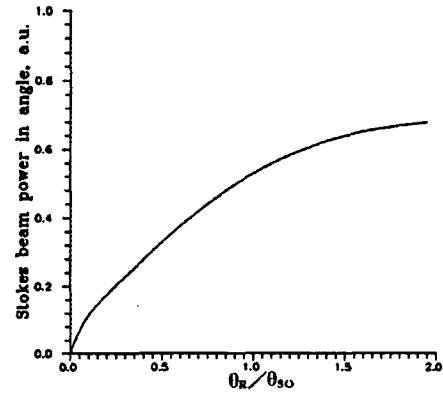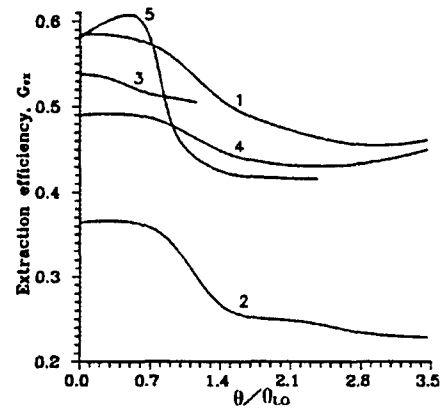
Fig. 5.12. Dependence of the coefficient of the efficiency of the pumping radiation use G_{ex} vs. tilt of the pumping beam (the numbering of the curves corresponds to that in the Fig.5.4).

It is possible to make the criteria CR_1 and CR_2 sufficiently smaller than 1. It can be done by means of modification of the geometric size of the amplifier (parameter C_L) and by focusing the pumping radiation. We have made two series of calculations so as to reveal the influence of the said factors onto the Stokes beam spatial structure. In the first series the parameter C_L was varied at h = 0, ρ = 1 and C_R = 0. In the second series we have varied the parameter ρ for h = 0 and for C_L = const. Pumping radiation was focused both to the plane z = 0 and to the plane z = 1.

The curves in the Fig.5.13 illustrate the character of the Stokes radiation divergence variation with the variation of the parameter C_L. The calculations were carried out for variation of C_L from 135 to 1000 and for the primary pumping beam, corresponding to the variant 3 in the Fig.5.3. In the Fig.5.14 are shown the distributions of the Stokes beam intensity, phase and angular distribution for C_L = 135 and G =3.
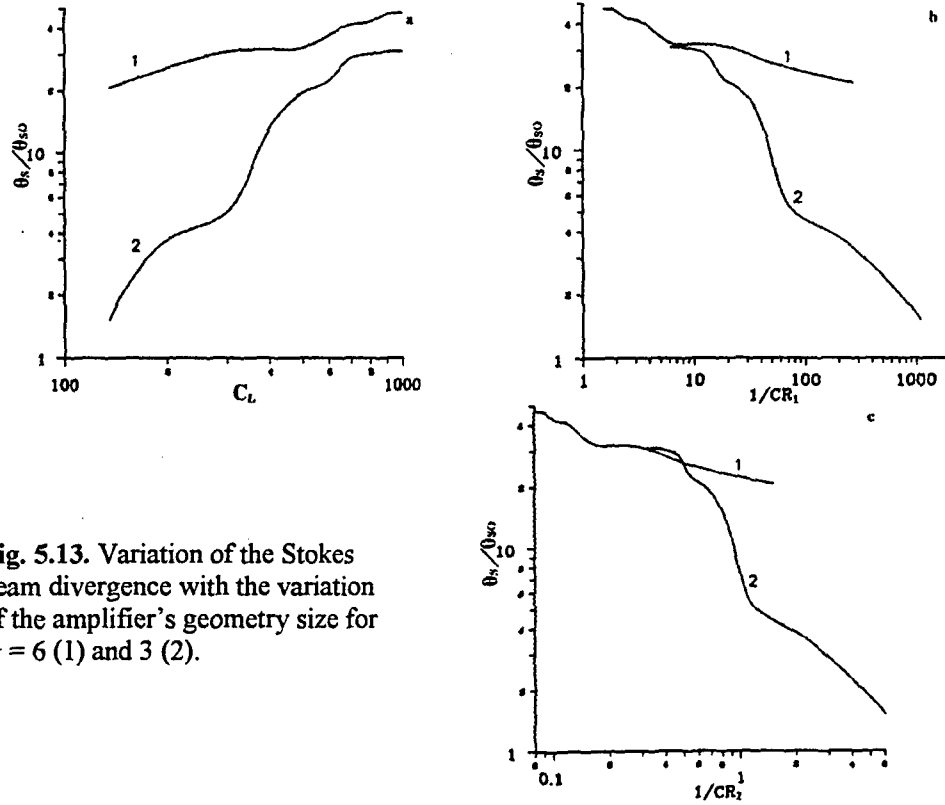
Fig. 5.13. Variation of the Stokes beam divergence with the variation of the amplifier's geometry size for G = 6 (1) and 3 (2).
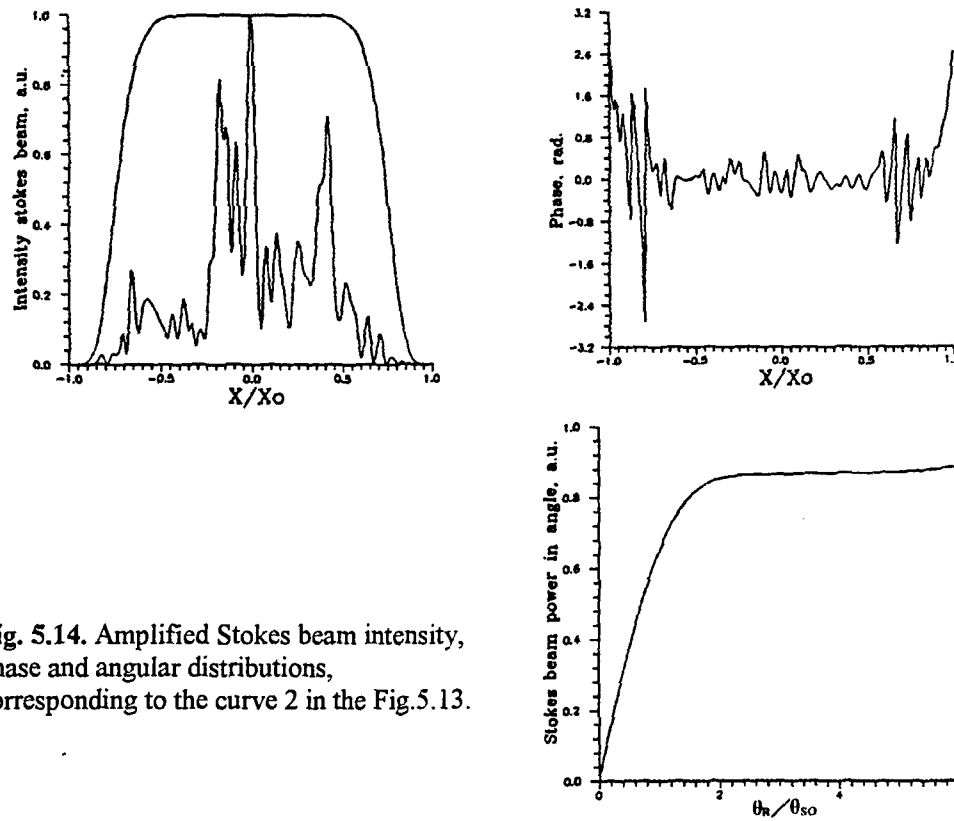

Fig. 5.14. Amplified Stokes beam intensity, phase and angular distributions, corresponding to the curve 2 in the Fig.5.13.

For the pumping beam focusing case the Stokes beam divergence reveals the same character of variation. Noteworthy, that the angular divergence of the converging beam is better than that of the diverging. Probably, this feature can be explained by the difference in the value of the local increment of SRS. Modification of the angular divergence of the Stokes beam with the pumping beam focusing is illustrated by the Fig.5.15. The calculations were carried out for C_L=1000 and for the pumping beam, corresponding to the variant 3 in the Fig.5.3. The curve 1 was calculated for the diverging pumping beam (R>0), while the curves 2-4 - for the converging beams (R<0). The curves 1-3 were calculated for the Stokes beam, described by the hyper-Gauss function for m=5, while the curve 4 corresponds to the Gauss beam. In the Fig.5.16 are shown the intensity, phase and angular distributions of the Stokes beam for ρ = 1.5 and G =3. The angular divergence of the pumping beam was equal $120\theta_{DG}$.
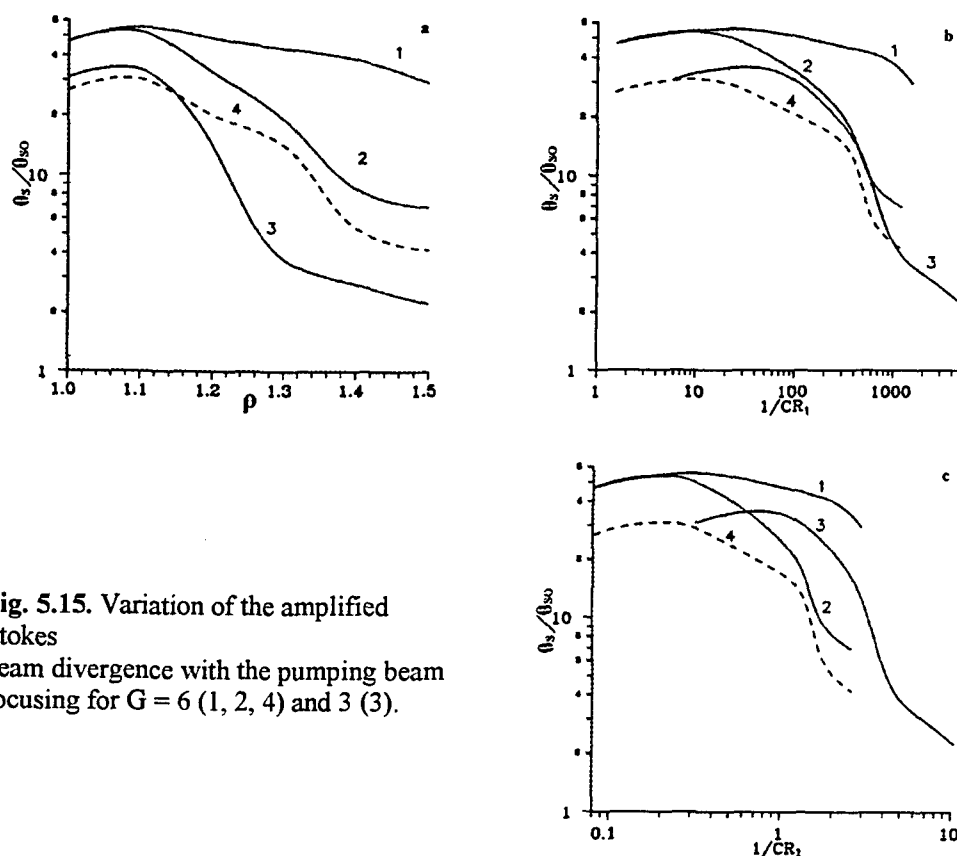

Fig. 5.15. Variation of the amplified Stokes
beam divergence with the pumping beam focusing for G = 6 (1, 2, 4) and 3 (3).
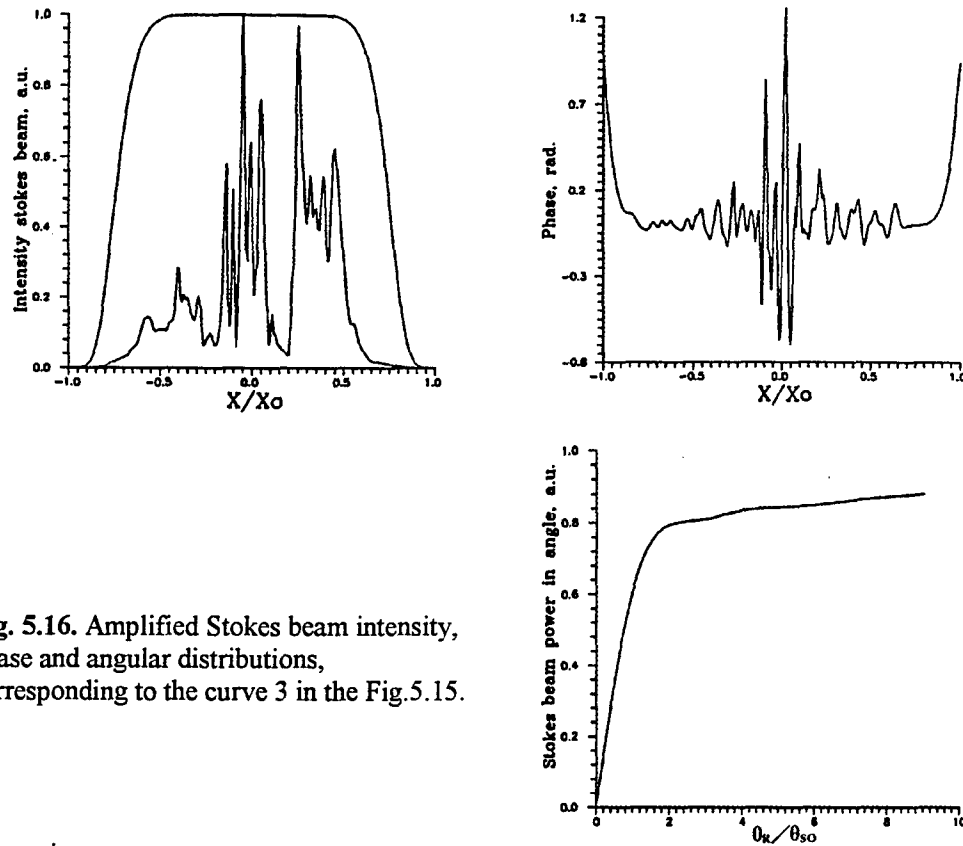
38

Fig. 5.16. Amplified Stokes beam intensity, phase and angular distributions, corresponding to the curve 3 in the Fig.5.15.

One can see from the Figures 13b,c and 15b,c that the angular divergence of the Stokes beam at the amplifier output reduces down to 1.5-2 diffraction limited angles if $CR_1<(10^{-4}-10^{-3})$ and $CR_2<(0.2-0.1)$. However, worth mentioning that the values of the criteria CR_1 and CR_2, for which the increase of the angular divergence of the beam via their amplification is insufficient, to a large extent depend on the geometry of the beams' interaction geometry. That is why it rather difficult to use these criteria in practice.

One can make the following conclusion of the presented results. Seemingly, the models of the plain waves and the model of the speckle-field, adequately describe the regime of the amplification in the field of the high divergent pumping wave of the Stokes wave without significant aggravation of its divergence when the divergence of the divergence of the pumping wave exceeds that of the Stokes wave in several hundred time.

39

Worth mentioning that the angular divergence of the Stokes wave strongly depends not only upon the considered factors, but also upon the ratio of its starting power to that of the pump. In the Fig.5.17 is shown for example the dependence of the Stokes beam divergence vs. the ratio $q=P_{SO}/P_{LO}$. The calculations were carried out for $C_L = 1000$, $h = 0$ and $C_R = 0$. The curves 1 and 2 correspond to the variant 1 in the Fig.5.3, and the curve 3 - to the variant 3 of the pump. The curves 1 and 3 were calculated for the case of the Stokes beam, described by the hyper-Gauss function for m=5, and the curve 2 corresponds to the Gauss beam. In the same Figure are shown the dependencies of the power gain G_S ($G_S = P_S/P_{SO}$) of the Stokes beam and of the efficiency of the pumping radiation use G_{ex} vs. the parameter q for its variation from 0.001 to 1. In the Fig.5.18 are shown the intensity, phase and angular distributions of the amplified Stokes beam, corresponding to the case of the minimal divergence.
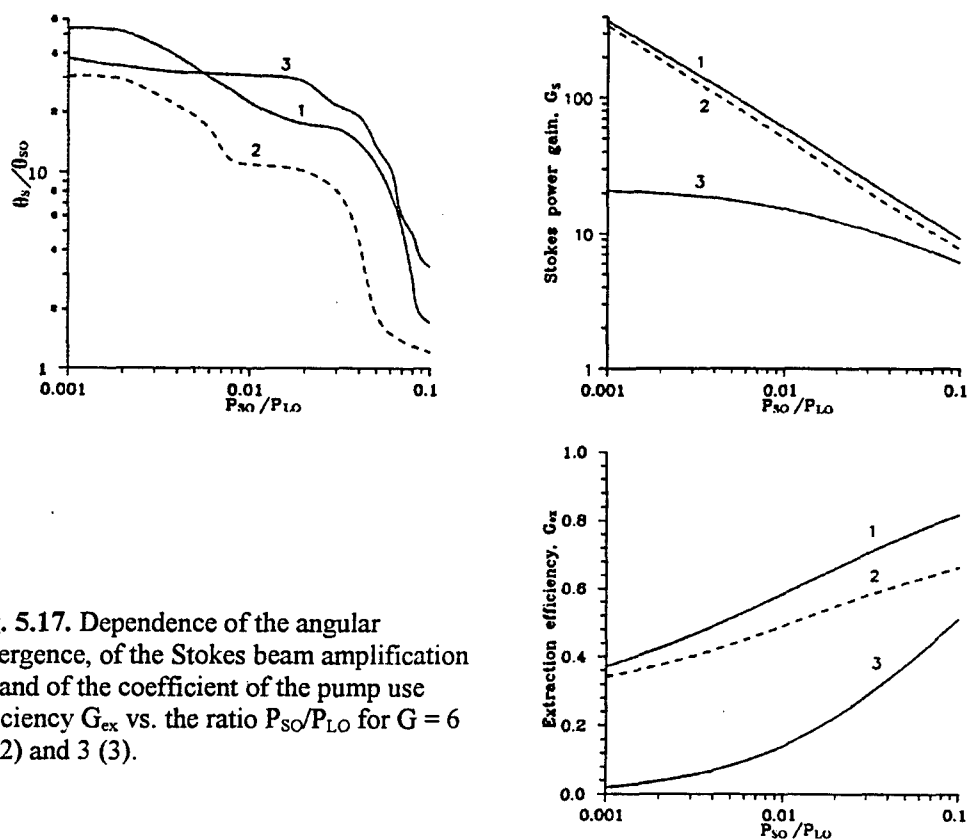

Fig. 5.17. Dependence of the angular divergence, of the Stokes beam amplification G_S and of the coefficient of the pump use efficiency G_{ex} vs. the ratio P_{SO}/P_{LO} for $G = 6$ (1, 2) and 3 (3).
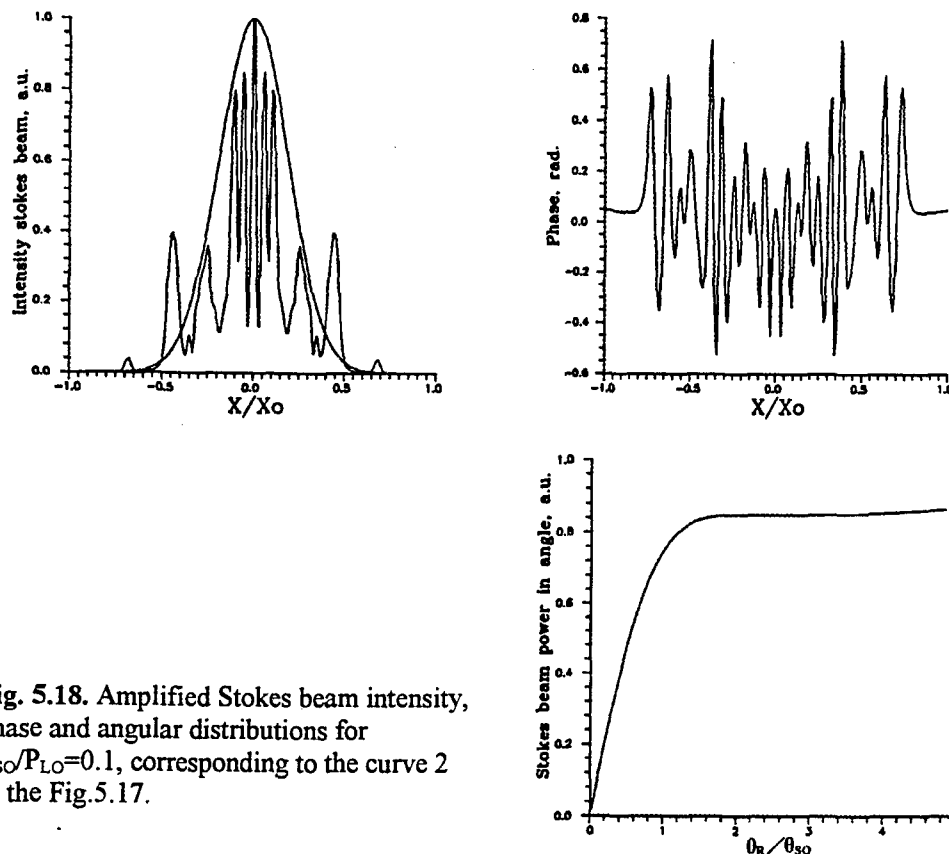
Fig. 5.18. Amplified Stokes beam intensity, phase and angular distributions for $P_{SO}/P_{LO}=0.1$, corresponding to the curve 2 in the Fig.5.17.

The given data indicates that under some specific conditions (say, the choice of the Stokes beam intensity profile) the amplification of the Stokes beam without significant deterioration of its angular divergence can be realized under the relatively low (some 10%) of the Stokes beam power to that of the pumping beam.

Conclusion

We can summarize as follows the main results of the numerical studies of the diffraction limited Stokes beams in the field of pumping by the beams with the wide angular spectrum:

- In the case, when the divergence of the pumping beam equals several dozen of the diffraction limited angles, the Stokes beam divergence can be efficiently improved by means of tilting the pumping beam. If this tilt is equal to some 1-3 angles of the pumping beam divergence, the amplified Stokes beam reveals nearly diffraction limited divergence, and its intensity distribution is efficiently smoothed.

- Seemingly, the models of the plain waves and of the speckle-field adequately describe the regime of amplification in the field of the pumping wave with the wide angular spectrum of the collinear Stokes wave without significant deterioration of its angular divergence in the case, when the angular divergence of the pump exceeds diffraction limit in several hundred times.

5.4. Experimental study of amplification

The experimental studies of the amplification were carried out with the use of the multi-mode laser, which was described in the Second Interim Report, and of the dual stage amplifier. (In this amplifier we have used the stages, which were created for the single-mode laser, where the rods were replaced by rods of a larger diameter). The half of the laser energy was sent by a beam splitter for the SRS-generator pumping, and the residual part was amplified in the laser amplifier and then used for the SRS amplifier pumping. SRS generation was realized with the use of the scheme of the pumping radiation into the volume of the zero mode with the consequent selection by the remote diaphragm, which was discussed in the Section 4. We have studied the amplification in collinear and in the quasi-collinear schemes. In the Fig.5.19 is shown the optical scheme, which was used for the amplifier studies. The maximum energy of the amplifier pumping was equal to either 108 mJ (divergence of 12 diffraction limits, produced by the cavity with the plain mirrors) or 80 mJ (divergence 22 diffraction limits, produced by the cavity, where one of the mirrors was concave). For both divergencies the diameter of the pumping beam in the crystal equaled 1.6 mm (the reason was approximately double difference of the beam diameters in the plane of the focusing lens). At the input of the SRS-amplifier crystal the energy of the Stokes beam with the near diffraction limited divergence was equal 9 mJ for lower pump divergence and 7 mJ for higher one. For the said parameters the maximal efficiency of the amplifier equaled 40% for lower pumping divergence. Similar to the calculations, the amplifier efficiency was determined as the ratio of the difference of the output and input Stokes signals to the energy of the wave, pumping the amplifier. No nonlinear absorption took place. Note that measured value was less than that obtained in the Section 5.1.3. The reason is that there was simulated the stationary process without account for the temporal overlap of the pulses. The pulse shapes of a output signal and passed without conversion pump are shown in the
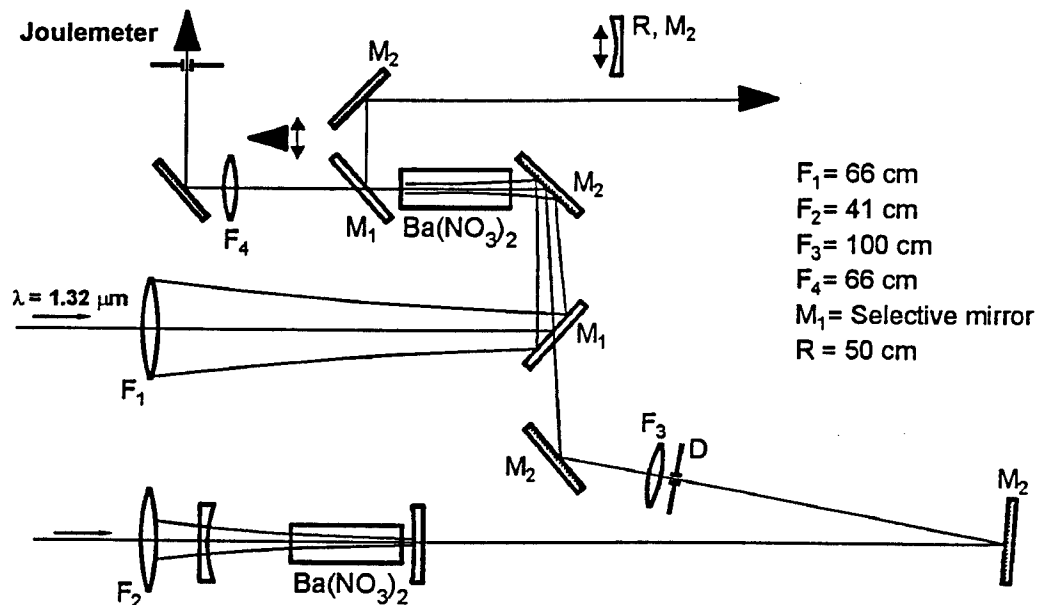

Fig. 5.19. Optical scheme for the amplifier studies.

F_1 = 66 cm
F_2 = 41 cm
F_3 = 100 cm
F_4 = 66 cm
M_1 = Selective mirror
R = 50 cm

λ = 1.32 μm

Fig.5.20. The higher efficiency was observed in the two-pass pumping scheme, which was realized by means of relay of the pumping beam back to the crystal with the use of the spherical mirror (see the Fig.5.19). In the Fig.5.21 is shown the dependence of the amplifier efficiency in the collinear amplification geometry vs. the pumping energy. As seen from figure it reveals the same character as all the previous dependencies of the efficiency vs. the pump, because the amplification from the spontaneous noise measured in previous sections the similar saturated process.
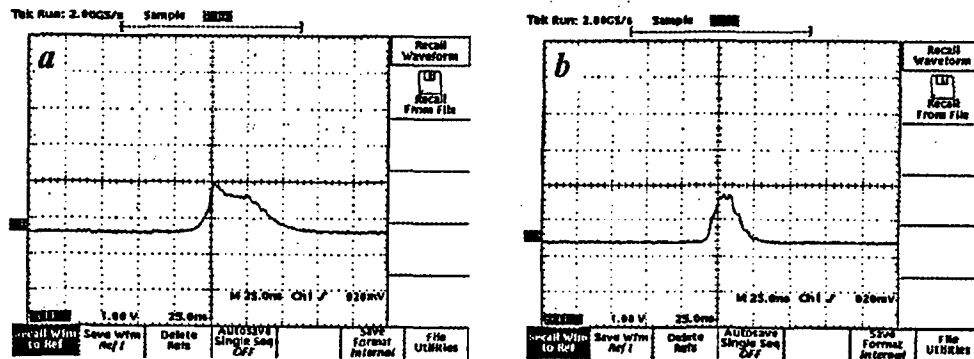
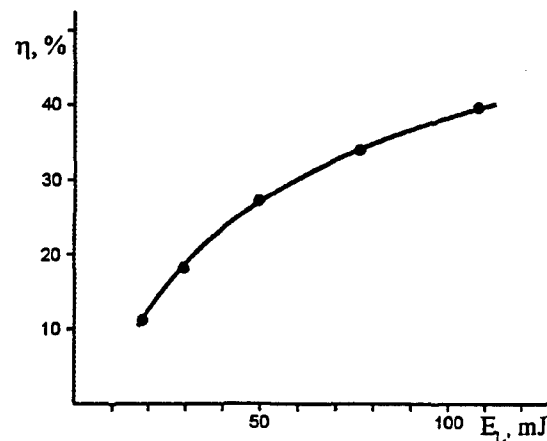**Fig. 5.20.** The pulse shapes of passed without conversion pump (a) and the output signal (b).

Fig. 5.21. The dependence of the amplifier efficiency in the collinear amplification geometry vs. the pumping energy.

Measurements of the weaker signal amplification were done with the energy of the pumping pulse less than the maximal value pointed out above. The reason is that, because the measurement of the weak wave amplification gain in the collinear scheme is impeded by the self-excitation of the amplifier. For the maximal pumping energy of 108 mJ the self-excitation resulted in generation of the Stokes radiation with the efficiency of 5-10% in the direction of the pump.

We can now calculate the value of the increment for the pumping intensity, average across the beam section. For pulse duration equaled 25 ns, beam diameter equaled 1.6mm and the gain equaled 0.0071 cm/MW, we can evaluate the said increment as $\approx$ 9. It is much smaller than the value of the threshold increment, which was given in the first Section. This contradiction can be explained in the following way. Nevertheless the butt-ends of the crystal are tilted, for the large diameter of the beam in the crystal there occurs some scattering, which provides the feedback. Another reason is that (as we have said already) the increment of the spontaneous

Fig. 5.22 . The dependencies for the collinear geometry of the gain and of the amplifier efficiency vs. ratio of the signal energy to the pump energy equaled 86 mJ.
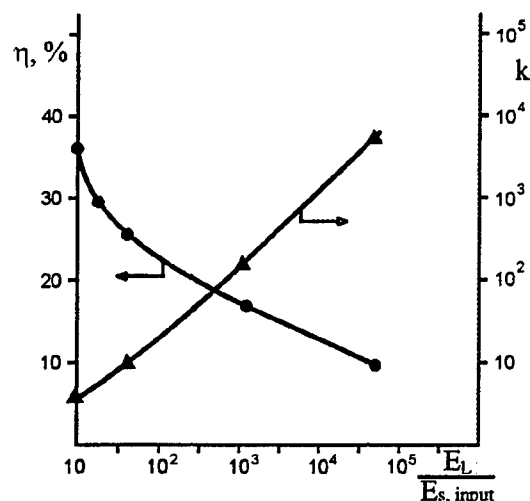
noise, which correlates with the pump, is twice as high. The dependencies of the gain and of amplifier efficiency vs. ratio of the signal energy to the pumping energy for the collinear geometry are shown in the Fig.5.22. We have observed the maximal gain of 5.6×10^3 for the conversion efficiency of 10% and the pump energy of 86 mJ , i.e. it corresponds (with neglection of saturation) to the increment of 8.63. This value exceeds the value of 7.3 which was evaluated from the calculation for such pump energy with the account for the gain, measured in the first Section and for the said beam diameter. Seemingly, in this case we once again observe the enlargement of the amplification coefficient due to the realization of the regime of the reproduction of the pump wavefront in the amplified Stokes radiation as it can be seen from the following results.

In the Figures 5.23 and 5.24 are shown the results of measuring of the divergence in the collinear and quasi-collinear schemes for the various values of the
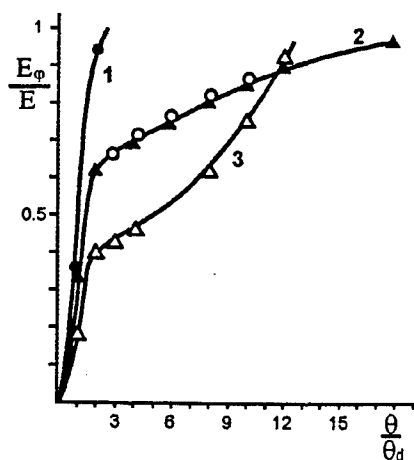
Fig. 5.23. The divergence of Stokes beams for the collinear amplification scheme.

1-input Stokes beam;
2-θ_L/θ_D =12, $E_{S,input}$=9 mJ ,E_L=86mJ(▲);
θ_L/θ_D = 22, $E_{S,input}$=7 mJ , E_L=80mJ (O)
3-θ_L/θ_D =12, E_L=86 mJ , $E_{S,input}$=2,5 mJ;
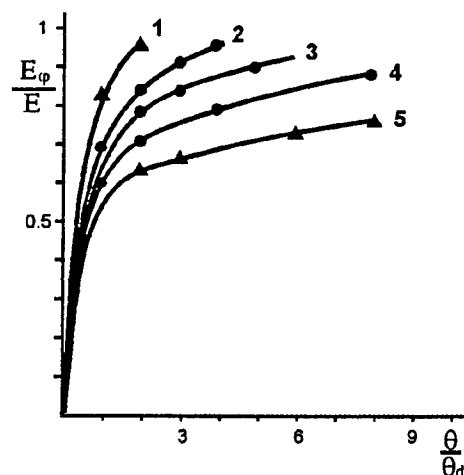
Fig. 5.24. The divergence of Stokes beams for the quasi-collinear amplification scheme with the angle in the crystal between Stokes beam and pumping beam $\theta=2\theta_L$ (θ_L/θ_D = 12)and for the collinear amplification scheme($\theta = 0$) with the same θ_L ,

1- input Stokes beam; 2,3 - θ =2θ_L, 4,5 - θ =0; signal amplification K=2 (2,4) and 2,7-(3,5).

44

gain and of the pump divergence as well as for the different values of input signal values. In the quasi-collinear mode of interaction beams crossed in the centre of the crystal at the angle equaled $2\theta_L$ (here θ_L - pump divergence in the crystal). One can see from the Fig.5.22 that in the case of the collinear geometry of interaction the spatial structure of radiation contains the nearly diffraction limited core and the wide wings. Just in agreement with the calculations the increase of the pump divergence from 12 to 22 diffraction limits is not accompanied by variation of the amplified signal divergence - notwithstanding the fulfillment in the experiment of the inequality of the plain waves criterion in nearly two orders of magnitude.

The reduce of the input signal energy under the constant pumping results in the reduce of the relative energy of the core, accompanied by the minor reduce of the energy, going to the maximal angle (due to the crossing of the curves 2 and 3 in the Fig.5.24); its shape becomes closer to the shape of the pump divergence contour. This is an evidence of the absence of the core while amplification of the weak signal, while the signal divergence becomes equal to that of the pump. Hence for weak signal the amplification is carried out in the mode of the wavefront reproduction.

For the equal gain (increment), the quasi-collinear amplification scheme reveals much smaller part of the energy, going to the wings, than it takes place in the collinear scheme (see curves 3 and 5 in the Fig.5.24 which represent equaled amplification),

The reduce of the pump intensity (the reduce of the gain) results in the increase of the relative energy in the core for both geometries of the amplification.

The important practical conclusion is that it is reasonable to use the quasi-collinear amplification geometry so as to improve the output divergence. The use of this method results, of course, in the reduce of the amplifier efficiency for the same pumping energy. The practical scheme, shown in the Fig.5.25, probably will improve the amplifier performance, because it provides for the averaging during the amplification and for the spatial overlapping of the interacting beams (one has to prevent, of course, the self-excitation of the amplifier).
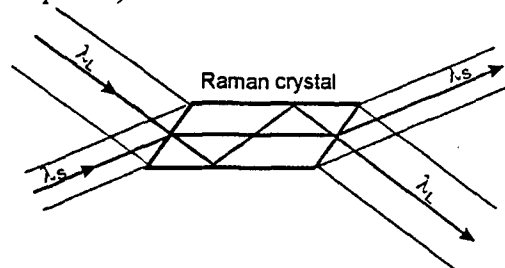
Fig. 5.25. Scheme for amplification.

All the described results qualitatively confirm the conclusions, drawn out from the numerical simulation. Let us once again enumerate the conclusions, which are confirmed by both theory and experiment:

1. Presence of the diffraction-limited core and of the wide wings in the single mode beam, amplified in the multi-mode pumping field.
2. Increase of the relative energy in the core with the growth of the input signal energy under the constant pumping level.
3. Significant reduce of the relative energy of the wings in the case of the quasi-collinear pumping when the angle exceeds in 1.3 times the divergence of the pump.

45

6. Main results

Let us in conclusion enumerate the main results of the work:

1. We have measured the gain and the constant, responsible for the thermal lens, in the crystal of barium nitrate.
2. We have established that in the focused beam the generation reveals the feature of the wavefront repetition up to the achievement of the saturation. Hence the Stokes beam divergence is close to that of the pump.
3. For the focused beam the efficiency of the first Stokes component generation is limited by the excitation of the second component. For the case of the focused single-mode beam it is higher than that for the multi-mode beam (35 and 27% correspondingly) due to the higher diffraction losses during the second Stokes component generation. In the scheme with the low quality cavity the efficiency of the first Stokes component generation with the wavefront repetition can be improved up to 41%.
4. We have realized in the experiment the 55% efficiency of generation of the single-mode first Stokes component, the six-times growth of the Stokes beam brightness with respect to that of the pump, generation in the focused beam of 1 W of the average power and the Stokes signal gain (amplification) of 5.6×10^3.
5. We have shown in the experiment that during the generation in the cavity it is possible to eliminate the influence of the depolarization onto the efficiency by using of the proper optimal orientation of the barium nitrate crystal.
6. We have theoretically and experimentally established the following. For the collinear amplification of the single-mode beam in the field of the multi-mode pump with the divergence of 10-20 diffraction limits and for the energy of the input signal of ~ 0.1 of the saturated pump energy, the structure of the amplified radiation contains the nearly diffraction-limited core, which contains approximately one half of the total energy, and the wide wings. Tilt of the pumping beam in the angle, exceeding its divergence, results in significant improvement of the amplified signal divergence.

References

1. William K. Bischel , Marc J. Dyer . Wave length dependence of the absolute Raman gain coefficient for the Q(1) transition in H_2 . J. Of the Optical Society of America B. Optical Physics. 1986, v.3, #5, p.677-682.
2. V.I.Bespalov, G. A. Pasmanik. Nonlinear optics and adaptive laser systems., Moscow, Nauka publishers, 1986 (in Russian).
3. B.Ya. Zeldovich, N.F. Pilipetsky, V.V.Shkunov .Wave front conjugation, Moscow, Nauka publishers, 1985, p.34 ,(in Russian).
4. N. Bloembergen., Nonlinear optics.,W.A. Benjamin, Inc., New York –Amsterdam, 1965.
5. S. A. Vitsinskii, V.K. Isakov, S.N. Karpukhin, I.L. Lovchii. Stimulated Raman scattering of copper-vapor laser radiation in a barium nitrate crystal., Kvant. Elektron.(Moscow) v.20, 1993 p.1155, [Sov. j. Quantum Electron.v.23, 1993, p.1001].
6. V.I.Bespalov, A.A.Betin, G. A. Pasmanik , Reproduction of a pump wave in stimulated scattering radiation. Proseedings of higher educational institutions, Radiophysc, v.21, #7, p.961-980 (in Russian).
7. Y. A. Anan'ev. Optical Resonators and Laser Beams, Nauka Publishers, 1990 (in Russian).
8. S.N. Karpukhin, A.I. Stepanov., Stimulated Emission From the Cavity Under SRS in $Ba(NO_3)_3$, $NaNO_3$ and $CaCO_3$ Crystals., Kvant. Elektron.(Moscow) v.13, 1572(1986) [Sov. J. Quantum Electron. v.16,1027(1986)].
9. Mezenov A.V., Soms L.N., Stepanov A.I. Thermal optics of solid-state lasers, J. of Soviet Laser Research, v.8, N5, 1987, p.427-549.
10. A. Z. Grasuk. Raman lasers, Kvant. Elektron.(Moscow), v.1, #3,1974, p.485-509 (in Russian).
11. Yu.E.D'akov, S.Yu.Nikitin. Kvantovaya Elektronika, 1987, v.14, No.10, p.1925-1957 (in Russian).
12. J. Goldhar, J. R. Murray, IEEE J. Quantum Electron. QE-18, 1982, No. 3, p. 399-409.
13. Y. R. Shen, The principles of nonlinear optics, John Wiley & Sons., 1984.
14. N.Ya.Vilenkin. Special functions and the theory of croup presentation. Moscow, Nauka, 1965 (in Russian).
15. A.A.Samarsky. Introduction to the numerical methods. Moscow, Nauka, 1987 (in Russian).
16. R. S. F. Chang, R. H. Lehmberg, M. T. Duignan, N. Djei, IEEE J. Quantum Electron., QE-21, 1985, No. 5, p. 477-487.

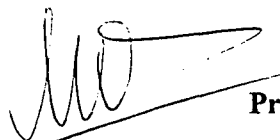Institute for Laser Physics of SC "Vavilov State Optical Institute"

&

Company Lasers and Optical System, Ltd.

Crystalline Media for SRS Conversion of

High Power 1.32 Micron Radiation

Interim Report #1

Director of the Institute   Prof. Arthur A.Mak

Principle Investigator   Sergey N.Karpukhin

St.-Petersburg

1997

1. Introduction

This Report is delivered on the completion of the studies in the frame of the Contract F61708-97-W0255, devoted to analysis the principal limitations of SRS conversion of 1.32 radiation carried out by the Company LOS Ltd., St.-Petersburg, Russia with the participation of the scientists of the Research Institute for Laser Physics, St.-Petersburg, Russia, and of the Research Center "Vavilov State Optical Institute", St.-Petersburg, Russia.

The use of stimulated Raman scattering (SRS) for Nd:YAG laser 1.32 μm emission conversion is rather promising idea, providing the possibility of realization of the completely solid-state source of the eye-safe radiation. Such a possibility was for the first time noted and experimentally tested in [1].

Most of the preceding papers on SRS in crystalline media were carried out with the use of pumping by 1.064 μm or its second harmonics. These activities revealed the novel crystalline media with the low generation threshold, demonstrated the possibility of the efficient energy conversion via SRS. It was shown that it is possible to obtain the diffraction limited radiation in the mode of phase conjugation, as well as to realize the amplification of weak wave without distorting it and to work in the kHz range of pulse repetition rates.

However, the results of these activities, as well as of studies of SRS in other media, had, at the same time, revealed some limitations of principal character, which are to be accounted for in design of SRS converters, including those pumped by 1.32 μm emission; in fact, a lot of general features of SRS process are valid across the wide spectral range and are to a large extent determined by general properties of the radiation, such as divergence and spectrum width, and by the spatial geometry of SRS excitation, such as SRS in focused beam, SRS in cavity etc.

2. Selection of crystals for Raman frequency conversion

The main parameter of the medium, which describes its applicability for SRS process, is the SRS gain. In [2] there was for the first time given the expression for this gain:

$$G = 2\lambda_s (d\sigma/d\Omega) I_p / h v_s \pi \Delta v$$

3

Here λ_S and ν_S are the wavelength and frequency of the Stokes radiation, $d\sigma/d\Omega$ - the cross-section of scattering from the single unit of the medium volume to the unit of the corporal angle, I_p - pump intensity and $\Delta\nu$ - linewidth of the spontaneous Raman scattering. The obvious conclusion from that formula would be the following. The best gain can be realized in crystals which reveal the highest value of ratio of the cross-section of scattering by the active molecular oscillation to the linewidth. However, it is impossible to find out the gain for this or that crystal by means of direct calculations: from the quantum theory it is known that the cross-section value depends on the outlook of the wave functions of this crystal electron states which is not known for the majority of crystalline media [3]. However, it is possible to derive one general principle of the search for the crystals with the highest gain.

It is well known from the classical theory that the scattering cross section is proportional to the square of the polarization derivative on the oscillation coordinate, calculated in the state of atomic equilibrium [3]. One can expect to find out the highest values of such a derivative in the crystals, containing in their structure the molecular complexes with the covalent atomic ties. The oscillations of the atoms, subject to such ties, result in strongest deformations of their common electron orbitals and thus in highest values of the said derivative [4].

So the search for the crystals with the highest gain of SRS process was done earlier by means of experimental evaluation of the media with such ties, namely nitrates, nitrites and sulfates of some metals. The search was carried out as the evaluation of SRS threshold in various polycrystalline media (the pressurized tablets of the medium powder [5,6]). This method is based on the inverse proportional character of this threshold dependence on SRS gain.

We have chosen the nitrates of several metals as the most prospective media. Further studies of the crystal growth processes resulted in choosing of two crystalline media, namely barium and sodium nitrates. The parameters of these crystals, important from the point of view of SRS excitation, are summarized in the Table 1. This Table contains also for the comparison purposes the same parameters for the natural crystal of calcite.

This Table 1 also contains the data on crystal of KGW (KGd(WO$_4$)$_2$). The SRS in this medium was the first time revealed in the Vavilov State Optical Institute

while investigating the picosecond generation in the laser, based on Nd-doped KGW active medium [7].

Table 1. Parameters of SRS crystals [8,9]

Materials	Polarization	v cm^{-1}	Δv cm^{-1}	g 10^3 cm/MW	
				λ_p =0.53 μm	λ_p =1.06 μm
Ba(NO$_3$)$_2$		1046 1047 /10/	1.5 0,56 /10/	47	11
NaNO$_3$	⊥ optical axis	1066	2.0	47	11
CaCO$_3$	- « -	1085	2.3	13	
KGd(WO$_4$)$_2$	n$_m$ axis	901.5	5.9		6
	n$_P$ axis	767.3	7.8		6

One can see from the Table that the barium and sodium nitrate crystals reveal the highest SRS gain. In KGW the comparatively high value of g ($g=G/I_p$) is accompanied by the large linewidth of the oscillation transition; such a combination makes this medium rather promising for SRS of radiation with the wide spectrum and for picosecond pulses of radiation.

3. SRS generation and amplification in crystals

Let us now discuss some experimental and theory results, which can help us to determine some limitations. We shall start with the results on studying the simplest scheme of SRS excitation via radiation focusing to the crystal volume [8,11]. In the Fig.1 is shown the experimental setup, which was used in these experiments. The multi-mode radiation from Nd:YAG and Nd:KGW lasers (λ = 1.064 and 1.067 μm) was focused into the crystal. In the Fig.2 are shown the results of measuring of the efficiency of conversion to all the Stokes components.

One can see that for the high threshold ratio in crystals of Ba(NO$_3$)$_2$ and KGW are realized the efficiencies of SRS conversion of ~ 70%. In KGW the pumping pulse energy was limited by the breakdown. It took place at the level of pumping pulse energy of ~ 10 mJ, i.e. at the intensity of breakdown of less than 1 GW/cm^2. However, in the pulse repetitive mode of pumping laser action these crystals revealed the bulk damage at the energy level which is much lower than the damage threshold for the single pulse action. So the thermal stress due to the Stokes loss can limit the use of this medium. The barium nitrate crystal could have been subjected to the action of 60 mJ pulses without damage.
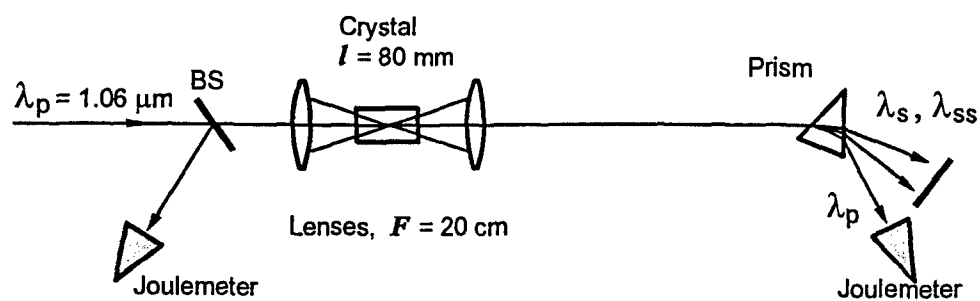
5

Fig.1. Optical scheme for investigation of the focused beam SRS.
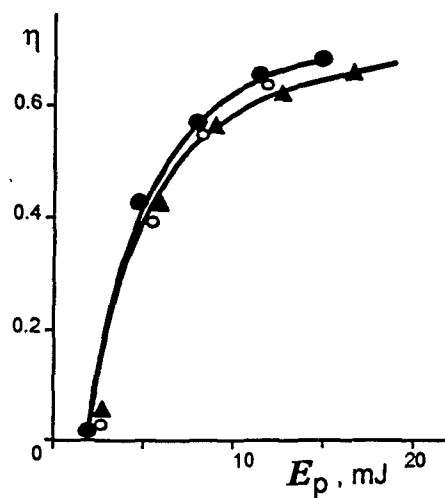
Fig.2. Energy conversion to all Stokes components efficiency (η) dependence vs. pump energy (E_p) for

the crystals: ▲ - $Ba(NO_3)_2$, ○ - $KGd(WO_4)_2$, polarization along the axis n_m,

● - $KGd(WO_4)_2$, polarization along the axis n_p.

Fig.3. Conversion efficiency and residual pump energy at the crystal output for SRS in $Ba(NO_3)_2$ for radiation from Nd:KGW laser (Fig.3a, $\Delta v_p =1.8$ cm^{-1}) and Nd:YAG laser (Fig.3b, $\Delta v_p =0.5$ cm^{-1})

The surface damage threshold of this crystal can be evaluated at the level 1.5 G/cm^2 (λ=1.06 μm). The crystal volume has to reveal higher threshold. In this crystal no thermal damage occurs at the level, typical for KGW, but the radiation is depolarized (see further).
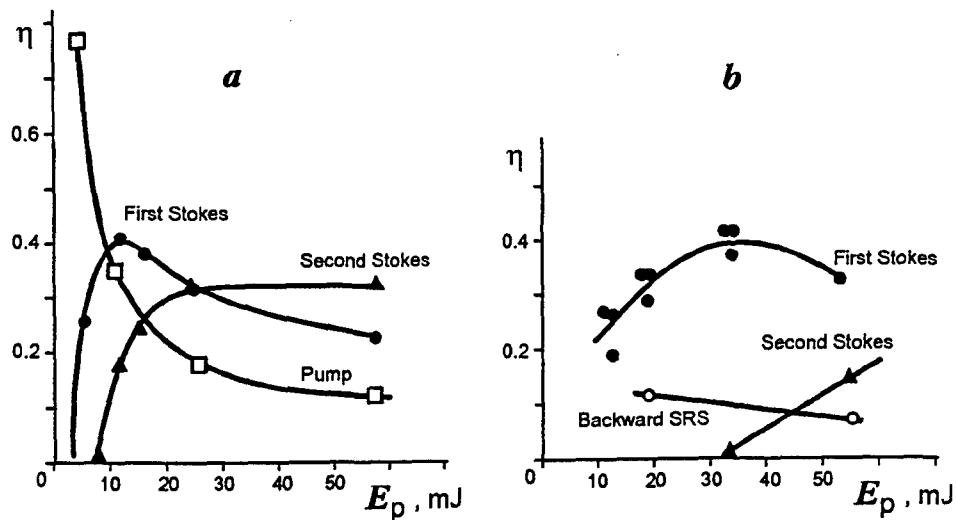
The most interesting case is that of maximal conversion to the first Stokes component. In the Fig.3 are shown the dependencies of the energy conversion to Stokes components vs. pumping energy for the case of focusing the multi-mode radiation with various width of spectrum [11]. One can see that at the conversion efficiency of 40% the excitation of second Stokes component reveals itself, limiting thus the conversion to the first one. The main role plays the SRS excitation by the first Stokes component.

Second Stokes component generation is supported by the parametric interaction of pump and first Stokes component waves. There is significant wave mismatch in this process: $\Delta k = k_p - 2k_S + k_{SS}$; here k_p, k_S, k_{SS} are correspondingly the wave vectors of pump, first and second Stokes components. Nevertheless, this process results in decrease of the second Stokes component generation threshold. For instance, in [12] the investigation of pumping by dual wavelength radiation revealed the decrease of the excitation threshold by weak component, and the efficiency of this process grew up.

In the case of pumping by the narrow linewidth radiation some part of radiation is scattered to the backward direction (Fig.3b). It means that there exists the competition between the processes of forward and backward generation of the first Stokes components. This competition is also to be regarded as the principal limitation of the conversion efficiency to the forward (or backward) Stokes component of SRS in focused beam. Some reduce of the role of this negative factor can be obtained by the proper choice of focal length of the lens. Such a possibility was earlier determined for the case of focusing to the crystal of the single mode beams, whose spectral width was limited by the pulse duration [13]. Short focal length resulted in preferably backward SRS generation, while longer - in preferably forward SRS process.

Observation of SRS in the cavity has also revealed the limitation of the energy and conversion to first Stokes component efficiency due to second component excitation [9,14]. The use of low selectivity mirrors at the high threshold ratio level,

8

which is necessary for the efficient conversion, did not provide complete dumping of the second Stokes component.

More efficiently the second Stokes component is dumped in SRS master oscillator - power amplifier schematics or in the case of SRS generation inside the pumping laser cavity [15]. These devices, of course, belong to the class of more complicated nonlinear devices. SRS in the cavity provides the possibility to realize the comparatively efficient device at the relatively small threshold ratio. The reason is lack for pump energy losses, for it is locked in the closed cavity. For instance, in [15] for barium nitrate pumping by 1.32 μm there was obtained the 12 mJ output to the first Stokes component with the efficiency 48 %. Scaling of these results gave the energy output of up to 250 mJ.

Now let us discuss the spatio-angular parameters of radiation and their connection with SRS generation energy and efficiency. In [11,13] it was shown that the forward SRS is accompanied by the so called effect of the wavefront reproduction, while the backward SRS results in phase conjugation of the scattered beam. In the Fig.4 is shown the optical scheme, which was used for measuring the divergence of the beam, realized via SRS of focused beam. In the Fig.5a are shown the results of measurements for the multy-mode pumping beam (E_φ is the energy in the angle φ and E - the total generation energy) [11]. One can see that for the low energies the scattered beam divergence coincides with that of the pumping beam, i.e. the effect of wavefront repetition takes place; note, that divergence of the Stokes beam is even slightly smaller than that of the pumping beam, because the low energy wings of the beam do not participate in the nonlinear process. The energy increase, however, results in more than double aggravation of the beam divergence due to the spatially incoherent mode of scattering.

One can expect that in the case of single mode pumping the growth of threshold ratio would also result in deterioration of forward SRS beam [13]. In addition, in the mode of the wavefront repetition the energy of single mode beam would be always smaller than that of multy-mode one, for the threshold energy is proportional to the beam divergence [16]. So in the case of use of focused beams the generation of diffraction limited forward SRS beam is possible only at the low energy level; for 1.32 μm this range is limited by 1 and 4 mJ. In the case of backward SRS the
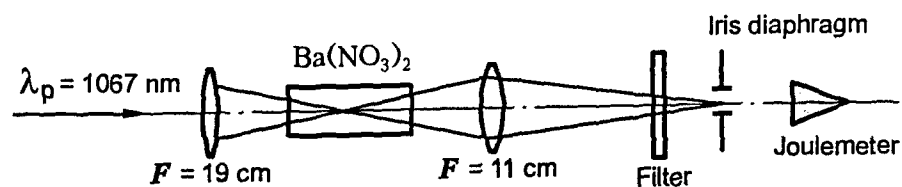
Fig.4. Optical scheme for measuring the angular divergence of the forward SRS radiation, excited by the focused beam.
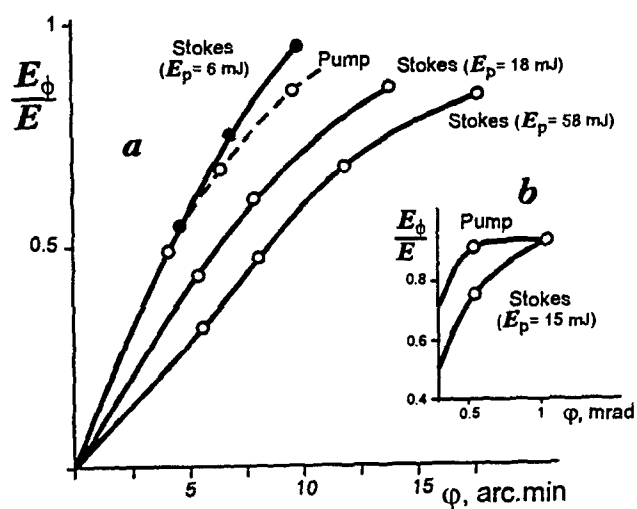

Fig.5. Dependence of the angular energy distribution E_φ/E vs. angle φ for multy-mode pumping (a) by radiation with $\lambda = 1.067$ µm, beam diameter $d \approx 5$ mm and for single mode pumping (b) by radiation with $\lambda = 0.532$ µm, $d \approx 6$ mm; the scheme with two crystals was used [13].

proper choice of the focal length of the lens provided at the high energy level (threshold ratio of ~ 2 orders of magnitude) the Stokes beam divergence of not more than 2-3 diffraction limited values (Fig.5b); the conversion efficiency in this case was ~ 35-40%. However, for the fixed energy of the backward scattered Stokes beam there is the principal limitation of the divergence improvement possibilities by the damage threshold of the crystal, because the reduce of focal length results in increase of the intensity in the focal plane as ~ $1/F^2$.

In the case of SRS generation in the cavity the nearly diffraction limited output beam was realized under the pumping by the beam, whose diameter is approximately equal to that of zero mode [14,15]. With this purpose the in [15] the waists of the cavity modes for the pump and SRS generation radiation were spatially matched in the center of barium nitrate crystal. In [14] it was shown that the increase of the pumping beam waist diameter over diffraction limited, but preserving pump intensity, results in the divergence growth.

Further increase of energy of scattered beam with the low divergence preservation is possible with the use of SRS amplification. The most interesting variant is that of single mode beam amplification under the multy-mode pumping. For the Nd:YAG laser typical divergence of multy-mode beam is somewhat ~ 2 mrad. Such a divergence of pump would, however, result in deterioration of the amplified beam divergence. The reason of such a deterioration [17] is as follows.

Let the pumping waves of SRS amplifier consists of two spatial components with the wave vectors k_{p1} and k_{p2} correspondingly and the amplified Stokes beam - the wave vector k_s (Fig.6). The action of pumping and Stokes waves excites in the medium the wave of molecular oscillations Q:

$$Q = \Sigma Q_i exp[i\ (\Omega t - q_i r)]\ , \qquad i=1,2$$

here $q_i = k_{pi} - k_s$ are the wave vectors of molecular oscillations. The scattering of pump components on the excited molecular oscillations results in generation of Stokes radiation with wave vectors:

$$k_{s1} = k_{p1} - q_1 = k_s$$
$$k_{s2} = k_{p2} - q_2 = k_s$$
$$k_{s3} = k_{p1} - q_2 = k_s - (k_{p2} - k_{p1})$$
$$k_{s4} = k_{p2} - q_1 = k_s - (k_{p1} - k_{p2})$$

11

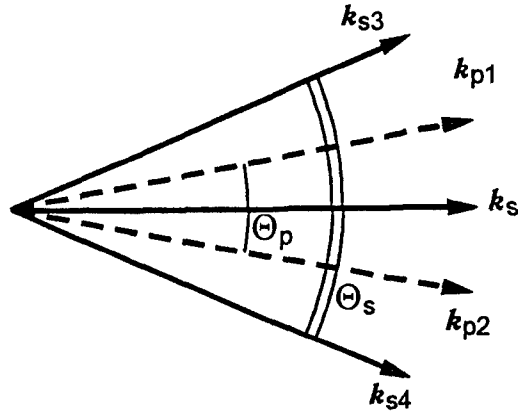Fig.6. Direction of the Stokes radiation amplification.

θ_p - divergence of pumping beam, θ_s - divergence of pumping beam
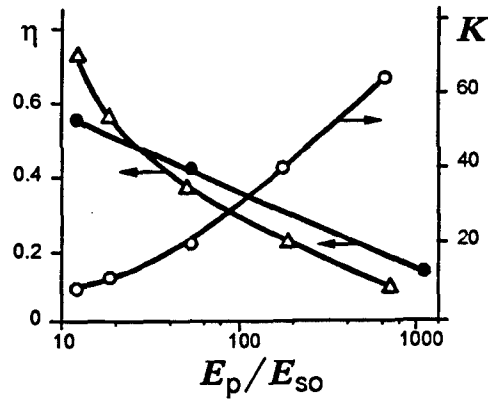

Fig.7. Conversion efficiency (η) and amplification (k) vs. ratio of pump energy to seed Stokes energy

(E_p/E_{s0}); $\theta_p = 16$ mrad, $\theta_s = 0.5$ mrad, $\triangle$, $\circ$ - two passes, $I_p = 16$ MW/cm^2,

$\bullet$ - single pass, $I_p = 24$ MW/cm^2.

One can see from these equations that two first wave vectors coincide with the wave vector of the amplified Stokes beam. It means that the pumping wave scattering on the wave of molecular oscillations, which was created with the said light wave participant, represents the Raman scattering without distorting the wavefront. At the same time the wave vectors k_{s3}, k_{s4} differ from the amplified beam vector. Generation of such waves is realized due to the parametric interaction of pump components with the input Stokes beam. This process results in wavefront distortions and thus in increase of the divergence of the amplified radiation. The mismatch of the parametric process of the waves with the wave vectors k_{s3}, k_{s4} is described by the equation:

$$\Delta k = |\, k_{s3}\,| - |\, k_s\,| = |\, k_{s4}\,| - |\, k_s\,| \approx \Theta^2_p k_p / 2 k_s$$

Here Θ_p is the diverence of the wave, pumping the amplifier. The dumping of the parametric interaction of waves and thus distortions-lacking amplification requires the fulfillment of the following relationship [17]:

$$(G\, k_s / k_p^2 \Theta_p^2)^2 \ll 1$$

Let us assume that the gain has the value in the typical range of G=0.5-1 cm^{-1}, which corresponds to the range of pump intensities of I_p=60-120 MW/cm^2. In our evaluation of G we have used the value of g=0.0086 cm/MW; it was recalculated from the value for λ_s = 1.064 μm (see Table 1) with the account for the spectral dependence of scattering cross-section: $d\sigma/d\Omega \sim v^4$ [3]. It was assumed that Θ_p= 2 mrad, λ_p= 1.32 μm, λ_s =1.53 μm (k= $2\pi/\lambda$). So for the left part of the formula we get the value of some 5-20, i.e. the relationship is not fulfilled. Hence the parametric process of multy-mode pump interaction with the amplified Stokes beam reveals itself as the principal limitation of the distortions-lacking amplification.

One can see from the discussed relationship that the negative influence of the parametric process can be reduced by means of pump divergence increase or by the quasi-longitudinal amplification with the comparatively large angle between the pump and amplified beam propagation directions [18].

For example, in [15], the single-mode pumping beam was intentionally distorted up to the divergence of 16 mrad by the etched plate. The plane of this

13

distorting plate was imaged into the crystal by special relay. In this experiment the signal with the divergence of 0.5 mrad was amplified without distortions. In the Fig.7 one can see the results of measurements of the amplifier efficiency and amplification gain vs. ratio of the pump and the input signal. In the dual pass (both for pump and amplified Stokes beam) scheme there was demonstrated the conversion efficiency of 74%. Higher ratio of the pumping beam energy to that of the input Stokes beam resulted in conversion efficiency deterioration due to the amplifier self-excitation.

4. Influence of medium heating onto SRS of pulse repetitive radiation

In this Section we present the preliminary novel results on quantitative analysis of the Stokes losses influence.

SRS is accompanied by the significant frequency shift in the value corresponding to the frequency of molecular oscillations. This energy deficit (Stokes losses) is released in the medium as the heat. For the pumping wavelength of 1.32 μm in the barium nitrate crystal the rate of Stokes losses equals 14%. In [10] in experiment there was measured the dependence of the molecular oscillation linewidth vs. temperature. It was determined that the temperature growth results in linewidth enlargement due to the stronger interaction between the active oscillation and other molecular oscillations in the crystal. So the gain is reduced.

Hence one can predict the deterioration of the SRS process efficiency. The strength of influence of the medium heating onto the efficiency of the pulse repetitive radiation SRS can be evaluated on the example of the SRS amplifier. Let the crystal is cylinder shaped. Both pumping and Stokes beams propagate along the cylinder axis, and the beam radius R_1 is less than the crystal radius R_2. Let us also assume that the crystal is cooled by cooling agent. In general case the temperature of the crystal surface would exceed that of cooling agent. The heat flow from this surface to the cooling agent is described by the equation [19]:

$$\chi dT_s/dn = \alpha \, (T_s - T_c)$$

In this equation χ is the thermal conductivity coefficient, α is the thermal exchange coefficient, T_s - surface temperature and T_c - cooling agent temperature. The derivative was taken in the direction, normal to the crystal surface. Let $W(z)$ is the average power, released in crystal volume unit. It includes not only the Stokes losses, but also the linear absorption of radiation in the crystal. Let us now assume the following

simplifications. Let us neglect the temperature gradient in the direction of the crystal axis. In this case the solution for the temperature in the practically interesting range of polar coordinate r values from 0 to R_1 can be derived analytically and looks like [20]:

$$T(z, r) = T_C + \frac{WR_1^2}{4\chi} \left(1 - \frac{r^2}{R_1^2} + \frac{2}{Bi} \right) + \frac{WR_1^2}{2\chi} \ln \frac{R_2}{R_1}$$

Here $Bi = \alpha R_2/\chi$ is the so called dimension-less criterion of similarity. Rather uncertain parameter is the value of the thermal exchange coefficient. It is known [19], that in the case of liquid cooling this coefficient value fills to the range of 0.1..1 W/cm^{2}K^0 (i.e. $Bi = 5..10$ for $R_2 = 0.5$ cm). In the case of gas cooling $\alpha < 0.01$ W/cm^{2}K^0 and, correspondingly, $Bi < 0.5$.

The following equations describe the interaction of the pumping and the Stokes waves with the account for the variation of the thermal power deposition in the unit of medium volume and thus variation of the gain:

$$\frac{dI_s}{dZ} = g(T) I_p I_s \qquad \frac{dI_p}{dZ} = -g(T) I_p I_s$$

$$W(Z) = F \frac{dI_s}{dZ} \frac{\Omega}{v_s} \tau + \kappa F \tau (I_C(Z) + I_P(Z))$$

Here I_p, I_s are the intensities of the pumping and Stokes components, F - repetition rate, k - absorption coefficient and τ - pulse duration.

We have calculated the amplifier efficiency η, determined as the ratio of the difference between output and input energy of the Stokes beam to the pumping energy, in its dependence on the input pumping power P. The function $g(T)$ was determined from the approximation of experimental dependencies in [10]. The results of calculations are shown in the Fig.8.

The calculation was carried out with the following set of parameters: $\chi = 1.1$ W/m K^0, $I_p = 50$ MW/cm^2, intensity of the input Stokes beam 5 MW/cm^2, crystal length 5 cm, $g = 0.0086$ cm/MW ($T = 300^0$K), pulse duration $\tau = 10$ ns, $R_1 = 0.3$ cm, $R_2 = 0.5$cm, absorption coefficient $k = 0.004$ cm^{-1}.
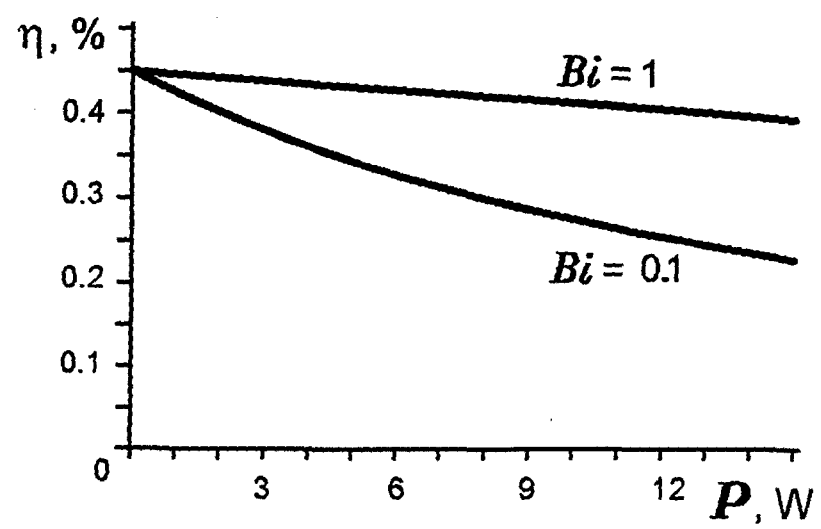
Fig.8. Dependence of amplifier efficiency vs. average power of pump

One can see from this Figure that the amplifier efficiency is strongly influenced by the Stokes losses in the case of non-efficient cooling of the crystal (low Bi). Note at the same time, that the crystals of nitrates, to the contrary with that of KGW, are rather hygroscope media. In this case the comparatively high value of Bi can be provided, for instance, by means of the contact with the surface of metal, cooled by some agent.

Let us now discuss another aspect of the Stokes losses influence onto the process of stimulated Raman scattering. It is the depolarization of radiation in the crystal of barium nitrate, induced in the pulse repetitive mode of action.

The crystal of barium nitrate is the cubic crystal of the symmetry m3. The cubic crystals do not reveal the birefringence, because in such a crystal the indicatrix of the refraction index is spherically symmetrical ($Bx_ix_i=1$, i=1,2,3, $B=1/n^2$, n - refraction index of the crystal). Thermal distortions of the crystal results in this sphere transformation into the ellipse, described by the equation:

$$B_{i,j}\, x_i x_j = 1 \qquad i,j = 1,2,3$$

Here $B_{i,j}$ is the tensor of the so called relative dielectric impermeability. In general case the modification of the indicatrix in comparison with its primary shape is described by the relationship [21]:

$$\Delta B_{i,j} = p_{i,j,k,l}\, \varepsilon_{k,l} \qquad i,j,k,l = 1,2,3$$

Here $p_{i,j,k,l}$ is the tensor of the fourth rank, describing the photoelastic effect, and $\varepsilon_{k,l}$ is the tensor of the second rank, which describes the thermally induced deformations. The crystal symmetry results in zero value of some components of the photoelastic tensor. So the modification of the tensor of the relative dielectric impermeability can be described in the simpler way [21]:

$$\Delta B_i = p_{i,j}\, \varepsilon_j \qquad i,j = 1,2..\ 6$$

In the same paper there was given the description of the tensor $p_{i,j}$ for the crystals of various symmetry classes. Let us write out the expressions for the components of tensor ΔB_i for the symmetry m3 and reorder the terms:

$$\Delta B_1 = p_{11}\varepsilon_1 + p_{1,2}\varepsilon_2 + p_{1,3}\varepsilon_3 = p_{11}\varepsilon_1 + p_{1,2}\varepsilon_2 + p_{1,2}[1+(p_{1,3}-p_{1,2})/p_{1,2}]\varepsilon_3$$

$$\Delta B_2 = p_{13}\varepsilon_1 + p_{1,1}\varepsilon_2 + p_{1,2}\varepsilon_3 = p_{11}\varepsilon_2 + p_{1,2}\varepsilon_3 + p_{1,2}[1+(p_{1,3}-p_{1,2})/p_{1,2}]\varepsilon_1$$

$$\Delta B_3 = p_{12}\varepsilon_1 + p_{1,3}\varepsilon_2 + p_{1,1}\varepsilon_3 = p_{11}\varepsilon_3 + p_{1,2}\varepsilon_1 + p_{1,2}[1+(p_{1,3}-p_{1,2})/p_{1,2}]\varepsilon_2$$

$$\Delta B_4 = p_{44}\varepsilon_4. \qquad \Delta B_5 = p_{44}\varepsilon_5. \qquad \Delta B_6 = p_{44}\varepsilon_6.$$

17

Let us now neglect the value of ($p_{1,3} - p_{1,2}$)/ $p_{1,2}$= - 0.06 (see Table 2) as very small in comparison with 1 in the expressions for ΔB_1, ΔB_2, ΔB_3. So the expressions for ΔB_i would be quite the same as for the class m3m of higher symmetry. So one can apply the existing theory of depolarization in YAG crystals for the analysis of the depolarization in barium nitrate crystal.

Table 2. Physical constants of barium nitrate crystal [21,22].

In the Table: n - refraction index for λ = 1.06 μm, β=dn/dT^0 , α- the coefficient of linear expansion (T =25^{0}C), χ - thermal conductivity coefficient (T=25^{0}C) and ν- Poisson coefficient.

n	$\beta \times 10^5$ degree^{-1}	$\alpha \times 10^5$ degree^{-1}	χ W/mK^0	ν	p_{11}	p_{12}	p_{13}	p_{44}
1.555	2	1.1	1.1	0.237	2.49	3.40	3.20	-0.021

The essence of this theory is as follows [21,23,24]. Let the crystalline active element is subjected to the thermally induced deformations. In each point of its transverse section with the polar coordinates $(r,\varphi)^1$ the axes of the ellipsis of the optical indicatrix are turned with respect to the direction **r** in the angle α= φ'- φ, where the angle φ' is to be determined from the equation:

$$tg2\varphi' = \xi \, tg2\varphi$$

One can see from this equation that for $\xi \neq 1$ the axes of the ellipses of the optical indicatrix, corresponding to various points of the crystal, do have in their orientation the emphasized direction (ξ=1 (φ' =φ) for the direction z || [111]^2). In the crystal of barium nitrate for the orientation of the geometric axis of the active element z || [001] ξ= 2p_{44}/(p_{11} -p_{12}) =0.04 and for z || [$\bar{1}$10] ξ=8p_{44}/(3p_{11} -3p_{12} +2p_{44}) =0.057. Such a low values of the parameter ξ mean that the axes of the ellipses in various points of the active element section are practically parallel. So, as we shall show further, it is possible to choose the crystal position with respect to the polarization vector in which the depolarization rate is minimal.

For the ray, which is parallel to the geometrical axis, and the coordinates (r,φ) the power in the depolarized component is determined by the equation:

$$a(r, \varphi)=\sin^2 2(\varphi'-\gamma)\sin^2 [\delta(r,\varphi)/2]$$

---

[1] Here φ is measured with respect to the plane, containing the geometry axis z and the crystallographic axis [100].

Here γ is the angle between the polarization vector and the plane, containing the geometry axis z and the crystallographic axis [100], $\delta(r,\varphi)$ is the phase shift in some point between the own polarization states of the optical indicatrix. The summary rate of depolarization across the section losses can be described analytically only for the directions of $z \parallel$ [001], [111], [$\bar{1}$10]:

$$A = \frac{1}{\pi} \int_{-\pi/4}^{\pi/4} \frac{(\xi\, tg2\varphi \cos2\gamma - \sin2\gamma)^2}{1+\xi^2 tg^2 2\varphi} \left[1 - \frac{\sin2G}{2G}\right] d\varphi$$

$$G = B\sqrt{\frac{1+\xi^2 tg^2 2\varphi}{1+tg^2 2\varphi}}$$

$$B = \frac{4\pi\alpha n_0^3}{\lambda} \frac{1+\nu}{1-\nu} \xi' \frac{WR_1^2}{4\chi}$$

Here W is the thermal power, released in the unit of volume, α - linear expansion coefficient, λ - Stokes beam wavelength, ν - Poisson coefficient, R_1 - radius of the channel of beams' interaction, χ - thermal conductivity coefficient, L - crystal length, $\xi' = p_{11}-p_{12}$, $3/4$ $(p_{11}-p_{12})$ $+1/2$ p_{44} and $p_{11}-p_{12}+4p_{44}$ correspondingly for $z \parallel$ [001], [$\bar{1}$10] and [111].

In the Fig.9 are shown the results of calculation according to the given expressions of A dependence vs. parameter B, which is proportional to the phase shift between r and φ polarization states. One can see that for $\gamma = 0°$ it is possible to obtain the significant reduce of depolarization for the directions of $z \parallel$ [001] and [$\bar{1}$10]. For the direction of $z \parallel$ [111] the rate of depolarization does not depend on the value of γ. This direction is less interesting with respect of intense pulse-repetitive radiation SRS.

The most interesting is the direction of $z \parallel$ [$\bar{1}$10], for it is the direction, in which it is possible to cut out the longest crystals of barium nitrate. Note, that the given expressions are valid for $z \parallel$ [$\bar{1}$10] when there is fulfilled the relationship $(p_{11}-p_{12} +p_{44})/(3p_{11}-3p_{12} +2p_{44})<<1$ [26]. However, the requirement of significant difference is not fulfilled, for the left side of this relationship equals in fact 0.32. It is impossible to evaluate the real situation for A by analytical means. So it is necessary to carry out the numerical calculations by Nye matrix method [21].

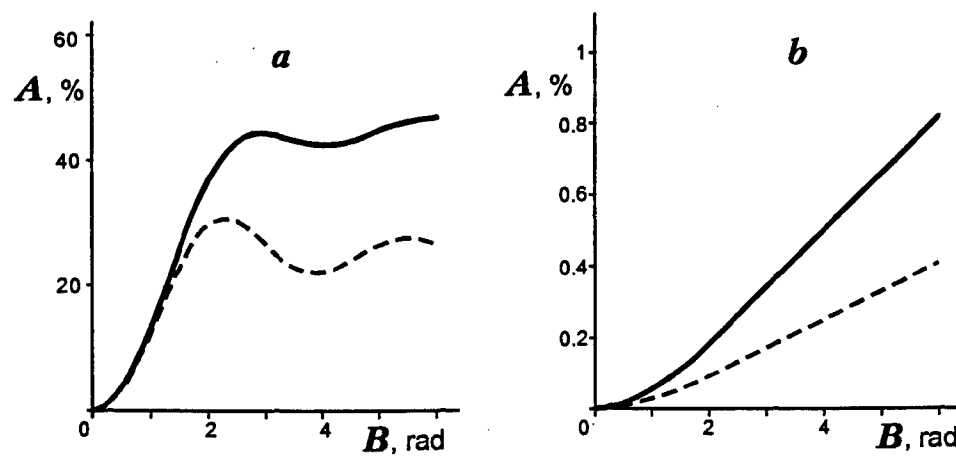[2] The figures in square brackets indicate the crystallographic direction in the crystal.

Fig.9. Dependence of depolarization rate A vs. parameter B.

Fig.9a: solid line - $z \| [\bar{1}10]$, [001], $\gamma = 45°$;

dotted line - $z \| [111]$, $\gamma = 45°$ and $= 0°$;

Fig.9b: solid line - $z \| [\bar{1}10]$, $\gamma = 0°$;

dotted line - $z \| [001]$, $\gamma = 0°$.

Earlier we have carried out the experimental measurement (in the pulse repetitive mode of laser action) of the rate of Stokes beam depolarization with the pumping by 1.064 μm radiation for this direction. For the average pumping power of 2 W the depolarized component contained ~ 25% of the total power for $\gamma = 45°$ and ~ 2-2.5% for $\gamma = 0°$. In [12] for $\gamma = 45°$ there was also observed the reduce of SRS conversion efficiency. Crystal tilt in 45° ($\gamma = 0°$) resulted in absence of such an efficiency reduce. These results indicate qualitative correspondence of experiment and above given discussion on the possibility to compensate for the thermally induced birefringence. However, the power level, when the depolarization is observed for $\gamma = 45°$ are much smaller than the theoretically predicted.

Let us evaluate the pumping power which is to result in 10% depolarization at 1.32 μm pumping. According to the calculated curve in the Fig.8a for such A we have $B=0.8$. Let us use in the equation for B the value of

$$ W = P\left(\eta \frac{\Omega}{v_s} + kL \right) \frac{1}{\pi R_1^2 L} $$

Here P is the average pumping radiation power, η - SRS conversion efficiency, Ω/v_s - ratio of the molecular oscillation frequency to that of Stokes wave, k - absorption coefficient. Solution for this equation gives us the value of P = 5.6 W. For the radiation of 1.064 μm we should have the value of P= 4.3 W; that value is much higher than that measured in real experiment.

In [12] there was revealed the violation of the energy balance for the input and output beams with the account for the Stokes losses. Possible reasons of such misbalance can be scattering to large angles, as well as nonlinear absorption (dual photon for the visible range of spectrum); it can occur for 1.064 μm as well. One can observe the violation of the energy balance at focusing for the pump energies, exceeding 15 mJ, analyzing the curves in the Fig.3a. One can see from this Figure that for the high pump energies the efficiency of conversion to second Stokes component alone is not changed, while the parts of the residual pump (at the crystal output) and of the first Stokes component are reduced. So the energy of the output radiation grows slower than that of input radiation. For the pump energy of 60 mJ the misbalance, accounting for Stokes losses, reaches 27%. It is rather difficult to separate the influence of the nonlinear absorption and of the scattering to large angles. At the same time the studies of the thermally induced birefringence can be regarded as an

21

instrument for the nonlinear absorption measurements. New studies are thus necessary.

As to the single axis crystal of sodium nitrate it is possible to neglect the influence of the thermally induced birefringence, for the induced retardation of r and φ phases would be much smaller than that of natural origin. The main difficulty in this crystal application results of its high hygroscopicity and thus difficulties in butt-ends processing.

5. Conclusion

In conclusion let us now enumerate the principle limitations, which are to accounted for while optimization of the crystalline SRS converters of high intensity 1.32 µm radiation.

- Optical breakdown of the crystal (limitation of the Stokes radiation energy).
- Generation of the second Stokes component (reduce of efficiency of the conversion to the separately first stokes component).
- Forward and backward SRS competition while generation in focused beams (reduce of either forward or backward SRS process efficiency).
- Parametric interaction of spatial components of the multy-mode pump with the amplified Stokes beam (radiation divergence increase).
- Medium heating in pulse repetitive mode of action due to the Stokes losses (efficiency reduce, thermally induced birefringence, thermal damage of the crystal).

6. References

1. S.N.Karpukhin, A.A.Nikitichev. Close IR range of spectrum radiation via SRS in barium nitrate. Proceedings of All-Union Conference Laser Optics'90, Leningrad, 1990, p.311 (in Russian).
2. Garmine E., Paudarese F., Townes C.H , Cogerently driven molecular vibration and light modulation ., Physical Review Letters , 1963, v. 11, p.160-163.
3. N. Bloembergen., Nonlinear optics.,W.A. Benjamin, Inc., New York –Amsterdam, 1965.
4. Eckhardt G., Selection of Raman Laser Materials., IEEE j. of Quantum Electronics, 1966, v. QE-2, №1, p.1-8.
5. Kondilenko I.I., Korotkov P.A., Maly V.I. Thermal dependence of SRS spectra of some salts of inorganic acids in crystalline phase. Journal of Applied Spectroscopy, 1974, v.21, №2, p.282-285 (in Russian).
6. Bortkevich A.V., Karpukhin S.N., Stepanov A.I. Study of some crystalline media for SRS converters, phase. Journal of Applied Spectroscopy, 1982, v.37, №2, p.332-334 (in Russian).
7. Ivanuk A.M., Ter-Pogasyan M.A., Shakhverdov P.A. et al. Picosecond laser pulses via intracavity stimulated Raman scattering in active element of neodymium laser. Optika I spektroskopiya, 1985, v.59, №5, p.950-952 (in Russian).

8. V.A. Berenberg,, S.N. Karpukhin, I.V. Mochalov, Stimulated Raman Scattering of Nanosecond Palses in KGd(WO$_4$)$_2$ Crystals., Kvant. Elektron.(Moscow) v .14,№9, 1987 .

9. S.N. Karpukhin, A.I. Stepanov., Stimulated Emission From the Cavity Under SRS in Ba(NO$_3$)$_3$, NaNO$_3$ and CaCO$_3$ Crystals., Kvant. Elektron.(Moscow) v.13, 1572(1986) [Sov. J. Quantum Electron. v.16,1027(1986)].

10. T.T. Basiev, W. Jia, H. Liu, P.G. Zverev, Raman Spectroscopic and Nonlinear Optical Properties of Barium Nitrate Crystal., OSA TOPS on Advanced Solid-State Lasers.,1996, v.1, p.554- 559.

11. V.N.Voitsekhovskii, S.N. Karpukhin, V.E. Yacobson, Single-cristal barium nitrate and sodium nitrate as efficient materials for laser-radiation frequency based on stimulated Raman scattering, J.Opt.Technol., v.62(11), 1995, p.770-776.

12. S. A. Vitsinskii, V.K. Isakov, S.N. Karpukhin, I.L. Lovchii .Stimulated Raman scattering of copper-vapor laser radiation in a barium nitrate crystal., Kvant. Elektron.(Moscow) v.20, 1993 p.1155, [Sov. j. Quantum Electron.v.23, 1993, p.1001].

13. S.N. Karpukhin, V.E.Yashin., Stimulated Emission and Amplification of Radiation Under SRS in Crystals., Kvant. Elektron.(Moscow) v.11, 1984, p.19982, (1984),[Sov. j. Quantum Electron. v14, 1337(1984)].

14. C. He, T. H. Chyba., Solid-state barium nitrate Raman laser in visible region. Optics Communications., v.135, 1997, p.273-278.

15. J.T. Murray, R.C. Powell, N.Peyghambarian, D.Smith, W.Austin, R.A.Stolzenberger., Generation of 1,5-μm radiation through intracavity solid-state Raman shifting in Ba(NO$_3$)$_2$ nonlinear crystals., Optics Letters, 1995, v.20, N9, p.1017-1019.

16. V.I.Bespalov, G. A. Pasmanik, Nonlinear optics and adaptive laser systems., Moscow, Nauka publishers, 1986 (in Russian).

17. Yu. E. D'yakov, S.Yu. Nikitin., SRS of the Laser Radiation with a Wide Angular Spectrum, Kvant. Elektron.(Moscow),v.14, N10, p.1925-1957 [Sov. J. Quantum Electron. v.17,p.1227-1247 (1987)].

18. Robert S.F. Chang, Robert H. Lenmberg, Michael T. Duignan, N. Djeu ., Raman Beam Cleanup of a Severely Aberrated Pump Laser., IEEE J.of Quantum Electronics v.Q.E.21,N5, 1985, p.477-487.

19. Mezenov A.V., Soms L.N., Stepanov A.I. Thermal optics of solid-state lasers, J. of Soviet Laser Research, v.8, N5, 1987, p.427-549.

20. Mikheev M.A., Mikheeva I.M. Principles of thermal transfer, Moscow, Energia publishers, 1977 (in Russian).

21. J.F. Nye, Physical Properties of crystals., Oxford at the Clarendon Press 1964.

22. Belevceva L.I., Voitzekhovsky V.N., Nazarova N.A., Romanova G.I., Shvedova M.V., Yakobson V.E. Basic properties of optical crystals of barium nitrate. Optiko-mekhanicheskaya promyshlennost, No.4, 1989 (in Russian).

23. L.N. Soms, A.A.Tarasov, V.V. Shashkin. On the Problem of Depolarization of Linearly Polarized Light by a YAG:Nd^{3+} Laser Rod Under Conditions of Thermally Induced Birefringence. Kvant. Elektron.(Moscow)., v.7, N3, 1980, p.619-621.

24. L.N. Soms, A.A.Tarasov, Thermal Deformations in Color-Center Laser Active Elements. 1.Theory., Kvant. Elektron.(Moscow).,1985, v.6, N12, p.2546-2551.

·Institute for Laser Physics of SC "Vavilov State Optical Institute"

&

Company Lasers and Optical System, Ltd.

Crystalline Media for SRS Conversion of High Power 1.32 Micron Radiation

Interim Report #2

Director of the Institute		Prof. Arthur A.Mak
Principle Investigator		Sergey N.Karpukhin

St.-Petersburg

1998

1. Introduction

This Report is delivered on the completion of the second stage of the work in the frame of the Contract F61708-97-W0255. According to the Contract provisions on the second stage we had to prepare the Q-switched laser system, operating at 1.32 micron wavelength in pulse repetitive mode up to 20 Hz and providing the output of 20 mJ in single mode and 150 mJ in multimode operation regimes, and had also to grow up the larger SRS-active crystal. The study was carried out by the Company LOS Ltd., St.-Petersburg, Russia with the participation of the scientists of the Research Institute for Laser Physics, St.-Petersburg, Russia, and of the Research Center "Vavilov State Optical Institute", St.-Petersburg, Russia.

2. Laser setup

The setup was created accounting for the possibility of studies of the single mode radiation amplification in the field of multimode pumping according to the schedule of the final stage of the Contract. The setup comprises two lasers with the synchronized starting up of the electrooptical Q-switches. One of these lasers operates in the single mode regime, while the other — in the multimode. It is also provided that in the experiments with the single mode beam the laser heads of one laser can be used for the amplification of the beam from the other one.

The functional scheme of the setup is shown in the Fig.1. The electrooptical switches of both lasers are controlled by one and the same modulator 1. The divider 2 of the Q-switch shutters driving frequency provided the variation of pulses rate at the fixed pulse rate of flash lamps, with repetition rate scaling 2,3,4,8,16. Thus it is possible to perform SRS studies with the variable thermal loading. Otherwise the variation of the lamp pump repetition rate could result in variation of thermal lens in laser YAG rod , and cause the variation of the pump radiation divergence and spatial structure.
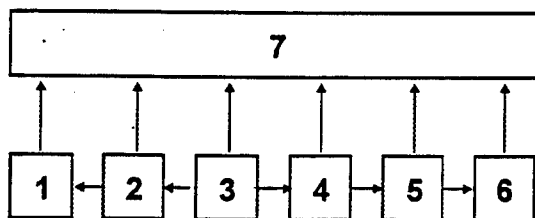

Fig.1. Functional scheme of laser setup.

1 — control unit for the electrooptical switches; 2 — the unit for the reducing of the repetition rate of the elctrooptical switching; 3, 4, 5 and 6 — power supply units for the flashlams; 7 — laser head.
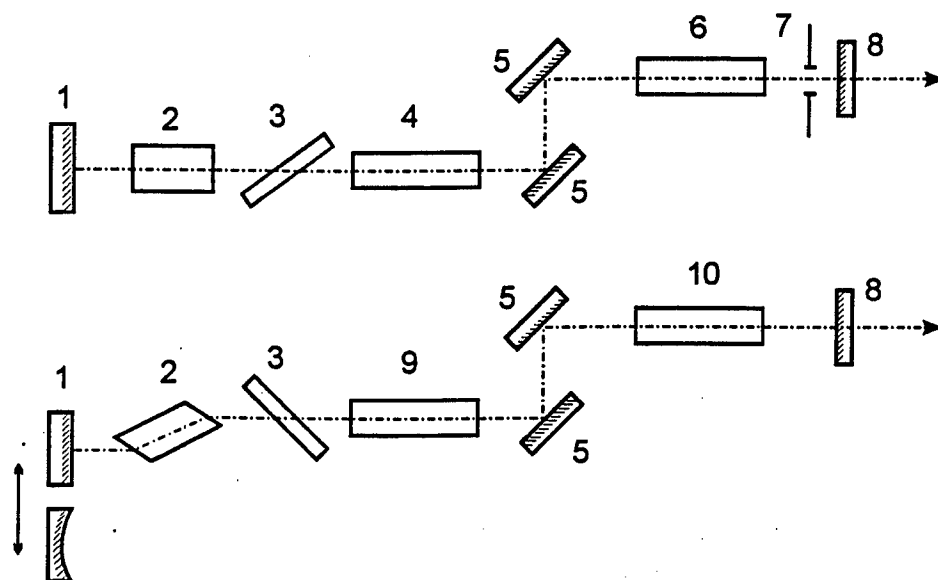
Fig.2. Optical scheme of laser setup.

1 — mirror, $R_{1.32/1.06}$= 99%/10%; 2 — electrooptical switches; 3 — polarizer; 4, 6, 9 and 10 — Nd:YAG crystals (4 — Ø5x65 mm, 6 — Ø4x65 mm, 9, 10 — Ø6.3x80 mm); 5 — $R_{1.32/1.06}$= 99,%/10% ; 7 — aperture Ø2 mm; 8 — $R_{1.32/1.06}$= 50%/10%.

The optical scheme of the pumping lasers is shown in the Fig.2. The cavities of both lasers (single mode and multimode ones) have similar lengths (~ 80 cm); their mirrors have the identical reflectivity. The crystals of Nd:YAG are pumped by the xenon flashlamps with the discharge gap length of 65 mm. Each of the cavities comprised two active elements, providing thus the possibility to reduce somewhat the pumping energy and the reflectivity of the coupling mirror. Such a reduce was necessary with the goal of reducing the intensity at the electrooptical Q-switch, which is made of lithium niobate. This medium has lower damage threshold, than the crystals of KDP and KDP* (DKDP), which are used for these purposes at 1.06 micron, but reveal significant absorption at 1.32 micron wavelength. Further reduce (~ 2 times) of the specific intensity at the edges of this crystal was obtained by means of these edges tilting at the Brewster angle. Each of the cavities also comprises two auxiliary spectrum selective mirrors, providing generation dumping at 1.064 micron (when these mirrors were absent we have observed the free run oscillation at this wavelength, reducing thus the Q-switched pulse energy and in the extra noise. We have fabricated two variants of the backward mirror for the cavity (position 1 in the Fig.2) — the plain mirrors and the concave with the curvature radius 2 m. In the second case we shall

realize the nearly semi-confocal cavity, which reveals the highest divergence of radiation among all the stable cavities with the exception of the so called conjugated cavity [1]. Such an operation mode is necessary for the studies of the regime of the averaging via the amplification (see the Report for the 1st stage of this work).

3. Pumping laser parameters

The energy of pulses was measured by the calorimeter. The energy of the multimode laser equaled 150 mJ. The energy of the single mode radiation was 10 mJ for the repetition rate 20 Hz and 8 mJ for the repetition rate 50 Hz; this energy was limited by the excitation of the second mode. The energy of 20 mJ, required by the Contract provisions was obtained after the amplification in two stages.

Fig.3. Divergence of radiation from the multimode laser.

(1) — with the plain backward mirror and (2) — with the concave backward mirror (semi-confocal cavity).
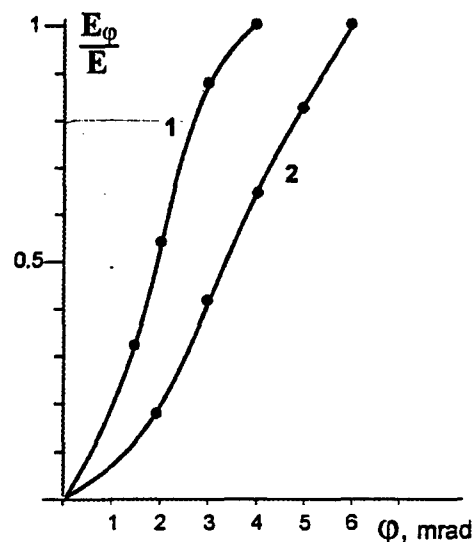
The divergence of the radiation was measured with the use of hard pinholes, positioned in the focal plane of the lens with the large focal length. The results of these measures are shown in the Fig.3. In the multimode laser, whose cavity was realized with the use of plain backward mirror the 0.8 of the beam energy filled into the angle of $\cong$ 2,5 mrad, while in the semi-confocal geometry it was $\cong$ 5 mrad. The far-field distribution of the single mode beam is shown in the Fig.4; its divergence was practically within the diffraction limit of 2.44 λ/d.

4

Fig.4. Far-field distribution of the single mode beam.
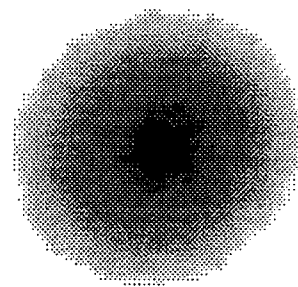
Pulse duration was measured with the use of the Tektronics oscilloscope TDS 744 (input bandwidth 500 MHz) and of the coaxial photosensitive element FEK-19 (bandwidth 1 GHz). The duration of the pulse (FWHM) was ~ 25 ns (see the oscillograms in the Fig.5).
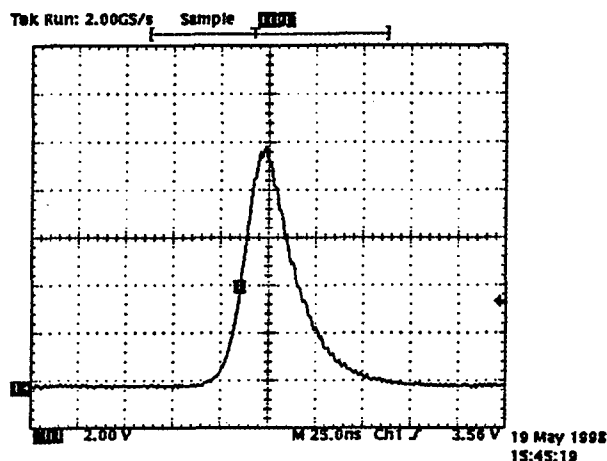
Fig.5. Oscillogram of laser pulse.

The width of the generation spectrum was measured using the second harmonics generation in KDP crystal 25 mm lengthl (ooe - interaction) .This an approach was valid because the generation spectrum is much more narrow than the width of frequency doubling synchronism (the last being about ~8 cm^{-1} for KDP with the crystal length spesified [2]). Three generation lines were detected , well resolved according to the doubling crystal angular position , which was interpreted as result of two lines generation in 1,3 micron region, viz. 1,319 and 1,344 micron. The brightest line corresponded to the doubling of 1,318 micron line. As long as the angle between beam direction and crystal axis increased, the weaker line appeared corresponding to frequency summation , and then the weakest line coupled with the 1,344 micron doubling was observed. The absolute wave lengths are given according to [3]. In the Fig.6 is shown the optical schematics which we have used for measuring the relative energy of these two components; it was determined that the energy emitted at 1.344 micron
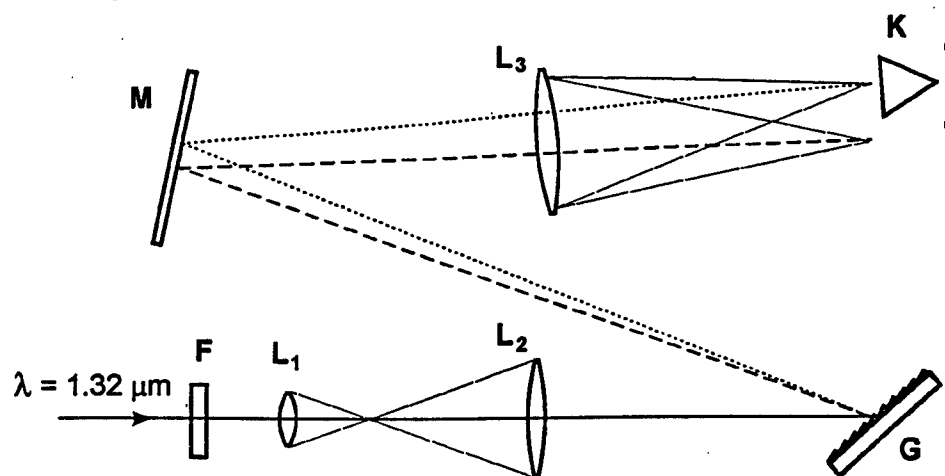
5

**Fig.6. Optical scheme for measuring
of energy distribution across spectral components.**

F-filter, $L_{1,2,3}$-lenses with focus length 5,70,150 cm ,G- diffraction
grating with 400 lines per mm , M-mirror, K-calorimeter.

was about 5% of that at 1.318 micron. Further, if it would be necessary, we plan to dump the weak component by the use of the intra-cavity interferometer with the appropriately small length and reflectivity. The spectrum width was measured with the use of the interferometers with the length of 1, 3 and 5 mm. The reflectivity of the mirrors was 90%. In the Fig.7 is shown an example of the interferogram, while the densitograms , recorded with the use of microdensitometer, are shown in the Fig.8. For the spectrum width evaluation from the densitograms, recoded with the 5 mm interferometer , the overlap of the neighboring interference orders was accounted. We have measured the relative density of the pattern near the center of the free interval (at the distance of 0,5 cm^{-1} from the line center). Such a measurement was realized with the use of the interferogram, recorded with the filter, transmitting 50% of the radiation. Assuming for the equal contribution of the neighboring orders, we could evaluate the result for the one interference order in the center of the free interval as 0,25 , or one half of the measured relative blackening. Accounting for this evaluation, we have then calculated the resulting spectrum width, using the formula for the gaussian shape of the generation line. The resulting value equaled 0.7 cm^{-1} ($\varphi(v)$ = exp($- v/\Delta v_g)^2$, $\varphi(0,5cm^{-1})$=0,25 for Δv_g =0,42 cm^{-1} , and $\Delta v = 2\Delta v_g \sqrt{\ln 2}$). For the length 3 mm, the influence of the neighboring order to the relative blackening was
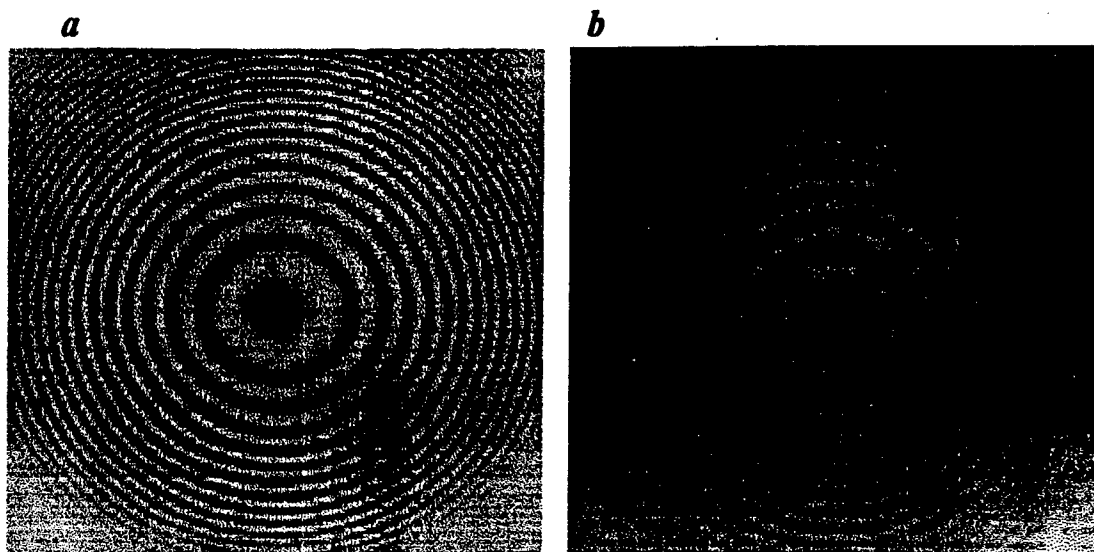
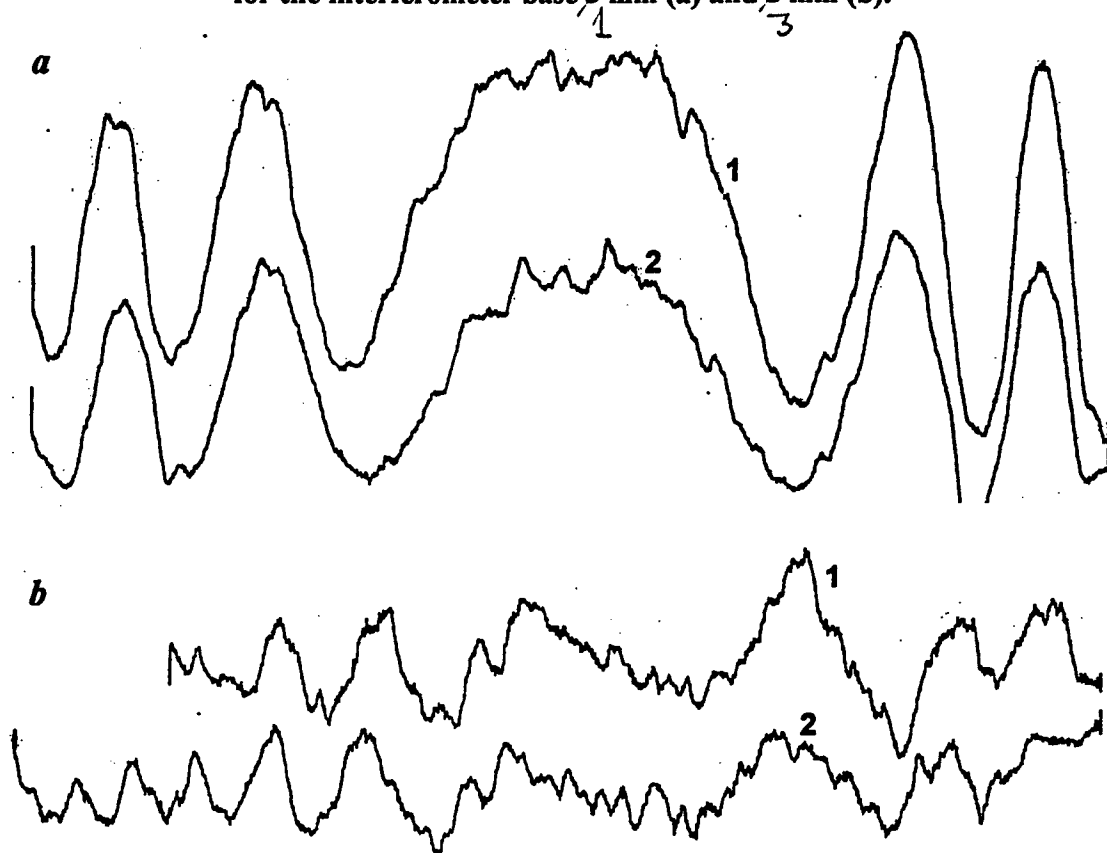**Fig.7. Interferograms of the 1.318 micron radiation for the interferometer base 3 mm (a) and 5 mm (b).**

Fig.8. Densitograms for the interferometer base 5 mm (a) and 3 mm (b) (1 — without the filter and (2) — with the filter, T=50%).

negligible, resulting in the close value of 0,75 cm^{-1} .So , for the spectrum width of second harmonic radiation we obtained medium value 0,73 cm^{-1} .Consequently for 1,319 μm we have value 0,37 cm^{-1}.

We have grown the crystals of barium nitrate, of sodium nitrate and of the KGW. Now the fabrication of the SRS active elements is in its progress — from the first two crystals with the size 10x10x60 mm and from KGW crystal — Ø5x60 mm.

4. References

1. Yuri A. Anan'ev. Optical resonators and laser beams. Moscow, «Nauka publishers», 1990, p. 87.

2. Optica i spectroscopiya. Volosov V.D., Kalinsev A.G. v.59, #5, p.1081-1084.

3. J.T. Murray, R.C. Powell, N.Peyghambarian, D.Smith, W.Austin, R.A.Stolzenberger. Optics Letters, 1995, v.20, N9, p.1017-1019.